Kaunas University of Technology

Faculty of Mechanical Engineering and Design

Investigation of Ultrasonic Techniques for Non-Destructive Testing of A-320 Wing Elevator

Master's Final Degree Project

Ribal ElBanna

Project author

Prof. Dr. Elena Jasiuniene

Supervisor

Kaunas, 2020

Kaunas University of Technology

Faculty of Mechanical Engineering and Design

Investigation of Ultrasonic Techniques for Non-Destructive Testing of A-320 Wing Elevator

Master's Final Degree Project

Aeronautical Engineering (6211EX024)

Ribal ElBanna

Project author

Prof. Dr. Elena Jasiuniene

Supervisor

Assoc. Prof. Dr. Saulius Japertas

Reviewer

Kaunas, 2020

Kaunas University of Technology

Faculty of Mechanical Engineering and Design

Riabl ElBanna

Investigation of Ultrasonic Techniques for Non-Destructive Testing of A-320 Wing Elevator

Declaration of Academic Integrity

I confirm that the final project of mine, Ribal ElBanna, on the topic „Investigation of Ultrasonic Techniques for Non-Destructive Testing of A-320 Wing Elevator“ is written completely by myself; all the provided data and research results are correct and have been obtained honestly. None of the parts of this thesis have been plagiarised from any printed, Internet-based or otherwise recorded sources. All direct and indirect quotations from external resources are indicated in the list of references. No monetary funds (unless required by Law) have been paid to anyone for any contribution to this project.

I fully and completely understand that any discovery of any manifestations/case/facts of dishonesty inevitably results in me incurring a penalty according to the procedure(s) effective at Kaunas University of Technology.

(name and surname filled in by hand) (signature)

Kaunas University of Technology

Faculty of Mechanical Engineering and Design

Study programme: Aeronautical Engineering (6211EX024)

Task of the Master's Final Degree Project

Given to the student: Ribal ElBanna

1. Title of the Project:

Investigation of Ultrasonic Techniques for Non-Destructive Testing of A-320 Wing Elevator

Ultragarsinių metodų, tinkamu A320 sparno neardomajai patikrai, tyrimas

2. Aim of the Project:

The aim of this project is to determine the most efficient and reliable technique for defect detection on A320 elevator.

3. Tasks of the Project:

- To analyze the existing NDT techniques for the inspection of composite structures and to select the most suitable ones for the inspection of A-320 elevator.
- Develop the A-320 elevator model using Civa software.
- Use two different Ultrasonic Transducers, Single Element Probe and Phased Array Transducer of 128 elements at frequencies 5MHz and 10MHz.
- Verify the results experimentally.
- Compare the experimental and simulated results.

4. Structure of the Text Part:

Introduction, Composite Materials, Analysis of NDT Methods Suitable of the Inspection of Aeronautical Components, Modelling Using CIVA, Modelling Results by Using Single Element Transducer, Modelling Results by Using PA Transducer, Experimental Results, Comparison of the Results of Different Transducers, Conclusion

Author of the Final Degree Project	Ribal ElBanna
	(abbreviation of the position, name, surname, signature, date)
Supervisor of the Final Degree Project	Prof. Dr. Elena Jasiuniene
	(abbreviation of the position, name, surname, signature, date)
Head of Study Programmes	prof. Artūras Keršys
	(abbreviation of the position, name, surname, signature, date)

ElBanna Ribal. Investigation of Ultrasonic Techniques for Non-Destructive Testing of A-320 Wing Elevator. Master's Final Degree Project / supervisor prof. dr. Elena Jasiuniene; Faculty of Mechanical Engineering and Design, Kaunas University of Technology.

Study field and area (study field group): Aeronautical Engineering (E14), Engineering Science.

Keywords: Ultrasonic Non-Destructive Testing, Phased Array, Modelling

Kaunas, 2020. 80 pages.

Summary

A non-destructive testing is used to evaluate and assess the quality of any material without causing damage for it. The aim of this project is to determine the most efficient and reliable technique for defect detection on A320 elevator. UT is used to inspect the A-320 elevator. The model using Civa software is developed for the ultrasonic inspection of A-320 elevator The inspection is performed by using different Ultrasonic transducers such as, single element probe and phased array transducer. Two different frequency ranges have been used: 10MHz and 5MHz in order to specify the most efficient and reliable technique for defect detection on the A320 elevator. It was determined, that higher frequency phased array inspection is more suitable. The results were verified experimentally**.**

ElBanna Ribal. Ultragarsinių metodų, tinkamu A320 sparno neardomajai patikrai, tyrimas. Magistro baigiamasis projektas / prof. dr.. Elena Jasiuniene; Kauno technologijos universitetas, Mechanikos inžinerijos ir dizaino fakultetas fakultetas.

Studijų kryptis ir sritis (studijų krypčių grupė): Aeronautikos inžinerija (E14), Inžinerijos mokslai.

Reikšminiai žodžiai: ultragarsinė neardomoji kontrolė, fazuotos gardelės, modeliavimas.

Kaunas, 2020. 80. p.

Santrauka

Neardomieji bandymai yra naudojami medžiagų ar konstrukcijų kokybei įvertinti jų nesuardant. Šio projekto tikslas yra nustatyti efektyviausią ir patikimiausią defektų aptikimo A320 sparne metodiką. Ultragarsinė neardomoji kontrolė naudojama A-320 sparno patikrai. Tinkamiausio metodo A-320 sparno patikrai parinkimui sukurtas modelis naudojant „Civa“ programinę įrangą. Patikrinimas atliekamas naudojant skirtingus ultragarso keitiklius, tokius kaip vieno elemento ir fazuotos gardelės. Buvo naudojami du skirtingi dažnių diapazonai: 10MHz ir 5MHz, siekiant nustatyti efektyviausią ir patikimiausią defektų aptikimui A-320 sparne. Nustatyta, kad sparno neardomąjai patikrai tinkamesnės aukštesnio dažnio fazuotos gardelės. Rezultatai buvo patikrinti eksperimentiškai.

Table of contents

List of figures

List of tables

List of abbreviations

A320 – Airbus 320

NDT – Non-Destructive Testing

CFRP – Carbon Fiber Reinforced Plastic

UT – Ultrasonic Testing

POD – Probability of Detection

PMCs – Polymer Matrix Composites

FRP – Fiber Reinforced Plastic

PE – Polyethylene

PP – Polypropylene

PA – Phased Array

PCA – Principle Component Analysis

1 Introduction

The Non-destructive testing techniques are able to evaluate and assess the quality of the component without causing damage to the part being tested. NDT techniques are widely used in the aerospace industries. However, the usage of composite materials in aerospace manufacturing companies such as Boeing and Airbus is significantly increased. Moreover, engineers use NDT to detect any defect in materials and structures, while these inspections are applied either during manufacturing or in service. Wing's damages and defects can be in different forms and shapes. In composite structures of the laminate type, the defects are mainly delamination between the different layers of the wing lining. The other defects of an A-320 elevator could be cracks inside the honeycomb, at a CFRP layer or a surface cracks. Eventually, the main purpose of the A-320 elevator inspection using NDT is to detect the surface and lower surface cracks and delamination that could be not visible. However, attenuation and energy losses may occur due to the variation of the ultrasound velocity between the layers. The other challenges in A-320 elevator inspection are the complexity of curvature shape and geometry. A320 elevator is a non-conductive material, which means only limited NDT techniques could be used such as UT, Thermography and Shearography. UT is widely used for wing inspections of sandwich structure to detect the surface and internal discontinuities by using only one side of the inspected part and non-hazardous for operators. Moreover, different frequencies could be used, for example 5 MHz and 10 MHz frequencies to detect various types of cracks at different intensities. As a result, different images could be demonstrated such as A-Scan and B-Scan that show the intensity and relative position of the defects. However, high skills is required for A-320 elevator inspection by using UT, and the inspection tools are expensive as well. The A-320 elevator is a heterogeneous component, and it consists of four different types of materials such as carbon fiber reinforced plastic (CFRP), Aluminum on the wing leading edge, fiberglass honeycomb core and polystyrene adhesive as shown in a figure 1.1.

Fig. 1.1. A320 elevator.

The objective of this project is to determine the most efficient and reliable technique for defect detection on A320 elevator.

To achieve the objective, following tasks had to be solved:

1. To analyze the existing NDT techniques for the inspection of composite structures and to select the most suitable ones for the inspection of A-320 elevator.
2. Develop the A-320 elevator model using a Civa software.
3. Use two different Ultrasonic Transducers, Single Element Probe and Phased Array Transducer of 128 elements at frequencies 5MHz and 10MHz.
4. Verify the results experimentally.
5. Compare the experimental and simulated results.

2 Composite Materials

Composite materials consist of a combination between two materials of different properties to produce another type of material that has a new mechanical characteristics differ from any initial ones. Composites are usually made of base matrix and reinforcements. However, the reinforcements are stronger than matrix; composites have better tensile strength and high properties because of different orientation of fibers and dispersions.

There are various Composite Structures such as:

- **Fibrous Composites** are consist of matrix and fibers. However, the fibers are long and thin of a diameter 20μm. Fibrous Composites have high mechanical properties.
- **Laminated Composites** are consist of several layers are bounded together such as sandwich structures, which are highly used in the aerospace industries.
- **Particle Composites** are made of a small fiber particles that dispersed in a matrix, which it produces high isotropic material.
- **Mixed Composites** composed of combining any of the previously mentioned of composite structures.

2.1. Polymer Matrix Composites

PMCs are a mixture of based resin as a matrix and fibers for the reinforcements, they are also known as fiber reinforced polymer (FRP). PMCs are commonly used in aerospace/aeronautics industries. However, the resin and fibers undergo with a various mixtures and chemical reactive components, while the resin define the final shape of the desired component. There are different types of resin such as:

- **Epoxy resins** are also known as a molecule of oxirane structure that consists of two carbon atoms and one oxygen atom. Epoxy resin have elastic modulus and strength, very good adhesion, high chemical resistance and low shrinkage. The main limitations are they brittleness and sensibility to moisture.
- **Polyester resins** are not expensive and easy for processing. The mixture is a combination of polyester and styrene solution, where it facilitates the molding process without a pressure. However, various optimizing products are used when the chemical reaction takes place to improve and increase the reaction speed such as, catalysts, accelerator and additives.
- **Phenolic resins** have high thermal resistance to chemical. However, it is used in complex shapes production because of the law viscosity and molecular weight.
- **Thermoplastics resins** such as polyethylene PE, polypropylene PP, polyphenylene sulfide PPS. These mentioned types of resins are widely used in aerospace manufacturing industries because of its thermal resistance, good mechanical properties at a high temperature and high moisture absorption. Moreover, thermoplastics resins are easy and fast to process, and high impact resistance.

2.2. Defects in Composite Materials of Sandwich Structure

The NDT are mostly used in the aerospace industries and manufacturers to ensure the quality of the material. However, the usage of composite materials in the Boeing and Airbus manufacturers have been increased. The sandwich structure damages and defects could be in a different form and shapes.

There are different types of defects and delamination in a composite sandwich structure, such as NOMEX as shown in a figure2.1. The defects in the sandwich structure material are classified as follows:

- Defect type A: the delamination between the external layers of the CFRP.
- Defect type B: loss of adhesion between the CFRP layer, coating and the honeycomb.
- Defect type C: cracks in honey comb which is parallel to the inspection surface.
- Defect type D: honeycomb layer is compressed.
- Defect type E: lack of adhesion between the inner layer of CFRP and honeycomb.
- Defect type F: fluid filtration occurs in honeycomb's core.

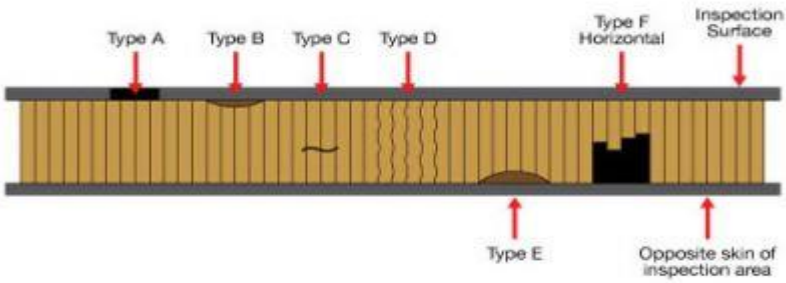

Fig. 2.1. Main defects of a composite structure. [7]

3 Analysis of NDT Methods Suitable For the Inspection of Aeronautical Components

There are different techniques for NDT. However, none of the available techniques can fully meet all the needs of NDT in composites. The UT is one of the most efficient and reliable techniques for the composites inspection.

3.1. Ultrasonic Methods

UT is widely used for non-destructive testing in aerospace industry, which it is mainly used for the inspection of the composites sandwich structure. However, the Multimode Acoustic Adhesion test is based on the transmitting and receiving signals to inspect wings and elevators of aircrafts. When the probe is placed over the inspected area as shown in a figure 3.1, it detects the adhesion loses, or it shows the reflecting signals with a different amplitudes. The amplitudes represent the intensity of the detected defects, and it is usually measured in dB. The amplitudes are demonstrated by an A-scan image.

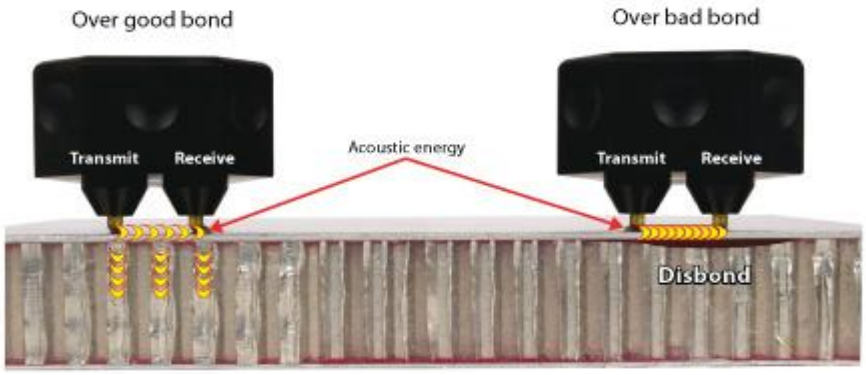

Fig. 3.1. Emission and reception mode for composites. [5]

Low frequency probes are usually used to detect the delamination and adhesion between the outer surface and the inner core. Moreover, a technique has been developed to detect the lack of adhesion between the inner core and the outer layer by using a probe of a bandwidth between 1 and 10MHz frequency that it produces waves and creates a resonance inside the probe. As a result, the loss of adhesion between layers will reduce the strength of the material structure.

Other advanced ultrasonic techniques is the ‘‘Phased Array’’ technique and it is used in a various application especially in aerospace industry. PA transducer is used to detect the defects and damages of the composite structures including wings and stabilizers.

The inspection of the Phased Array covers a wide range area since it consists of many elements. Moreover, the results that could be obtained from the Phased Array testing are presented by the three images such as A-scan, B-scan and C-scan of Omni-scan. However, the scan images allow us to determine the size of the defect/delamination, location and its position from the inspection area.

3.1.1. Phased Array Inspections

Recently, the PA technique is widely used for NDT of an aircrafts including wings, elevators and fuselage. However, The PA technique can be adjusted to a different focus types by electronic sound beams. Another advantage of PA transducer in comparison with a Single element transducer, it present different scan images (B-scan, C-scan, S-scan) rather than only A-scans.

Moreover, Large CFRP parts are inspected with a multi-channel facilities. The probe moves automatically on the upper surface area of the wing. The probe consists of a 96 individual transducers (channels). The maximum inspection area is 13m, with a step size speed of 100mm/s. Special software tools such as an OMNISCAN is used to represent the A-scan and B-Scan images as shown in a figure 3.5.

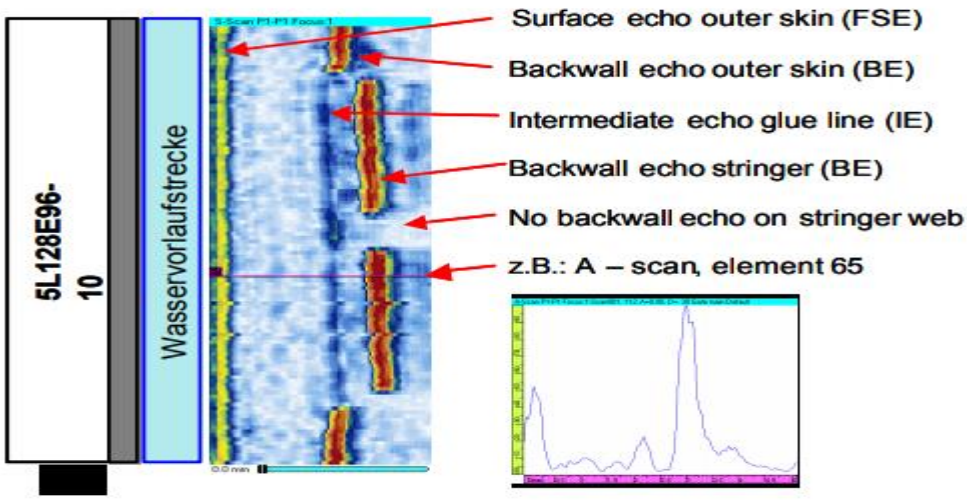

Fig. 3.2. B-scan and A-Scan images of A-320 wing. [28]

Advantages of using Ultrasonic Phased Array:

- Possible to detect surface and internal discontinuities.
- Only one side is needed for inspection.
- Law setup preparations.
- Nonhazardous for operators.
- Receive detailed images (A-scan, B-scan and C-scan).
- Applicable for different types of materials.
- It provides instantaneous results.

Advantages of using Ultrasonic Phased Array:

- Skill and training for the operators are expensive.
- Rough and irregular shapes are difficult to inspect.
- Expensive tools and devices.

3.1.2. Lamb Waves Technique

Lamb Wave technique is one of the most effective techniques to test complex and large shapes such as wing section. However, the undamaged section is called normality and damaged part is called abnormality where the impact damage is detected.

The advantages of the Lamb Wave are less energy consumption, easy preparation. Lamb waves have different shapes in nature. The speed of each sample varies with respect to its frequency due to the variation of Ultrasonic wavelength velocity. Moreover, high velocities propagation from 800m/s to 6000m/s could reach high amplitudes.

The major disadvantage of a PZT-generated Lamb wave is that the received noises could not be avoided. Lamb waves using a contactless laser may lead and cause interference and as a result inaccurate data. [6]

3.1.3. Laser Based Ultra-Sound

Advanced technologies manufacturer and industries recently are using more the composite materials such as carbon fiber reinforced plastic (CFRP) especially in aerospace industry for example, it is widely used in the wings, fuselage, stabilizer, rudder and fins. Fiberglass (GFRP) are used in order to make the structure of the material thicker with a light weight such as honeycomb, where the structure is strong as well.

When a focused beam signal is transmitted to a solid surface, one part of the energy is reflected and the other part is absorbed and transform into heat. However, the temperature is increased near the surface and produce high pressure, which it may increase the temperature of the material. The acoustic waves are produced in different directions corresponding to longitudinal, shear, transverse and surface waves. Figure 3.10 represents C-scan image of the delamination of Falcon 10 jet composite wing using Based Laser Ultrasonic method.

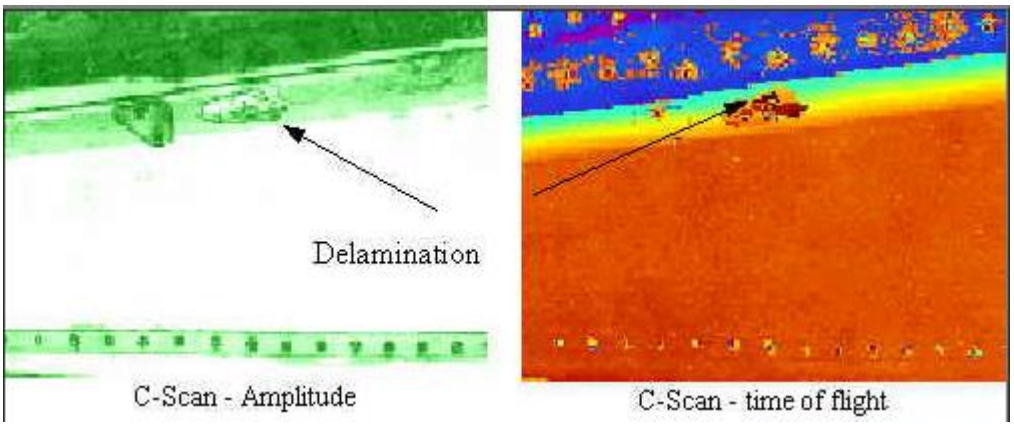

Fig. 3.3. Laser Ultrasonic C-scan of Falcon jet 10 wing. [9]

Advantages and Limitations of Lamb Based Ultra-Sound

- No liquid coupling.
- Very high tolerance.
- Inspection of limited access area.
- Proven sensitivity for a wide range of materials.

The main disadvantages of Lam Based Ultra-sound testing is being lower sensitivity, higher impedance, high operational skills is required, and high equipment cost.

3.2. Shearography Testing

Shearography Technique is an advanced testing method for NDT where it is applicable in various industries including aerospace. However, this technique is a laser based that measures the variation of the phased angles. Moreover, it is non-contact and useful to inspect large areas such as wings and fuselage of aircrafts.

Shearography technique use the reflective light to detect the displacement deformation on the surface. However, it is applicable to inspect a wide range of materials such as homogeneous and heterogeneous. Besides that, it is non- contact technique and can part can be inspected by using only one face. On the other hand, the problem with shearography technique is that can cause damage to the part when applying load or heat. The other drawback, shearograghy is more applicable with rough surfaces while smooth surfaces can cause interference and lead to receive wrong inspection results. Moreover, personal skills is required while performing this technique and good lightning is required to get better results. [2]

3.3. Other NDT Techniques for Inspection of Sandwich Structure Composite Material

There are various and different types of a NDT techniques that are used in aerospace industry such as Ultrasonic, Shearography, Thermography, Lamb-Waves testing and Acoustic Techniques. Airliner and manufacturer use these techniques on different applications to identify and detect any defect without causing damage to the component. However, some techniques require high skills for operators since some of them are hazardous and need experience.

3.3.1. Radiography Technique

This method is widely used in non-destructive testing especially in aerospace industry. However, different radiographic records are produced by electromagnetic radiation such as X-ray or Gamma rays. Hoever, it is used for wings inspection of laminate composite structure to detect porosity, water ingress, cracked core and loss of adhesion. [9]

Advantages of Radio Graphic method:

- Defects can be detected internally and externally.
- Significant detections for variations.
- Very few material limitations.
- No preparing required.
- Can detect hidden areas.

Limitations of Radio Graphic method:

- Hazardous for operators.
- High skills are required.
- Slow process.
- High cost.

3.3.2. Visual Testing

It is based on the illumination of the test surface and on the eyesight of technicians. Visual testing requires training, for example knowledge of the material, and it has specific range of equipment. However, it is significantly used in aircraft and wing inspections, where in most cases the inspections include checking the welded parts and its location.

Advantages of Visual Testing technique:

- Low cost.
- Non expensive tools.
- Instantaneous inspections.

- No preparation required.
- Law skills required.

Limitations of visual testing:

- Only surface defect detection.
- No detailed images.
- Slow process.

3.3.3. Acoustic Technique

Acoustic Technique use waves below 500 KHz, and different devices are used, such as external mechanical device (Piezoelectric transducer) and acoustic emission. It is used in various application especially in aerospace industry to detect the defects and damages of the composite structure of the aircraft including wings and stabilizers. There are two different types of acoustic method such as tap testing and acoustic emission testing. However, the tap testing is used to check for large surface discontinuities, which they are close to the surface. Moreover, the advantage of using Acoustic technique is that it has low cost, easy and noncomplex procedure, and very useful for sandwich structure components. However, requires hearing skills and dependent on the operator, damage size and depth could be accurately detected, and needs verification by other NDT methods. [20]

Advantages of Tap Testing Method:

- Low cost.
- No coupling fluid is needed.
- Limited training needed.
- Good for sandwich structure materials

Disadvantages of Tap Testing:

- Hearing skills is required.
- Defect size cannot be determined.
- Lacks reliability.
- Requires verifications by other NDT methods.

However, the acoustic emission testing is a result of stress waves produced by a sample, when it is applied to an external load, and it is widely used in aircraft inspections to detect cracks and delamination.

Advantages of Acoustic Emission method:

- Crack growth can be detected in time.
- Control of specimens during mechanical loading.
- Good for health monitoring.

Disadvantages of Acoustic Emission method:

- High external load is required.
- Hard to detect small discontinuities.
- Affected by noises and attenuations.

- Needs verification from other NDT methods.
- Technical skills is required.

3.3.4. Thermography Technique

Thermography Testing is correspond to the measurement of the surface temperature of an object that is applied to thermal source. However, each body above the absolute zero emits an electromagnetic radiation known as thermal radiation, where it is based on the analysis of the thermal images taken on a surface of the inspected part. This method has various advantages, where measurement can be done without contact with the inspected area and fast results obtained without any preliminary treatment, and it is widely used in aviation and aircraft industry, where it used to inspect water ingress and failure installations. [24]

Advantages of Thermography Testing:

- Fast results.
- Non-contact.
- Portable.
- Can detect water ingress in honeycomb.

Disadvantages of Thermography Testing:

- Poor resolution on thick section.
- Low sensitivity.
- Only the close to the surface area can be inspected.

3.4. Conclusion

There are various types of NDT techniques, and they are widely used in aerospace industry especially for wings and stabilizers inspection.

Shearography testing in comparison with Ultra-sound techniques is based on a thermal laser inspection. However, it is widely used in the aerospace industries for large inspections such as, wings and fuselage. Shearography testing is more applicable with rough surfaces while smooth surfaces can cause interference and lead to a wrong and non-accurate results. Moreover, shearography testing can cause damage to the part when applying load or heat, which it will not be suitable for A-320 elevator's inspection. Moreover, this type of techniques require high operational skills and experience; inspection tools are expensive.

Other inspection technique such as, Radiography testing is widely used in the aerospace space industries and manufacturers. It is used for wings inspection to detect porosity, water ingress, cracked core and loss of adhesion. However, it is not applicable for A-320 elevator because it requires high operational skills, it is danger because it produce high radiations, and it is an expensive technique.

4 Modelling Using CIVA

The experiment is simulated by using a CIVA software, which it is developed especially for NDT applications, However, different NDT method could be simulated using CIVA software such as Ultrasonic, Eddy-current and Radiography technique. Moreover, CIVA is very useful and efficient tool to design, verify, and optimize inspection procedures. Furthermore, different transducers are possible to use, such as a single element and a phased array. The results are shown through the of A-scan, B-Scan and C-Scan image.

4.1. Sample Description

The A-320 elevator drawing is designed by using CIVA software. The area of the A-320 model is 580*360 mm^2. However, the A-320 elevator consists of four layers, which they are correspond to the CFRP, adhesion and honeycomb. Moreover, The ultrasound velocity and density of each material are identified to obtain accurate results.

The A-320 elevator is made up of four main parts and different types of materials. Table 4.1 represents the different parts of an A-320 elevator and its specifications. However, the thickness of a fiberglass honeycomb core is 14.32 mm. There are two parts of CFRP, where the thickness of the top part is a 0.45mm and at the button is 0.75mm. The thickness of a polystyrene adhesive is a 0.35mm.

Table 4.1. A-320 elevator material parameters.

	Part 1	**Part 2**	**Part 3**	**Part 4**
Material	Polystyrene (adhesive)	Carbon fiber reinforced plastic	Fiberglass honeycomb core	Carbon fiber reinforced plastic
Thickness mm	0.35	0.45	14.32	0.75
Ultrasonic velocity m/s	2340	3070	2740	3070
Density g/cm^3	1.04	1.55	2.66	1.55

4.1.1. Case Study 1: Modelling of Angular Defects

Case study 1 consists of three different size defects with different angles. However, defect1 is positioned vertically with respect to the surface, defect2 is placed parallel to the surface at a 0.35mm depth, and defect3 is placed at angle 45 degrees as shown in a figure 4.1.

Table 4.2. Different size defects and different angle.

	Defect 1	**Defect 2**	**Defect 3**
Length (mm)	20	20	20
Width (mm)	10	55	15
Depth (mm)	13	9	12
Angle (◦)	90	0	45

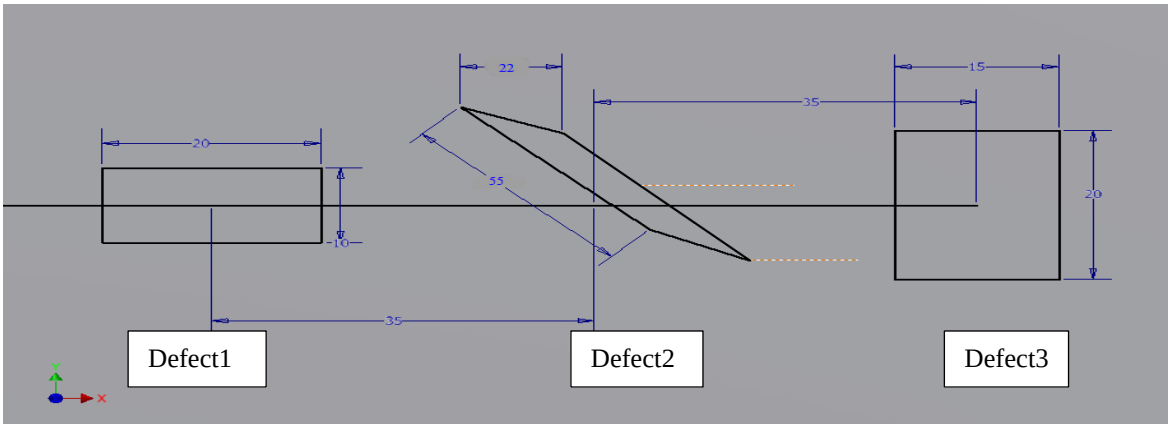

Fig. 4.1. Angular defects.

4.1.2. Case Study 2: Modelling of Same Size Defects at Different Depths

Case of study 2 represents the inspection of the same size defects. The area of each defect is a 10*10 mm^2. However, defect1 is located at a height of 0.35mm below the surface, between CFRP layer and paint and adhesion layer. Defect 2 is placed at a 0.6mm height, where it represents the delamination at the CFRP layer. Eventually, defect 3 is located at a 0.8mm below the surface. Moreover, the distance between the defects is a 35mm.

Table 4.3. Same size defects with a different depth.

Delamination/ Dimension	**Delamination 1**	**Delamination 2**	**Delamination 3**
Length, mm	10	10	10
Width, mm	10	10	10
Depth parallel to surface, mm	0.35	0.6	0.8

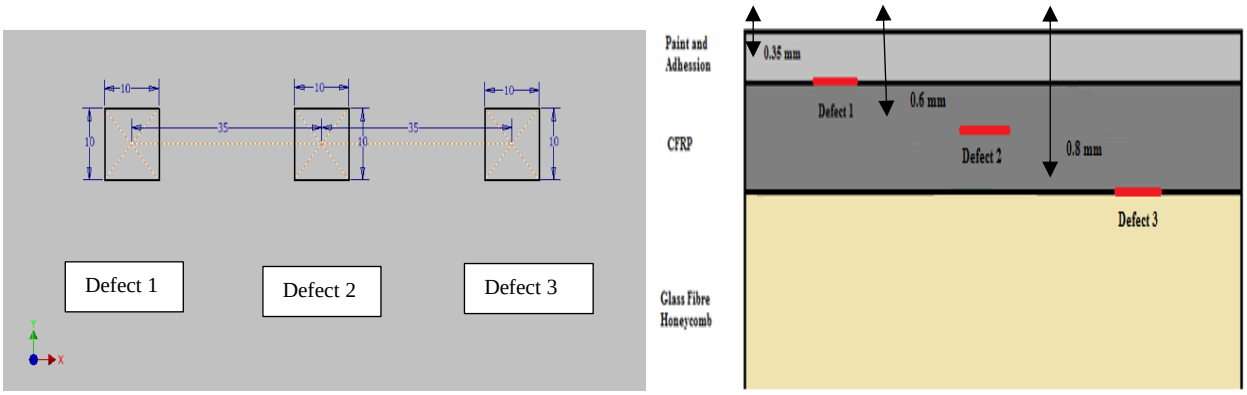

a) Top view b) Side view

Fig. 4.2. Same size delamination at a different depth.

Figure 4.2 represents the dimensions of the same size defects at a different depth. The top view shows the same size defects, which they are parallel to the upper surface. The side view represent the depth of each defect between the layers of an A-320 wing model.

4.1.3. Case Study 3: Modelling of Different Size Defects

Case study 3 represents the modelling of the three different size defects by using Civa software. The three defects are designed by using Civa program as shown in a figure 4.3. The purpose of modelling a different size defects is to detect the maximum amplitude of the defects. However, study case3 is divided into three sections.

- **Section1** represents the defects at 0.35mm depth (between paint/adhesion and CFRP).
- **Section2** represents the defects at 0.6mm depth (at CFRP layer).
- **Section3** represents the defects at 0.8mm depth (between CFRP and honeycomb).

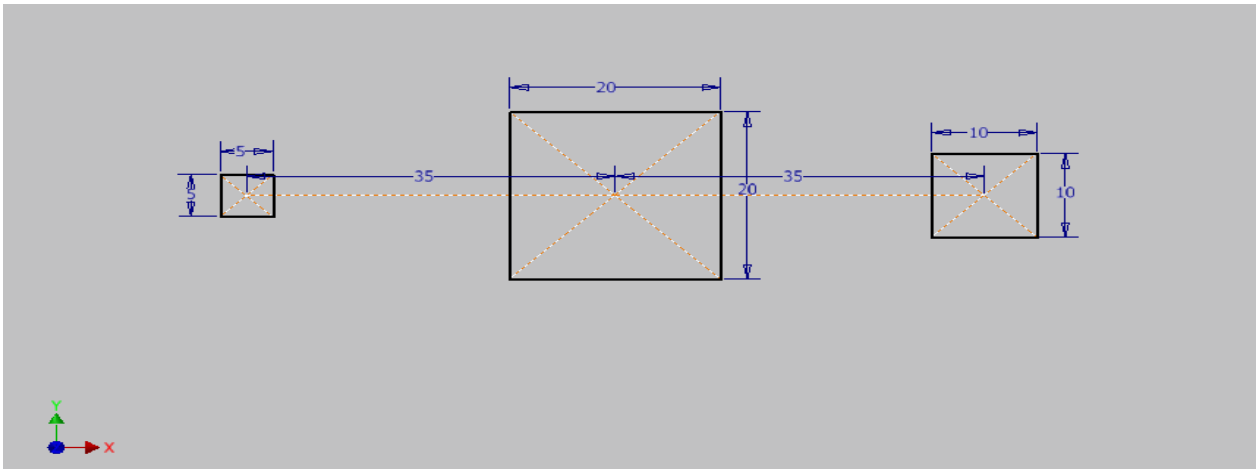

Fig. 4.3. Different Size defects.

The ultrasonic transducers used for inspection are single element probe and phased array transducer. There are two types of inspection correspond for PA transducer that are determined by the single point focusing and null delay law. Table 4.4 represents the parameters of the three size defects.

Table 4.4. Different size defects is positioned at three sections.

Sections	Section 1			Section 2			Section 3		
Defects no.	Defect1	Defect2	Defect3	Defect2	Defect2	Defect3	Defect 3		
Length mm	5	20	10	5	20	10	5	20	10
Width mm	5	20	10	5	20	10	5	20	10
Depth mm	0.35	0.35	0.35	0.6	0.6	0.6	0.8	0.8	0.8

4.2. Single Element Probe Modelling Setup

The inspections have done by using a different ultrasonic tools. The frequencies of the circular single element probe are 5 MHz and 10MHz. The diameter of the probe is a 10mm. The probe type is on contact to the surface. However, we have used a flat wedge geometry since the defects are located near to the surface.

Table 4.5. Single element probe parameters.

Transducer	Single element probe
Shape	Circular
Type	Contact
Diameter	10 mm
Frequency	5 MHz and 10 MHz

Figure 4.4 represents the A-scan reference signal at time = 3.2 µs along horizontal axis and amplitude 100 points along the vertical axis and 1,024 total number of points.

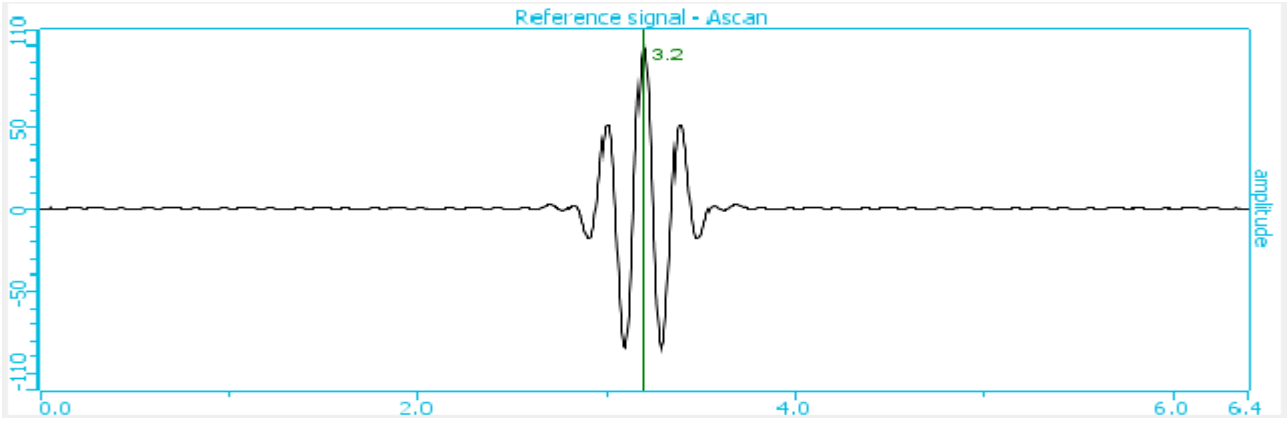

Fig. 4.4. A-Scan signal reference.

Moreover, the inspection has done on the three different delamination at different depths. the inspection is performed along y direction of a offset x=130 mm and offset y= 52 mm as shown in a figure 4.5.

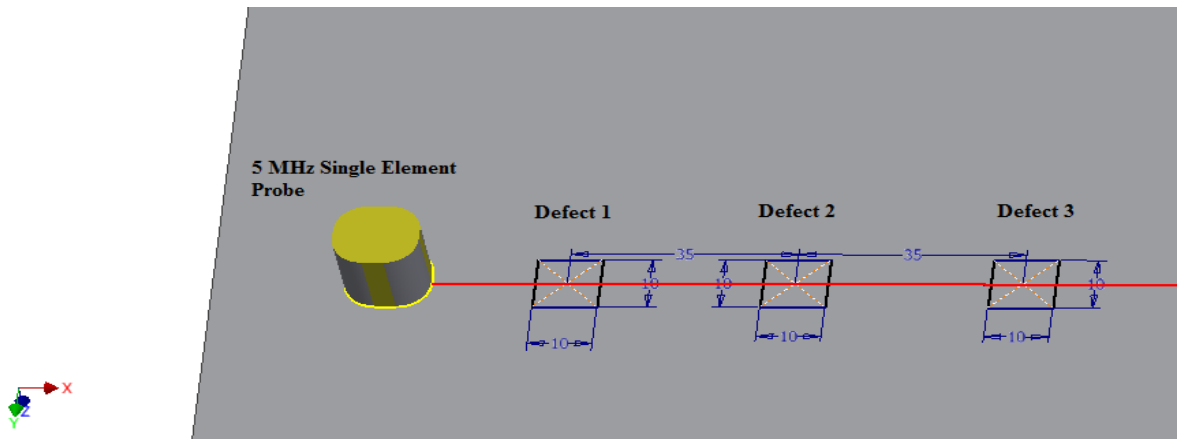

Fig. 4.5. Inspection of the same size defects

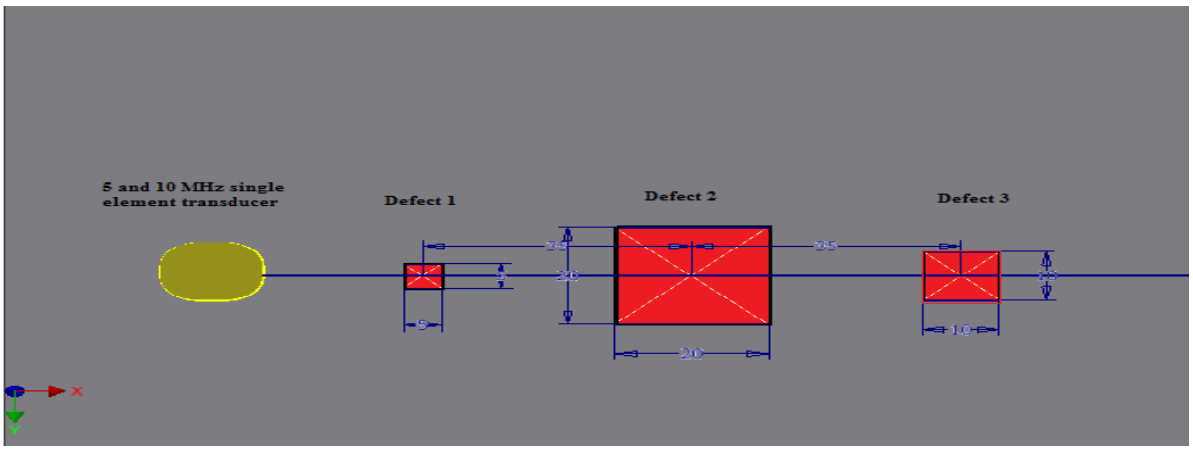

Fig. 4.6. Inspection of the different size defects.

Figure 4.6 represents the single element transducer at 5 MHz and 10 MHz inspection of three different size defects 5*5 mm^2, 20*20 mm^2 and 10*10 mm^2, where the height of the all defects is a 0.35mm.

4.3. Phased Array Modelling Setup

The latest method of UT is the PA inspection. There are two types of PA transducers: linear-single point focus and null delay law. However, the results are based on two different frequencies 5MHz and 10MHz

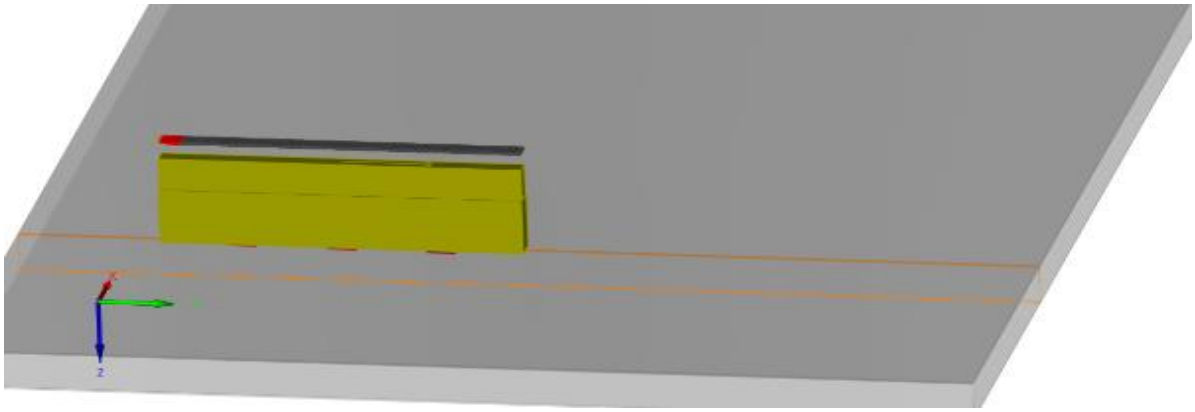

Fig. 4.7. Phased array inspection using Civa.

The single point focusing PA generates a fixed sound beam with a fix angle focusing (longitudinal or transverse). On the other hand, the non-linear delay law PA produces fix sound beams with more complexity of delay combinations, where the beam could be steering or focusing as shown in a figure 4.8.

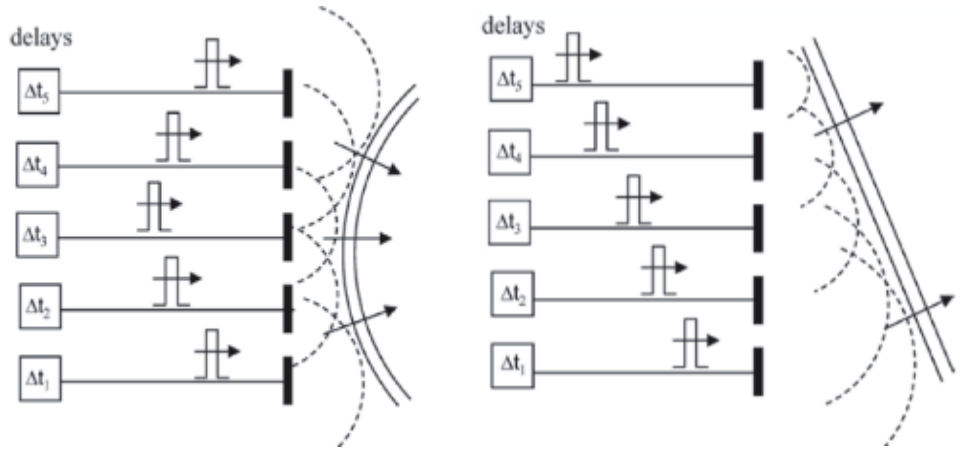

a) Single point focusing beam b) Null-delay law beam

Fig. 4.8. PA focus types. [29]

The main parameters of the linear transducer array are active pressure, passive aperture, probe width, gap between adjacent element, pitch or center to center distance as shown in a figure 4.9.

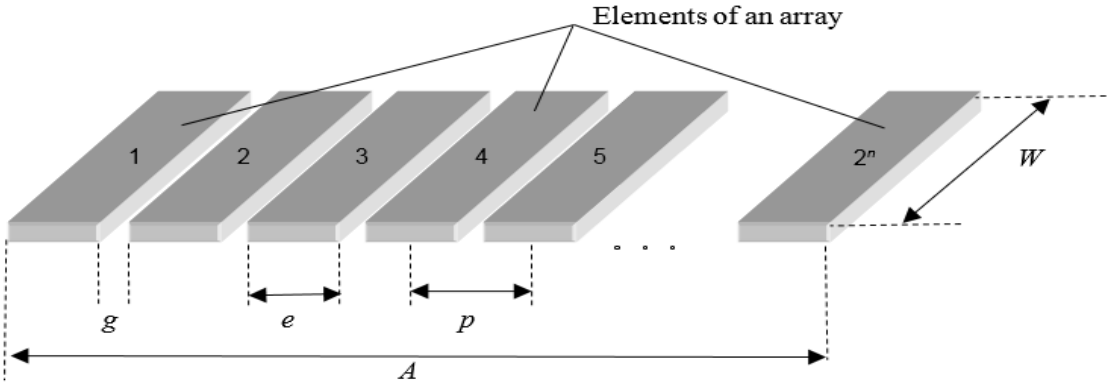

Fig. 4.9. Transducer array parameter.

Table 4.6. Main parameters of PA

Transducer	5L128-128X7-NW3	10L128-64X7-NW1
Frequency	5 MHz	10 MHz
Number of elements	128	128
A-total aperture	128 mm	64 mm
Elevation	7 mm	7 mm
P-Pitch	1 mm	0.5 mm

The patterns of the linear phased array are consist of 128 element and 8 consecutive element. However, the space between each element is a 0.1 mm, and the dimension of each element width is a 1mm as shown in a figure 4.10.

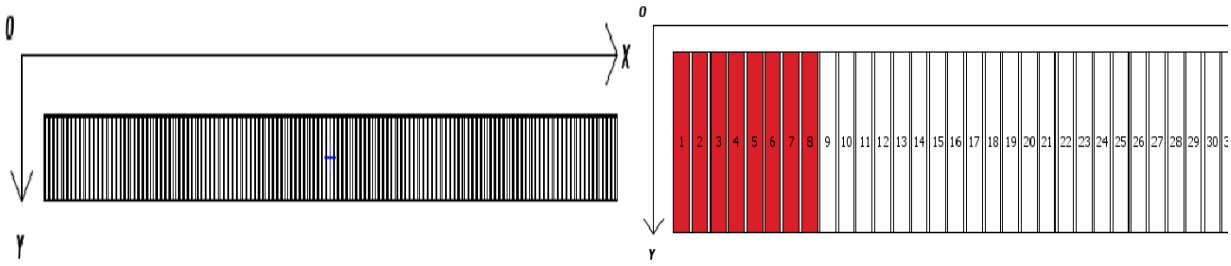

Fig. 4.10. Total number of elements and sequencing.

Figure 4.11 shows the variation of emission and reception of the consecutive elements, where the horizontal axis represents the position of the elements/channels. The vertical axis represents the time interval between the sequencing elements, which it is measured in µs. Moreover, the mid- channels 4 and 5 represents the peak time amplitude approximately 0.1 µs, and it is decreased progressively to reach 0µs at channels 1 and 8 as shown in a table 4.7.

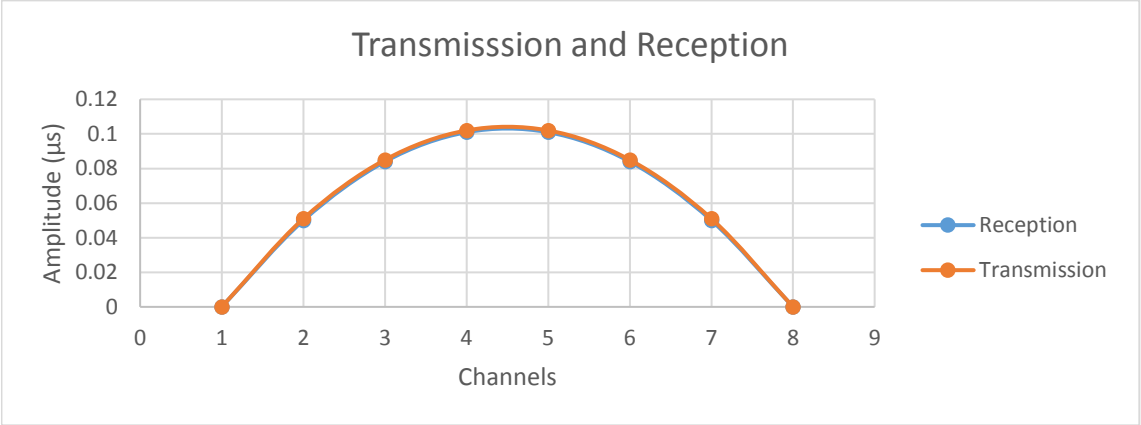

Fig. 4.11. Transmission and reception signals of the sequencing elements.

Table 4.7. Sequencing elements and time amplitude.

Channel	A.Transmission	D.Transmission (µs)	A. Reception	D. Reception (µs)
1	1	0	1	0
2	1	0.05	1	0.05
3	1	0.084	1	0.084
4	1	0.101	1	0.101
5	1	0.101	1	0.101
6	1	0.084	1	0.084
7	1	0.05	1	0.05
8	1	0	1	0

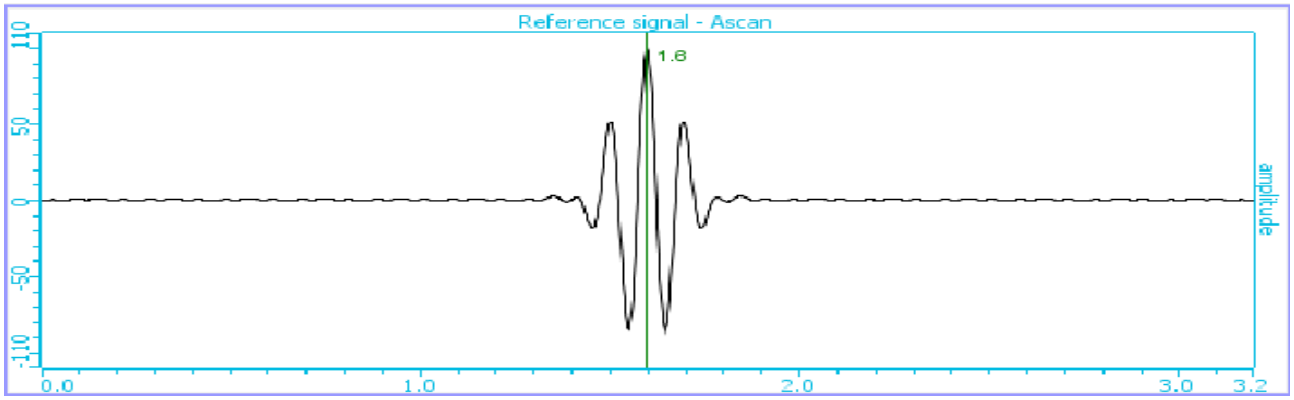

Fig. 4.12. Phased array A-scan reference signal.

The probe type is on contact to the surface. However, we have used a flat wedge geometry for phased array transducer since the defects are near surface. Table 4.8 represents the wedge dimensions.

Table 4.8. Phased array wedge dimensions.

Length1 (L1) mm	Length2 (L2) mm	Width (L3) mm	Height (L4) mm
64	64	10	22

Figure 4.13 represents the linear phased array inspection of the three different size defects 5*5 mm^2, 20*20^2 mm and 10*10^2 at a different depths as presented in section1, section2 and section3.

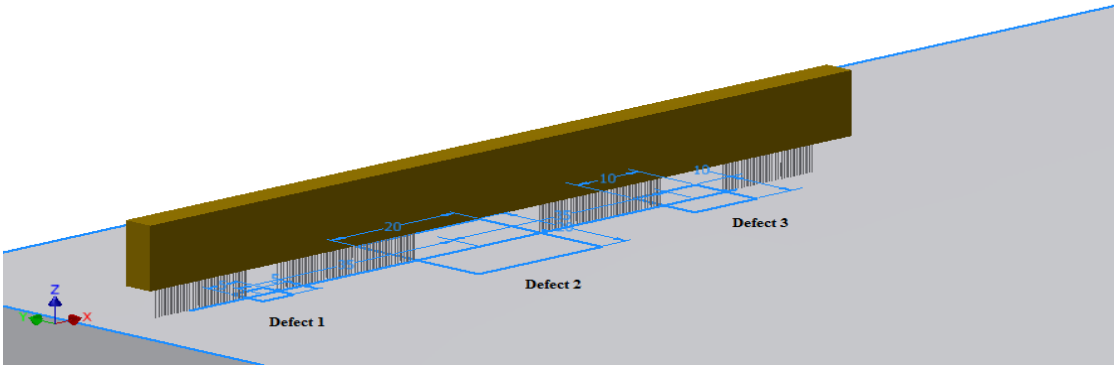

Fig. 4.13. Different size defect inspection using PA transducer.

4.4. POD Analysis

CIVA software is capable to compute for the probability of detection. However, the assessment and evaluation of the POD curves correspond to the estimation of the likelihood of the flows. The POD procedures are:

1. Determine the characteristic parameters for the POD computational analysis.
2. Define the variable parameters.
3. Select the uncertainty distribution for each variable such as normal or uniform distribution
4. Run the simulation based on Monte-Carlo function for the uncertain parameters.
5. Analyze the received POD curves.

All the flaws/defects are defined as characteristics, and the variables are defined as uncertain parameters. Moreover, in all tests the number of the characteristic values is 50 S.I, and the sample/character is 2 S.I.

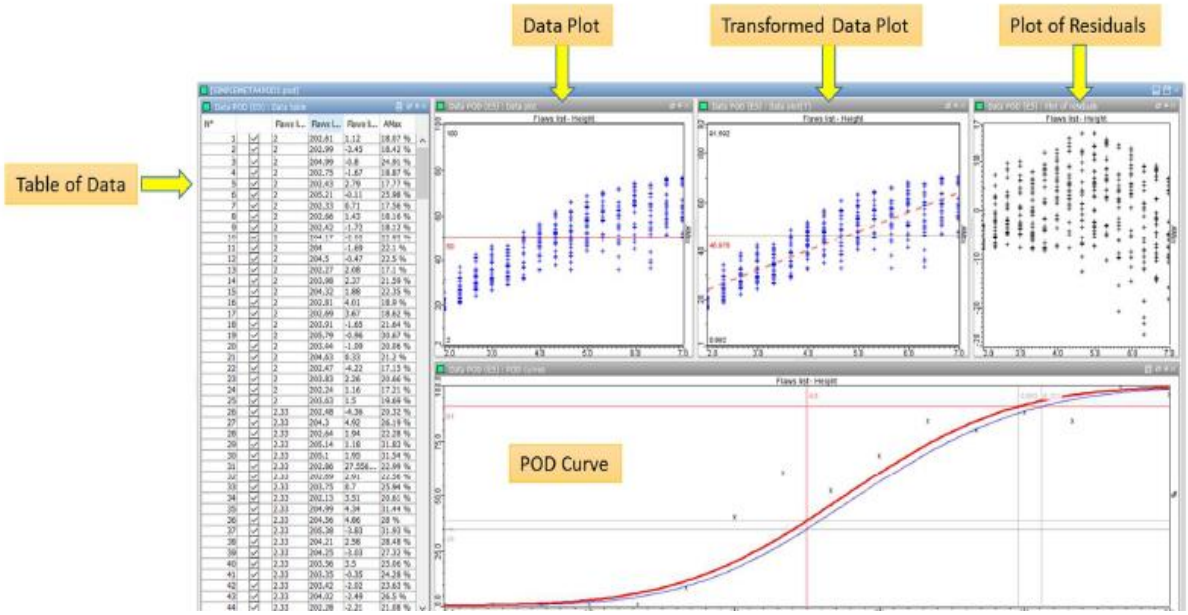

Fig. 4.14. POD analysis panel. [30]

Figure 4.14 represents the POD analysis panel in terms of signal response and algorithms. However, POD analysis displays different plots such as Data plot, Transformed Data plot, Residual plot and POD Curve.

Moreover, the table of data represents all the possibilities of the random values of the uncertain parameters. However, the attenuation and noises can be detected by the thresholds linked plot cursors.

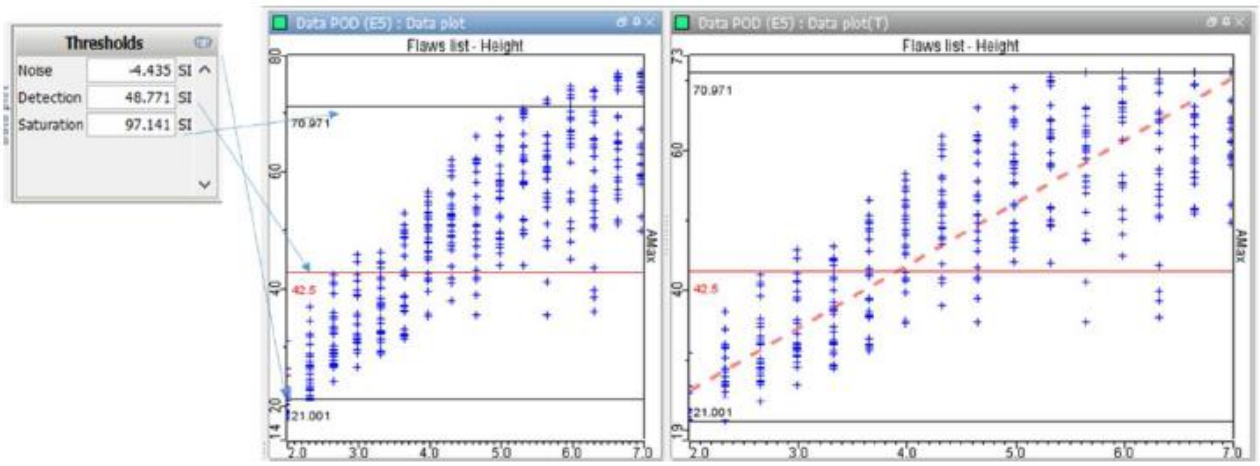

Fig. 4.15. Attenuation, noise and saturation thresholds. [31]

5 Modelling Results by Using Single Element Transducer

The inspection of the study cases1 is based on different types of ultrasonic transducers. The following results show A-scan and B-Scan images of the defects are correspond to the inspection of the single element probe with a 10mm diameter, and two different frequencies 5 MHz and 10MHz. However, the probe has circular shape and on contact to the surface.

5.1. Results of Case Study1

To detect the defects at a different positions, single element transducer of 5 MHz has been used. However, the results below show different amplitudes and intensities. The peak amplitude represents high detection of the defect as shown in a figure 5.1(b) . The running setup is consisted of 210 number of steps and 0.5 mm step size. After almost 30 minutes of a running progress, A-scan and B-scan images have been received as shown in a figure 5.1 and 5.2 respectively. The scanning simulation is based on a 3D simulation.

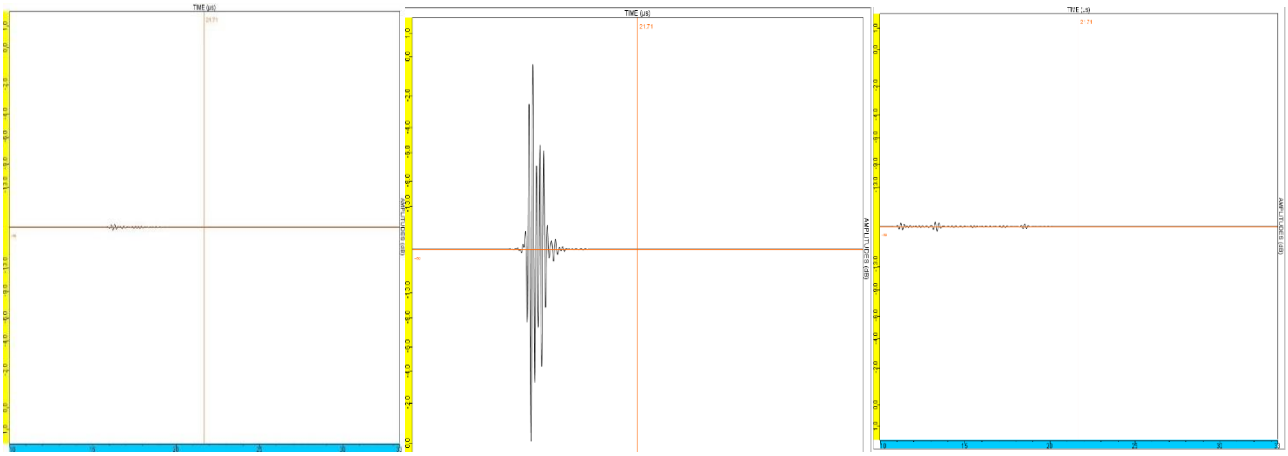

a) Vertical Defect b) Parallel to surface defect c) Angular defect

Fig. 5.1. A-Scan of defects with different sizes.

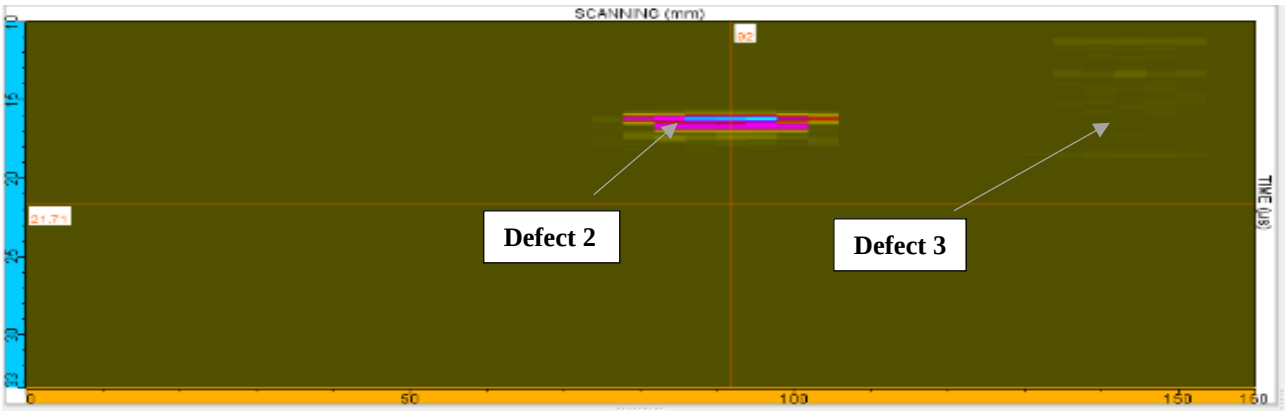

Fig. 5.2. B-Scan image of the angular defects.

Figure 5.1(a) represents the A-scan image of the vertical defect, and it is perpendicular to the surface. The maximum amplitude of the defect1 is a -0.1dB. Therefore, defect1 is not detected properly. However, at a defect2, the amplitude/intensity have decreased significantly, the amplitude at defect2

is a -13dB. The maximum amplitude of a defect3 is -6dB, where the defect3 is almost visible as shown in the B-scan image in a figure 5.2.

The results of the case study2 are regarding to the same size defects 10*10mm^2 as shown in the previous chapter of a figure 4.2(a). The inspection has performed by using circular shape single element probe at 5MHz and 10MHz frequency. The probe type is on contact with the surface, and the probe diameter is a 10mm. However, a flat wedge geometry is attached to the beam side of the transducer to separate the surface reflecting signals and the defects reflecting signals, also to improve the quality of A-scan and B-scan images.

5.1.1. Results of Case Study 2 at 5MHz Frequency

The aim of this task is to inspect the same size delamination of 10*10 mm^2 at a different alignments. The first delamination is located between the polystyrene adhesive and carbon fiber, the second delamination is placed between the carbon fiber and fiberglass honeycomb, and the third delamination is positioned inside the carbon fiber reinforced plastic at a 0.8mm height.

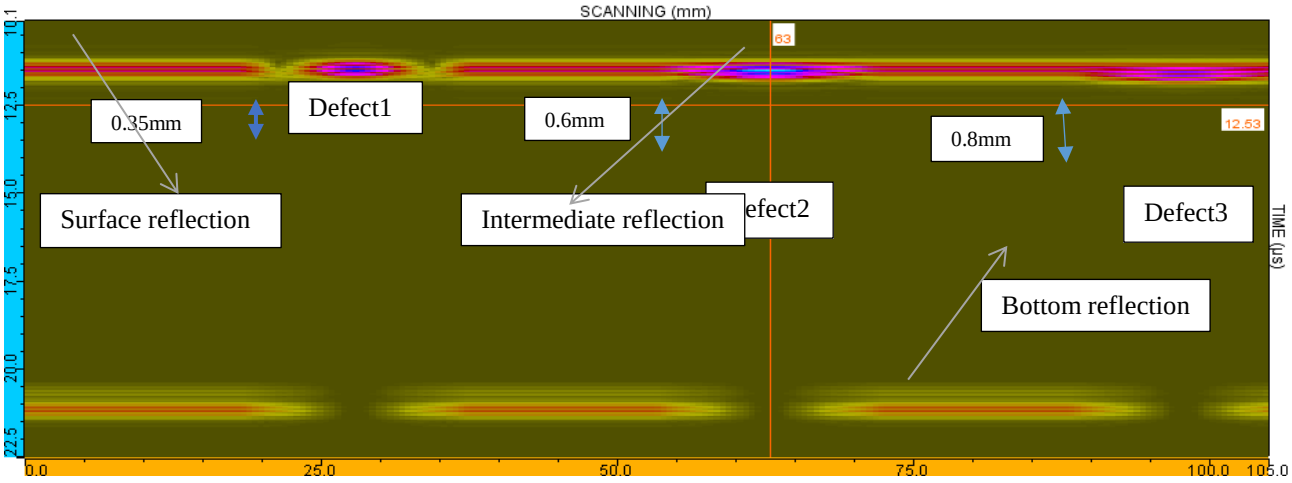

Fig. 5.3. B-scan image at 5MHz.

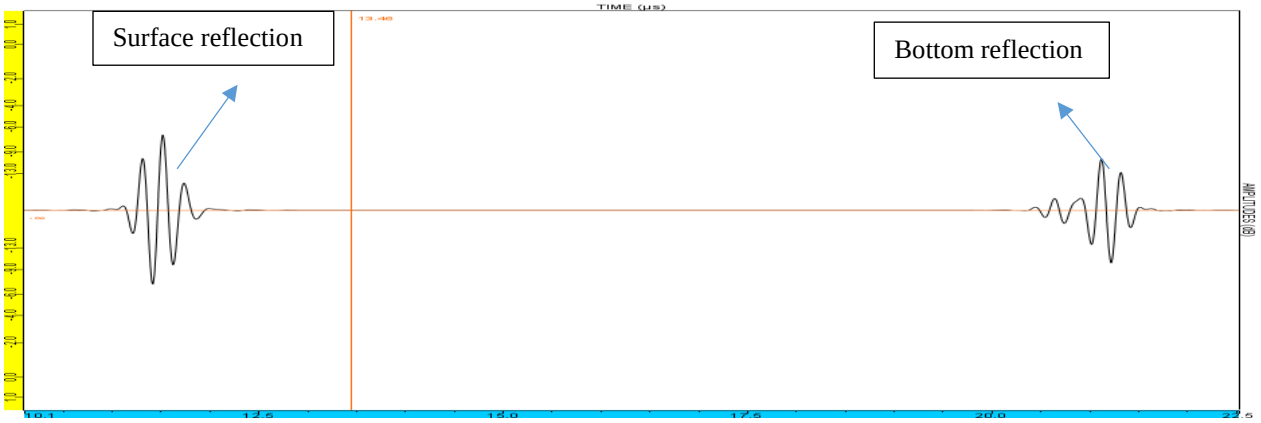

Fig. 5.4. A-Scan at no delamination section.

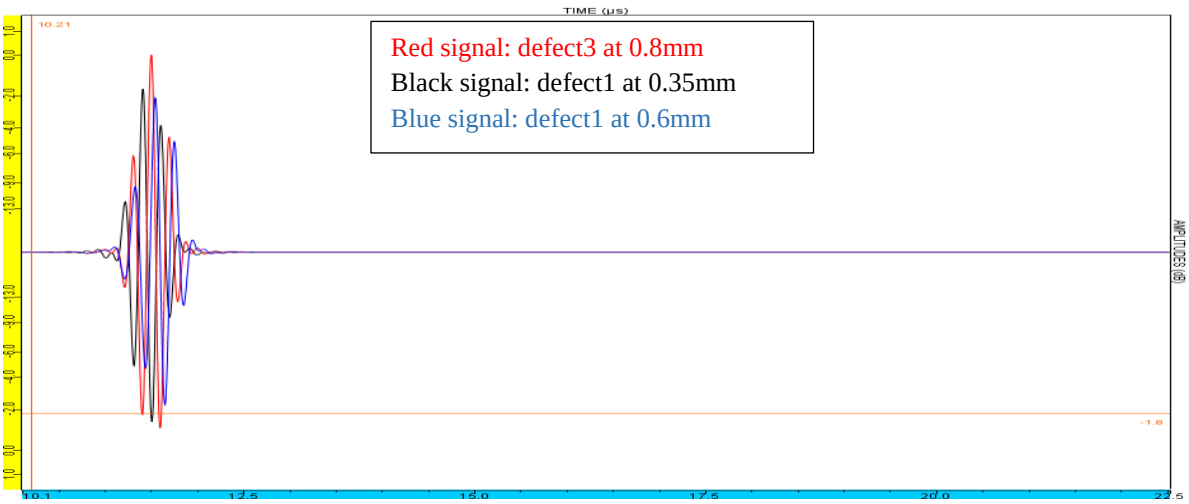

Fig. 5.5. A-Scan image Delamination at 5 MHz.

Figure 5.5 represents the maximum amplitudes of the three defects by using A-scan image. The red signal represents the defect3, and it is located at depth 0.8mm below the surface of theA320-elevator. The maximum amplitude of a defect3 is -2.2dB. However, the amplitude has increased progressively to 0dB in defect 2, and the maximum amplitude for a defect1 is -1.3dB. The causes of the variation of the amplitudes is due to a different factors such as attenuation, energy losses and beam reflections. The bottom and surface reflections are represented by an A-scan image as shown in a figure 5.4, while the first reflection is related to the surface and the second reflection belongs to the bottom side.

5.1.2. Results of Case Study 2 at 10MHz Frequency

For the same type of defects, another experiment was done to detect the delamination at a different depths by using **10MHz** frequency..

The running setup consists of 210 steps and 0.5mm step size, and the inspection is based on 2D simulation. In addition, the results of the amplitudes are demonstrated by an A-scan image, and the position of the defects are presented by a B-scan image as shown in a figure 5.6 and 5.8 respectively.

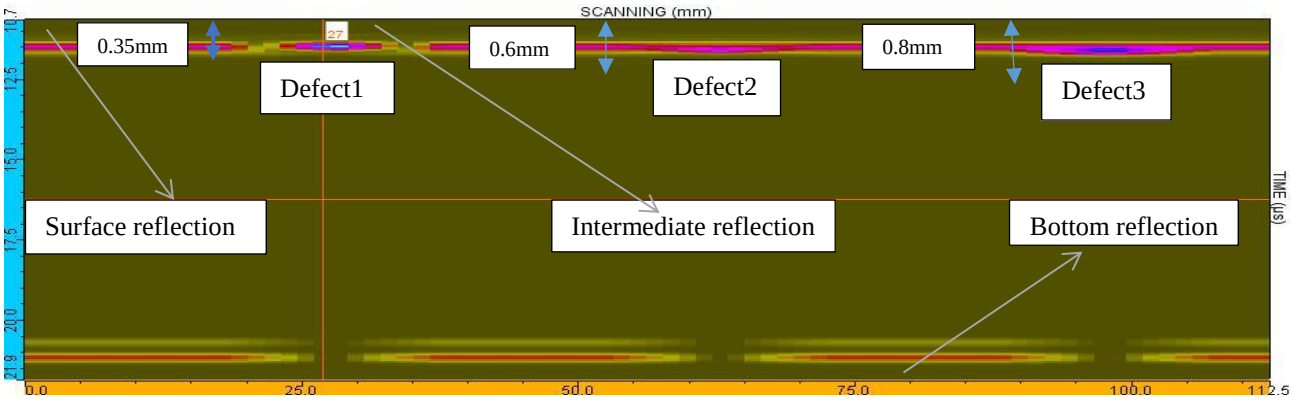

Fig. 5.6. B-Scan of the same size defects at 10 MHz.

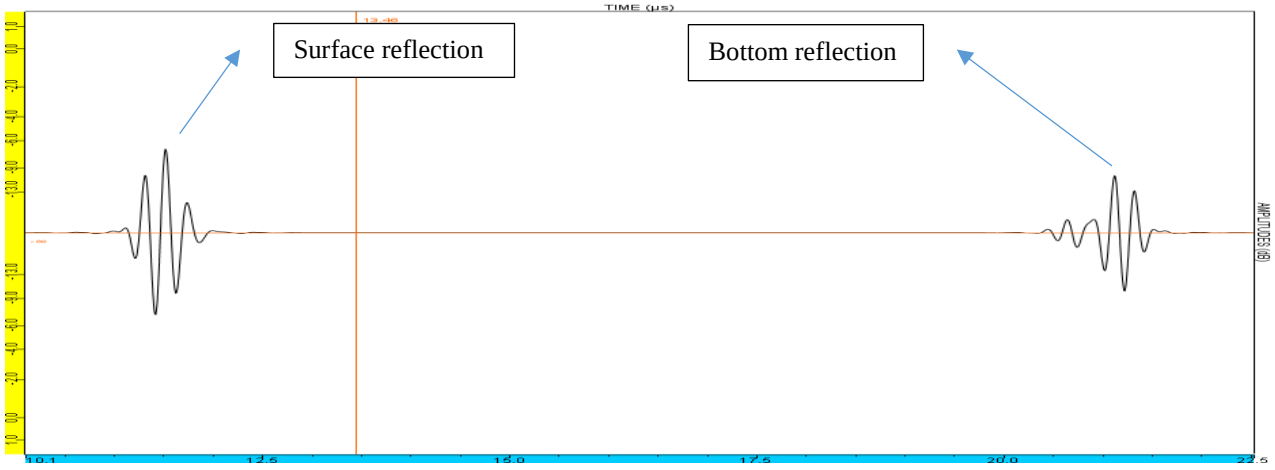

Fig. 5.7. A-Scan at No delamination section.

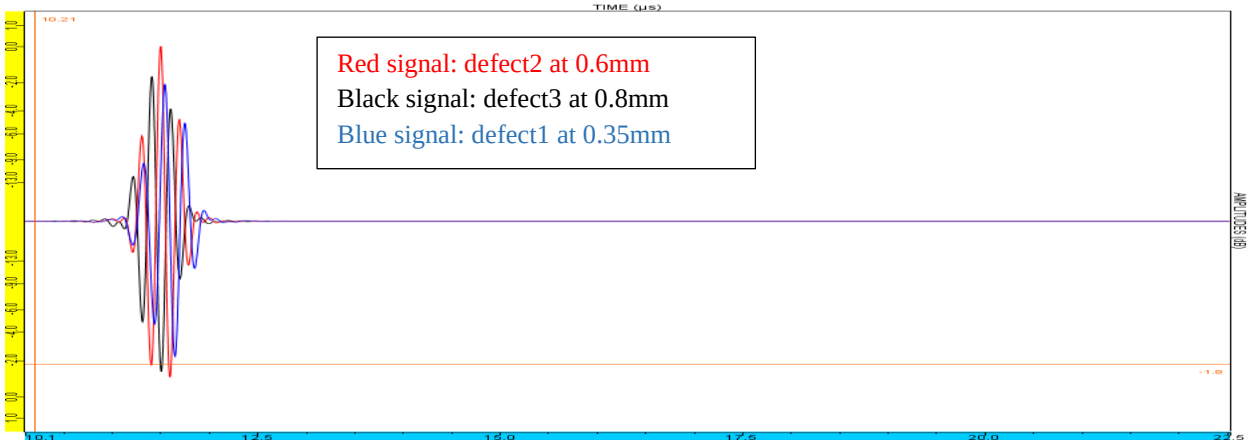

Fig. 5.8. A-Scan image at a10 MHz.

Figure 5.8 represents the comparison of the three different delamination at 10MHz frequency. The red signal represents the maximum amplitude of a defect2 at a depth 0.6mm below the surface, wjere it reached peak amplitude -9.7dB. However, the black signal represents the delamination at 0.8mm depth, and it reached maximum amplitude -8.3dB. The blue signal shows the reflection of the defect1, and its maximum amplitude is -7.3dB as shown in a table 5.1. The maximum amplitudes of the reflecting signals are shown in a figure 5.9.

Table 5.1. Same size defects amplitude.

Frequency / Defects	**0.35 mm depth**	**0.6 mm depth**	**0.8 mm depth**
	Measured Max Amp. (dB)	Measured Max Amp. (dB)	Measured Max Amp. (dB)
5 MHz frequency	-1.3	0	-2.2
10 MHz frequency	-7.3	-9.7	-8.3

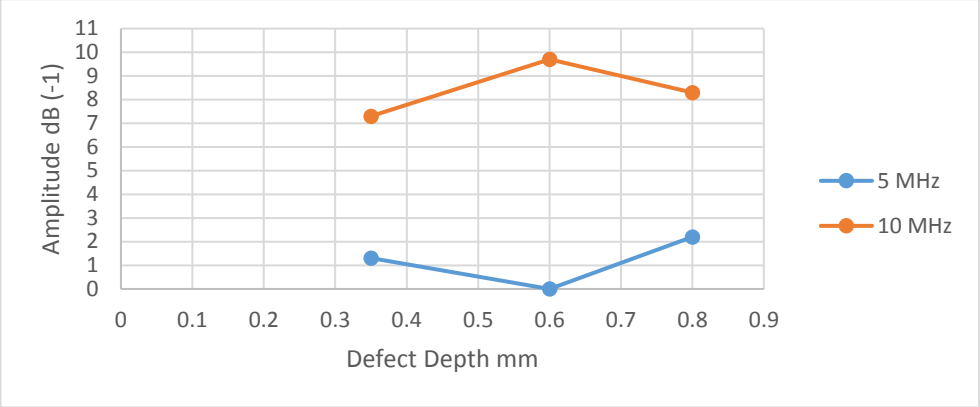

Fig. 5.9. Depth versus amplitude of the same size defects.

5.2. Results of Case Study 3

The following data shows the results of the three different size defects, which they are 5*5mm^2, 20*20mm^2 and 10*10 mm^2 as shown in a chapter 4 of a figure 4.3. The inspection is performed by using single element probe of 5MHz and 10MHz frequencies. Furthermore, the distance between each defects is identical and equals to a 35mm. To obtain realistic and accurate results, the defects are inspected at different depths such as, 0.35mm, 0.6mm (at CFRP) and 0.8mm (between CFRP and honeycomb). Each depth has different ultrasound velocity. For example, the ultrasonic velocity for composite material is a 3070m/s. Case study 3 is divided into three sections as mentioned in the modelling chapter.

5.2.1. Results of Section 1 Using 5MHz and 10MHz Frequencies

The following results correspond to a test is done by using a 5MHz single element probe at a 0.35mm depth. The running setup is 210 steps/0.5mm step size. After almost 15 min of a running progress, B-scan and A-scan images have received as shown in the figures 5.10 and 5.11 respectively.

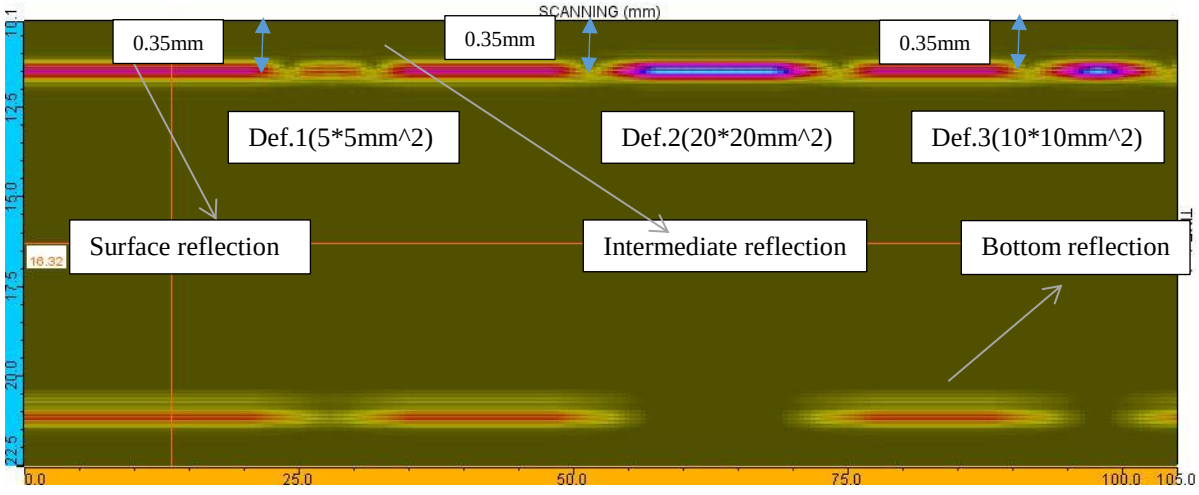

Fig. 5.10. B-Scan at a 0.35mm depth and 5MHz frequency.

Figure 5.10 shows a B-scan image at 0.35mm depth using 5MHz Single Element Transducer, where the sizes of the defects are very clear. However, the color of the intermediate reflections are different due to the variation of the intensity in each defect. The blue color shows high intensity of the defect, while the red color represents low intensity.

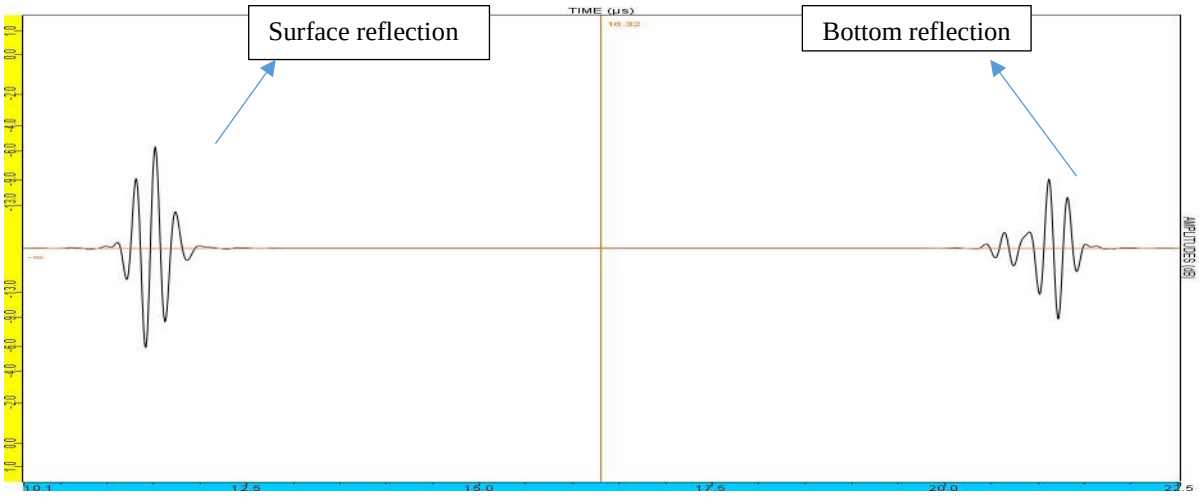

Fig. 5.11. A-Scan image at no delamination.

Figure 5.11 represents A-scan image that it shows two different separated signals, the first signal is related to the reflection of the surface of A-320 elevator, while the second signal to the right represents the bottom.

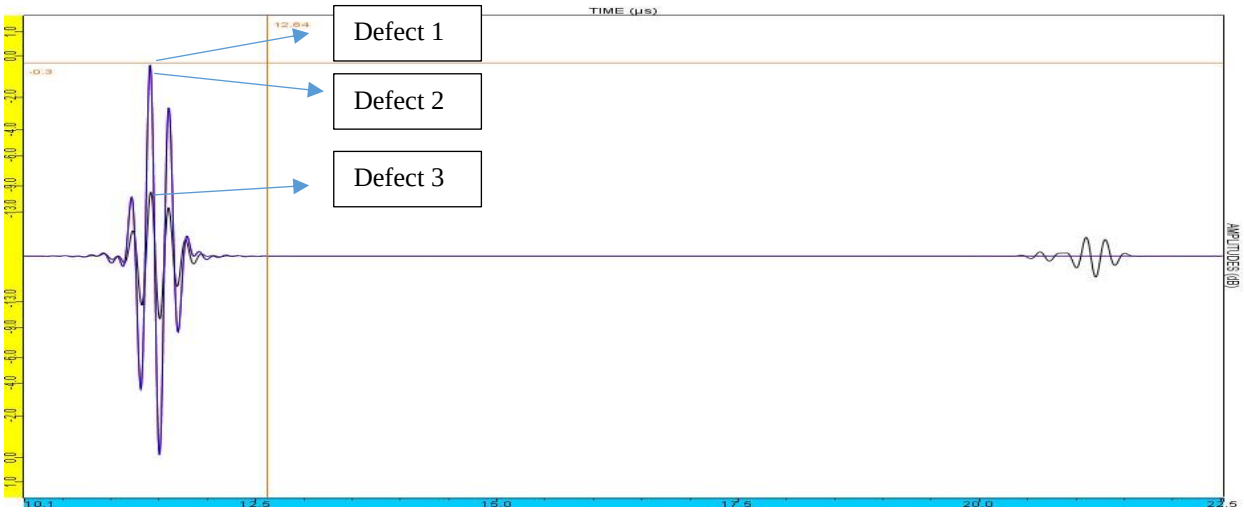

Fig. 5.12. A-Scan image of the three delamination at a 5 MHz frequency.

Figure 5.12 represents the comparison between the three different delamination. the maximum amplitude of a defect1 is -9.3dB. The black signal represents the defect2, which has lowest amplitude 0dB. The amplitude is slightly increased 0.1dB at defect3.

Second test has done for the same defects' conditions, but by using a **10 MHz** frequency. The running setup is 210steps/0.5step size. Figure 5.13 shows B-scan image at 10MHz frequency. However, the resolution of defects is high and very clear. Moreover, B-scan image shows different reflections on the ssurface, bottom and intermediate. A-scan image represents the maximum amplitudes of each defect with different intensity levels.

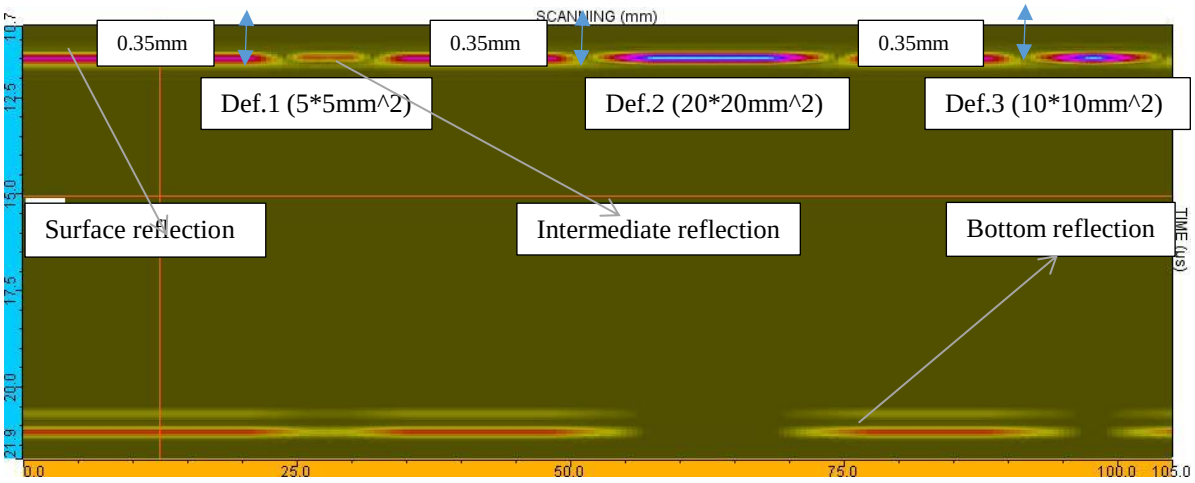

Fig. 5.13. B-Scan image of the different size defects at a 0.35mm and 10 MHz frequency.

Figure 5.14 shows an A-scan image of a two different signals, the first signal is related to the reflection the surface and the second signal represent the reflection of the bottom side.

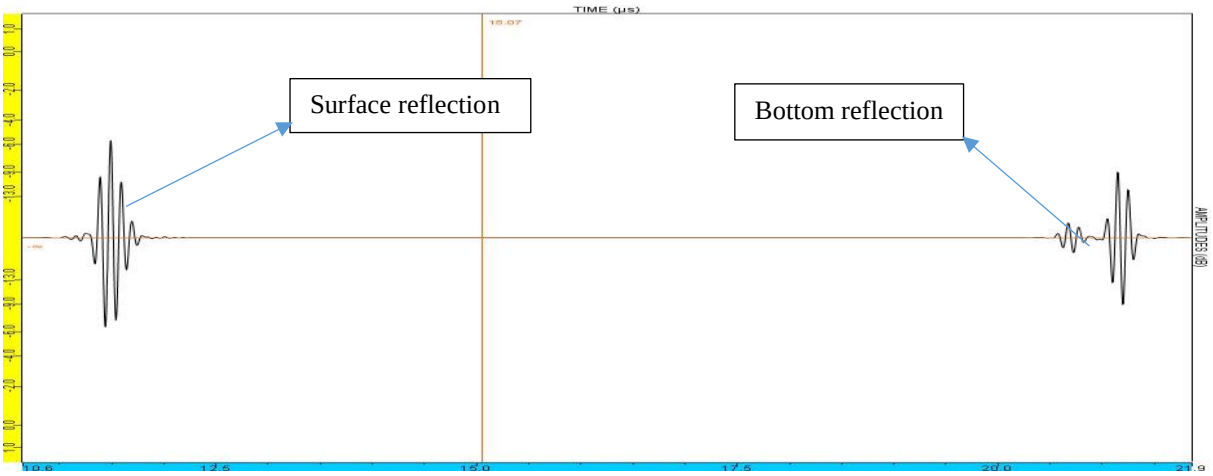

Fig. 5.14. A-Scan image at a no delamination section.

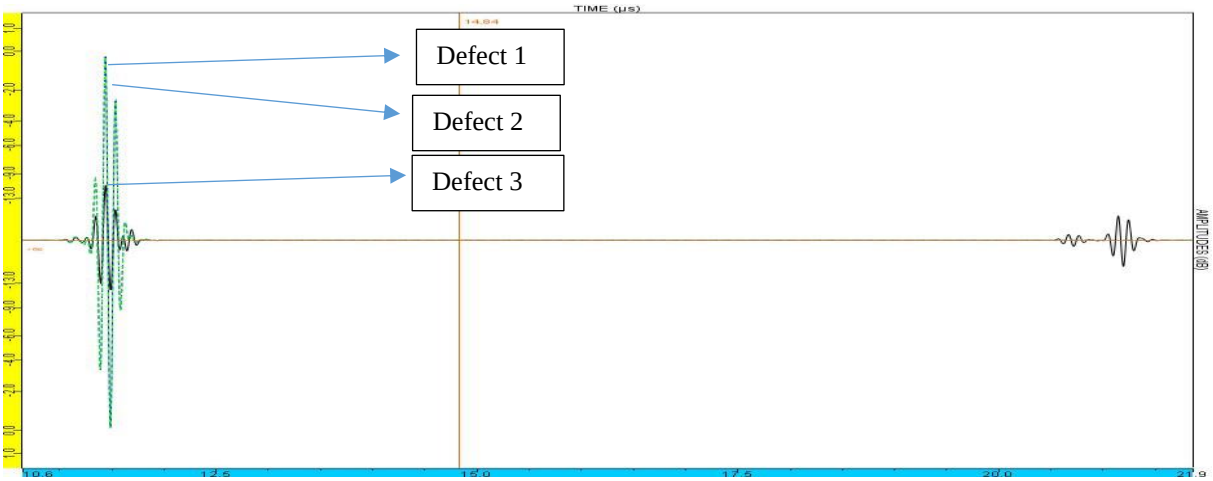

Fig. 5.15. A-Scan image of the delamination at 10 MHz.

Figure 5.15 represents the comparison between the three different size delamination at a 5MHz frequency. The defect1 represents the highest amplitude -9.9dB, then the intensity decreased to -0.8dB at defect2 and -0.2 at defect3 respectively. The reference value is a 16.654 points.

Table 5.2. Different size defects amplitudes at 0.35 mm depth.

Frequency / Defects Size	5*5 mm^2	10*10 mm^2	20*20 mm^2
	Measured Max Amp. (dB)	Measured Max Amp. (dB)	Measured Max Amp. (dB)
5 MHz frequency	-9.3	0	-0.1
10 MHz frequency	-9.9	-0.8	-0.2

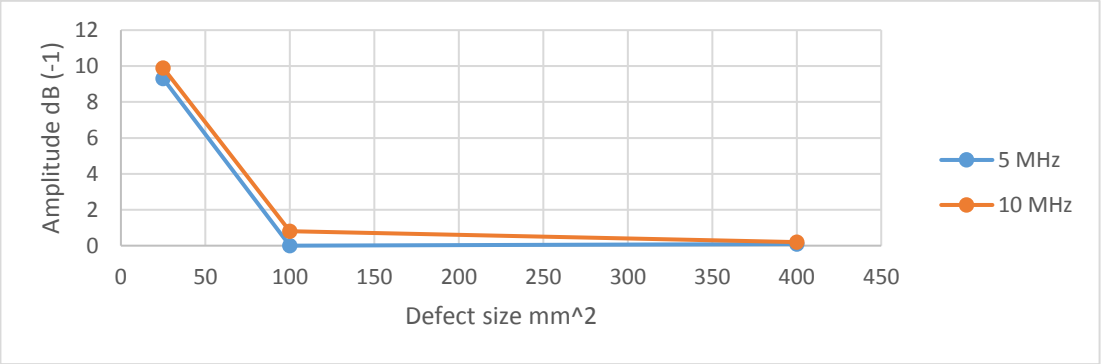

Fig. 5.16. Maximum measured amplitudes of the defects at section1.

5.2.2. Results of Section2 Using 5MHz and 10MHz Frequencies

The following results are obtained at a 0.6mm depth. Similarly, a 5MHz Single Element Probe is used for the first inspection, and 10MHz frequency for the second inspection. The B-scan image shows the position of each defect, and the A-scan image identifies the intensity that is expressed in a dB and. The different size defects are clearly visible as shown in a figure 5.17 and the intensity is presented by dark blue color.

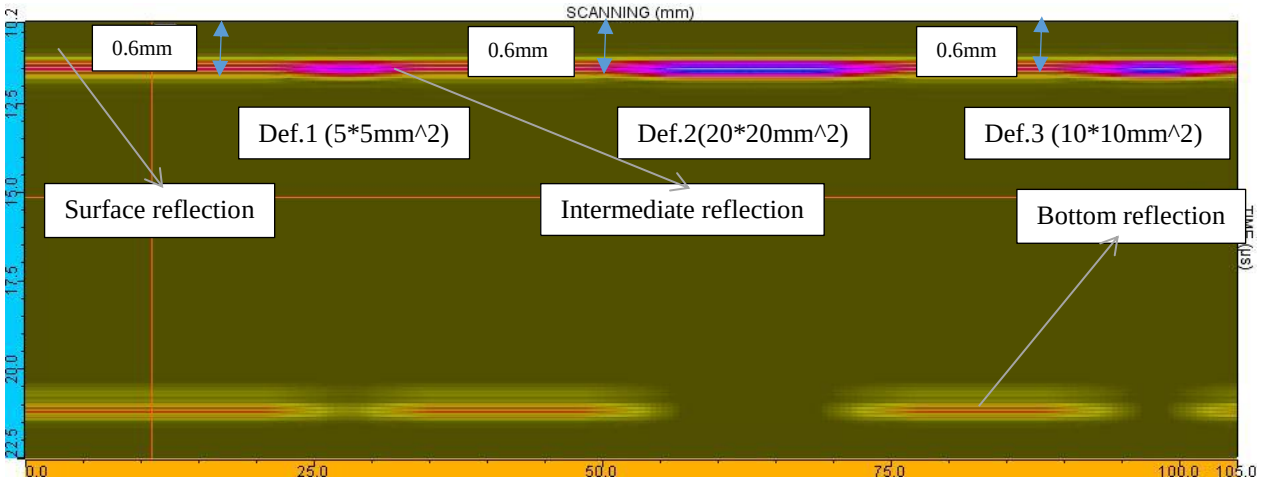

Fig. 5.17. B-Scan Image at 0.6 mm depth and 5 MHz frequency.

Figure 5.18 represents the initial step of the probe at no delamination position. However, there are 2 different separated signals. The left signal is reflected from the upper surface and the second signal is reflected and received from the bottom of the sample.

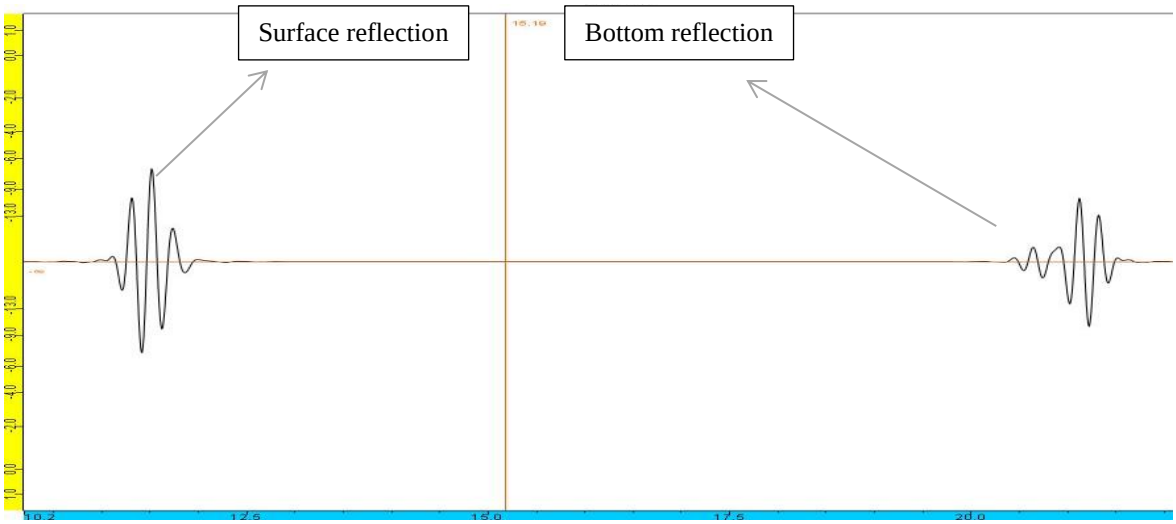

Fig. 5.18. A-Scan image at no delamination step position.

Fig. 5.19. A-Scan image of the three delamination at 10 MHz.

Figure 5.19 represents the comparison of the three different size defects. The maximum amplitudes are shown by different colors. Each color is referred to a specific defect. However, the peak amplitude is correspond to a defect1 where it reached -2.1dB, and the minimum amplitude is related to defect2 where it is reached 0dB. The maximum measured amplitude for defect3 is a -0.2dB as shown in a table 5.3.

Moreover, a second experiment has been done for the same type defects but at frequency **10MHz**, and 10mm diameter of a single element probe. Similarly, the running setup is 210steps/0.5mm step size. Then, different images such as A-scan and B-scan have received as shown in the figure 5.20 and 5.21 respectively.

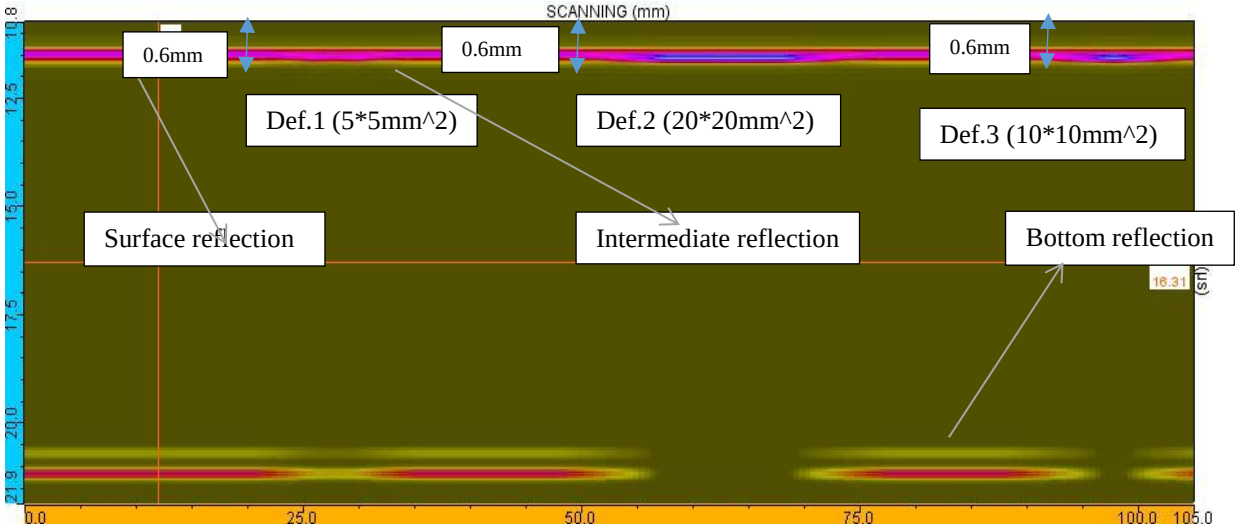

Fig. 5.20. B-Scan image at 0.6 mm depth and 10 MHz frequency.

Fig. 5.21. A-Scan image of three delamination at 10 MHz frequency.

Figure 5.21 represents the comparison between the three different delamination at a **10 MHz** frequency. The reference value is 16.811 points. The reference value is used to calibrate the signals from 10 MHz to 5MHz frequency. However, the maximum reflection at defect1 is a peak amplitude -13.9dB and -9.7dB at a defect2. The largest defect (20*20mm^2) has reached maximum amplitude -9.8dB at 10MHz frequency as shown in a table 5.3.

Table 5.3. Amplitudes of different size defects at a section2

Frequency / Defects Size	**5*5 mm^2**	**10*10 mm^2**	**20*20 mm^2**
	Measured Max Amp. (dB)	Measured Max Amp. (dB)	Measured Max Amp. (dB)
5 MHz frequency	-2.1	0	-0.2
10 MHz frequency	-13.9	-9.7	-9.8

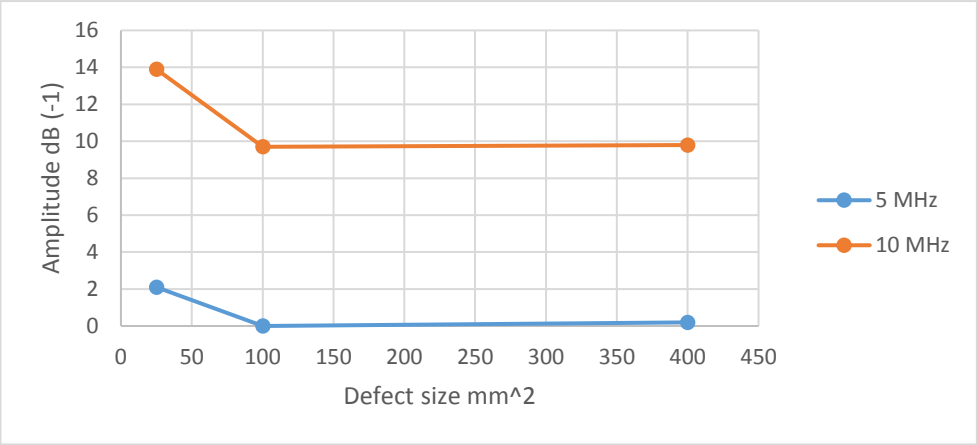

Fig. 5.22. Maximum amplitudes of different size defects at a section 2.

5.2.3. Results of Section3 Using 5MHz and 10MHz Frequencies

The results of section3 represents the defects of the different sizes at a 0.8mm depth. The inspection is performed by using 5MHz and 10MHz single element transducer of a 10mm diameter. After running the simulation, A-scan and B-scan images have been received as shown in a figure 5.23 and 5.24.

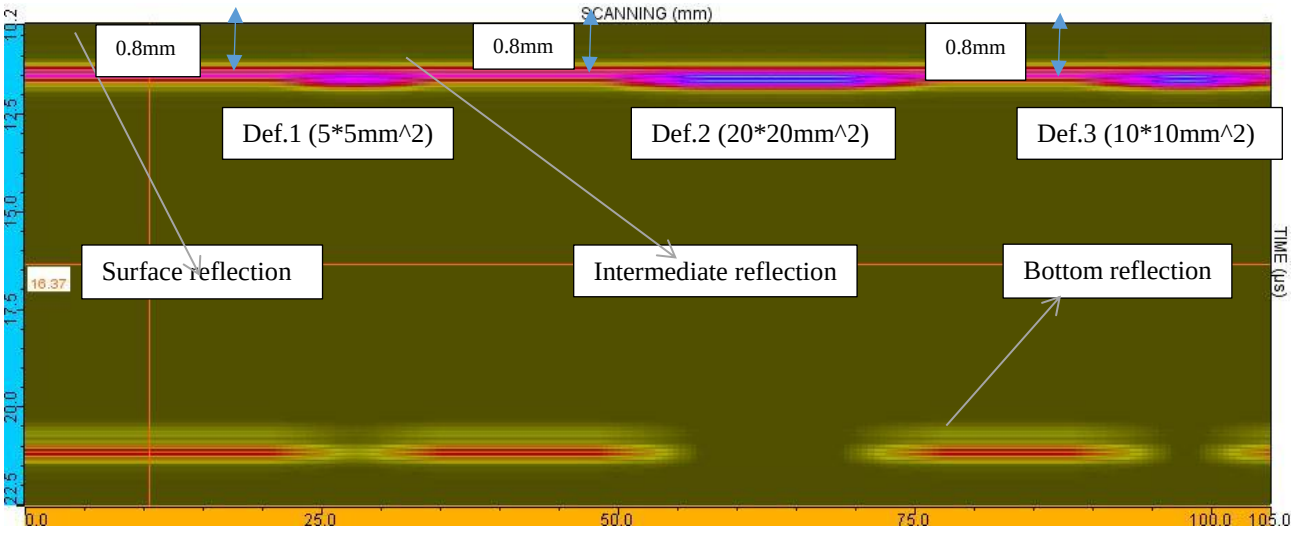

Fig. 5.23. B-Scan image of the three defects at a 5MHz and 0.8 mm depth.

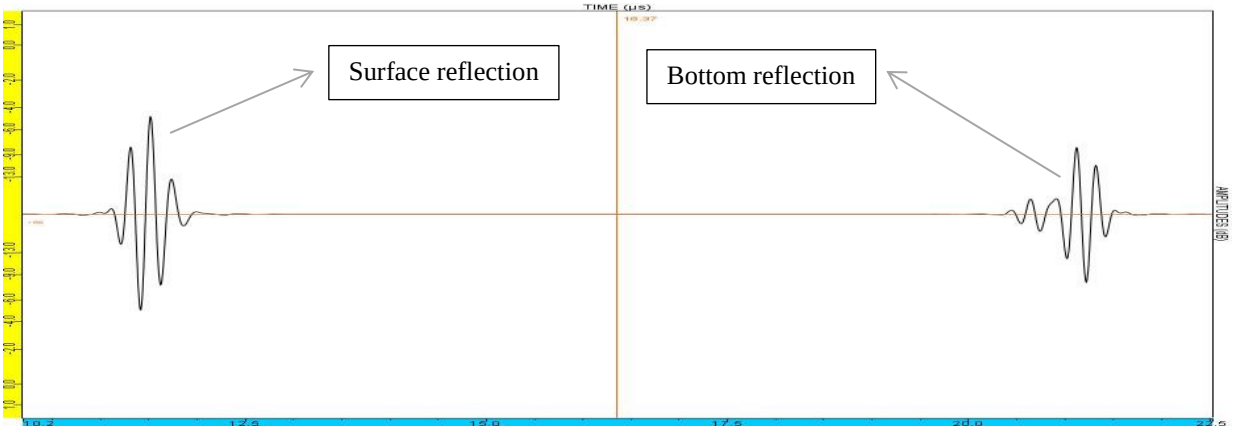

Fig. 5.24. A-Scan image at no delamination step position.

Figure 5.24 represents the initial step of the probe at no delamination position. However, there are 2 different separated signals, where the left signal is reflected from the upper surface and the second signal is reflected and received from the bottom of the sample.

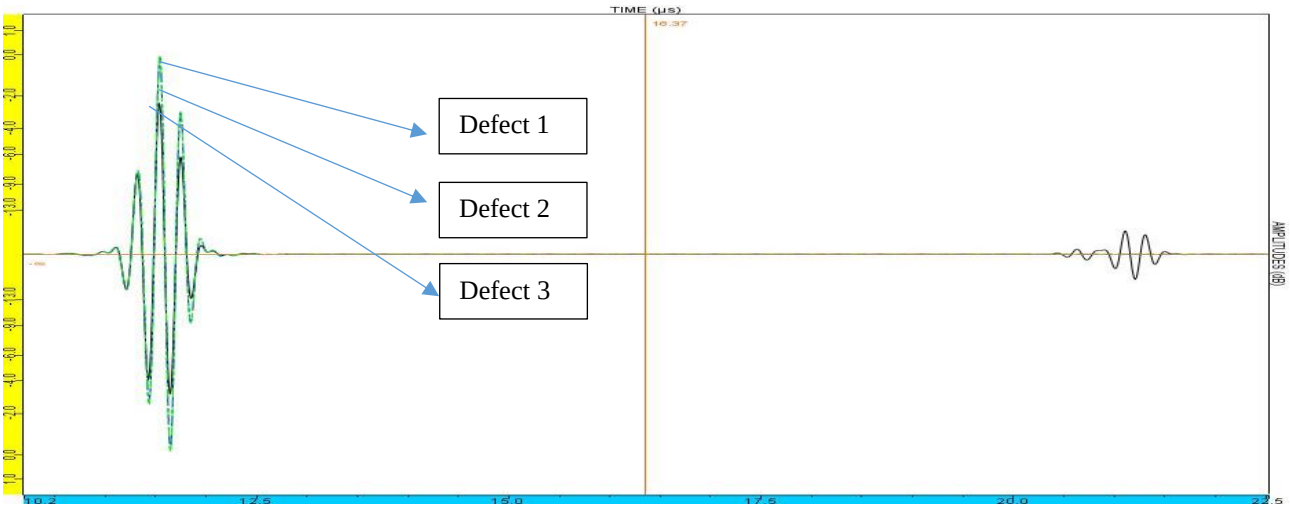

Fig. 5.25. A-Scan image of the three delamination at 5 MHz frequency.

Figure 5.25 represents the variation of the amplitudes at a 0.8mm depth. The maximum amplitude reached by defect1 is -2.4dB at a 0.35mm below the surface. The amplitude at a defect2 has increased significantly to 0dB, while the amplitude at defect3 of a size 3*3mm^2 is -0.2dB.

Moreover, another experiment was done for the same defects conditions but at **10MHz** frequency. However, there is an inverse proportional relation between the frequency and the wavelength. The running setup is a 210 steps/0.5mm step size, and the simulation is a 2D. Similarly, same images have been received such as A-scan and B-scan images that represent the defects' amplitude/intensity and position respectively. Figure 5.26 shows a B-scan image of the different size defects, and figure 5.27 represents the A-scan image.

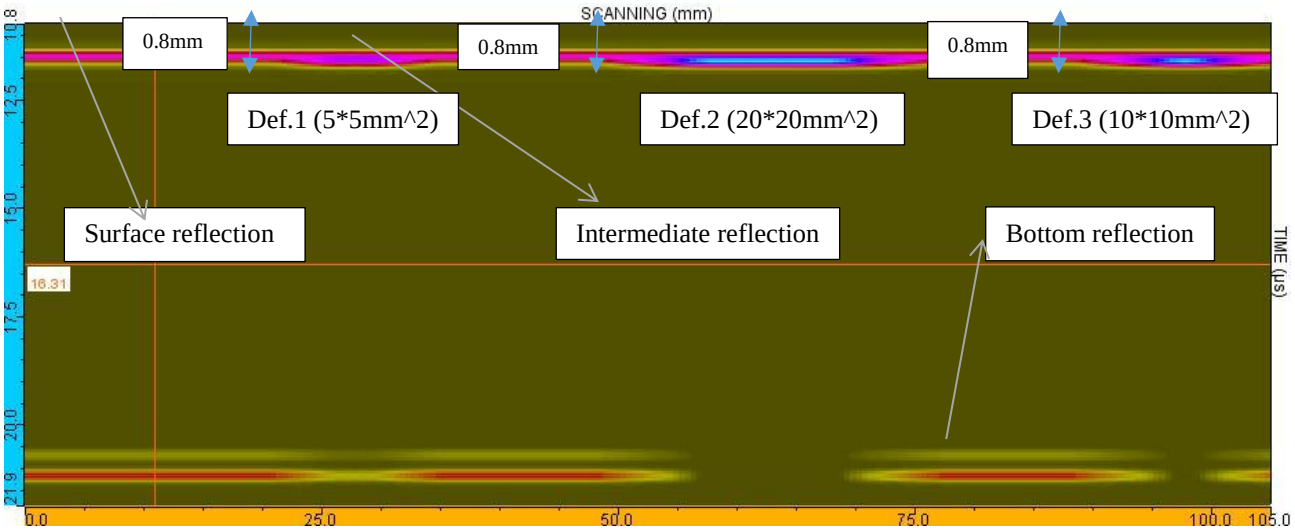

Fig. 5.26. B-Scan image at 0.8 mm depth and 10 MHz.

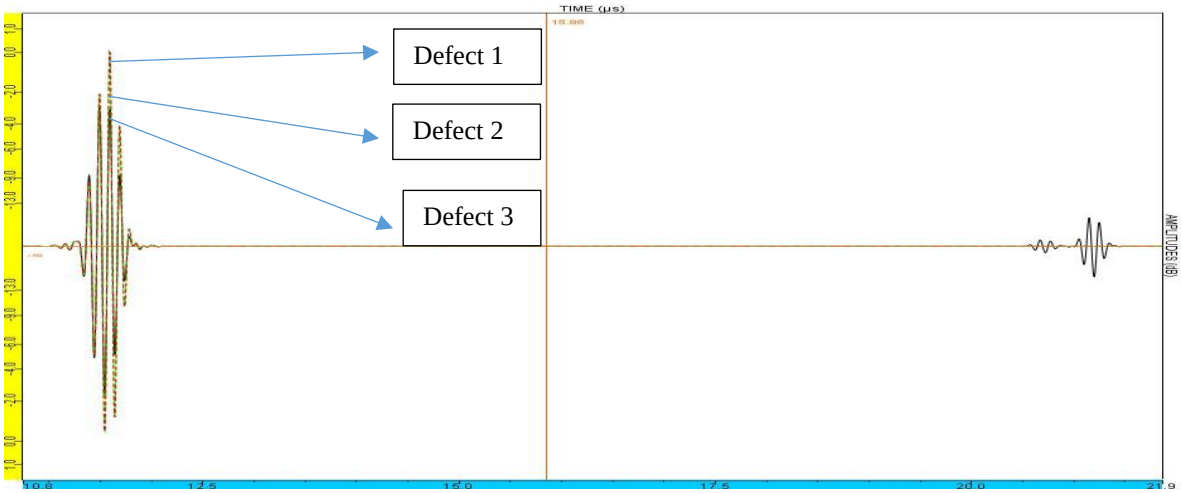

Fig. 5.27. A-Scan of the three different size defects.

At 10MHz frequency the intensity has significantly increase as shown in a figure 5.27. However, the amplitude at defect1 became -8.3dB at a 10MHz frequency instead of -2.4dB at 5MHz. The intensities at defect2 and defect3 have reached -6dB maximum amplitude. The lower amplitudes at 10MHz frequency shows that the resolution and accuracy have significantly increased. Table 5.4 shows the variation of the amplitudes as a function of defects size.

Table 5.4. Different size defects amplitudes at 0.8 mm depth.

Frequency / Defect's Size	**5*5 mm^2**	**10*10 mm^2**	**20*20 mm^2**
	Measured Max Amp. (dB)	Measured Max Amp. (dB)	Measured Max Amp. (dB)
5 MHz frequency	-2.4	0	-0.1
10 MHz frequency	-8.3	-6	-6

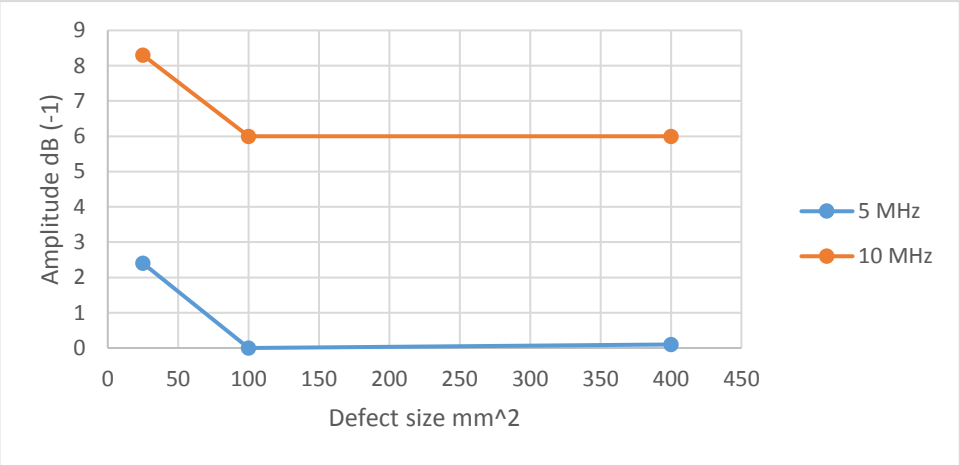

Fig. 5.28. 5 and 10 MHz inspections of different size defects at 0.8 mm depth.

5.2.4. Conclusion

In a case study1, the parallel defects to the surface/delamination is significantly detected by using 5MHz single element transducer. The amplitude has increased sharply to almost 0dB at the vertical defects, which shows a high attenuation and week reflecting signals at a vertical defect . For case study2, the maximum amplitude has reached at defect3 is a -9.7dB at 10MHz frequency. On the other hand, the intensity for a defect2 is sharply increased to 0dB at 5MHz frequency, which it shows less intensity. Moreover, the maximum amplitudes of the different size defects at a study case3 shows that the small defects such as 5*5mm^2 is significantly detected by using 10Mhz single element transducer. The maximum measured intensity is -9.9dB.

6 Modelling Results By Using PA Transducer - Single Point Focusing

The results of the tests by using Phased Array transducer will be divided into different subchapters as it is shown below. However, each subchapter is regarding to a specific frequency and different defect depth. Moreover, two different transducers are used such as 5L128-128X7-NW3 (5MHz) and 10L128-64X7-NW1 (10MHz). The results will be shown according to the Single Point Focusing type. Furthermore, the results of the different size defects will be presented in a three sections. Section1 is related to the results of the different size defects' inspection at a 0.35mm depth. Section2 shows the defects at a 0.6mm below the surface. Eventually, Section3 represents the different size defects at a 0.8mm depth.

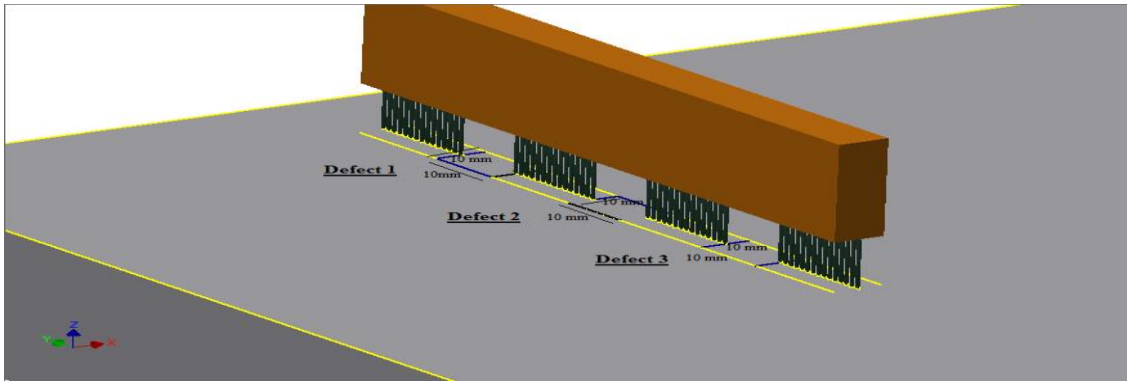

Fig. 6.1. Inspection by using Phased Array transducer.

6.1. Results of Case Study2 Using PA Transducer

This test shows the variation of the intensities relating to the same size defects at different depths. The focusing type for this test is a Single Point Focusing. The defects are equidistant at a 35mm each, and identical of a 10*10mm^2 as shown in a figure 6.1. However, two types of transducers have been used such as 5L128-128X7-NW3 and 10L128-64X7-NW1. The frequencies are 5MHz and 10MHz

6.1.1. Results of Case Study2 by Using 5L128-128X7-NW3 PA (5MHz)

The first results are correspond to 5MHz frequency and 5MHz PA transducer. The PA transducer consists of 128 elements and 8 sequencing elements. However, the running setup is 210 steps/0.5mm step size, and the simulation is based on 2D inspection. Moreover, a different A-scan and B-scan images have been obtained at the end of the simulation as shown in the figures 6.2 and 6.3.

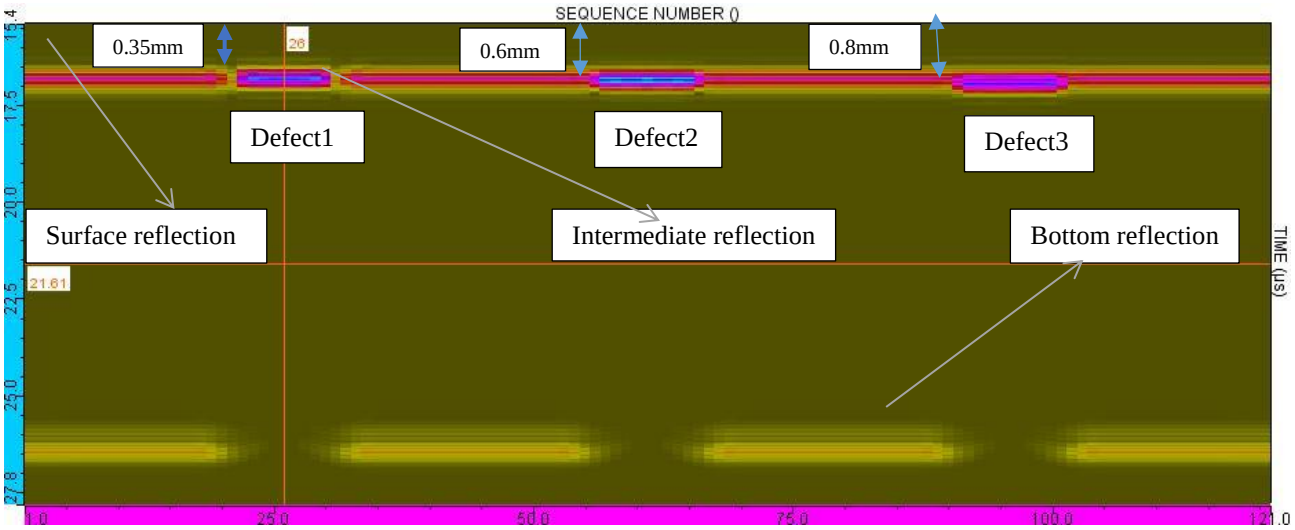

Fig. 6.2. B-scan image of study case 2 at 5MHz frequency.

Figure 6.2 shows a B-scan image of same size defects. However, this image shows a different reflections such as surface, intermediate and bottom reflections. Moreover, the resolution of the defects is very high, and the depth of each defect is very clear as well.

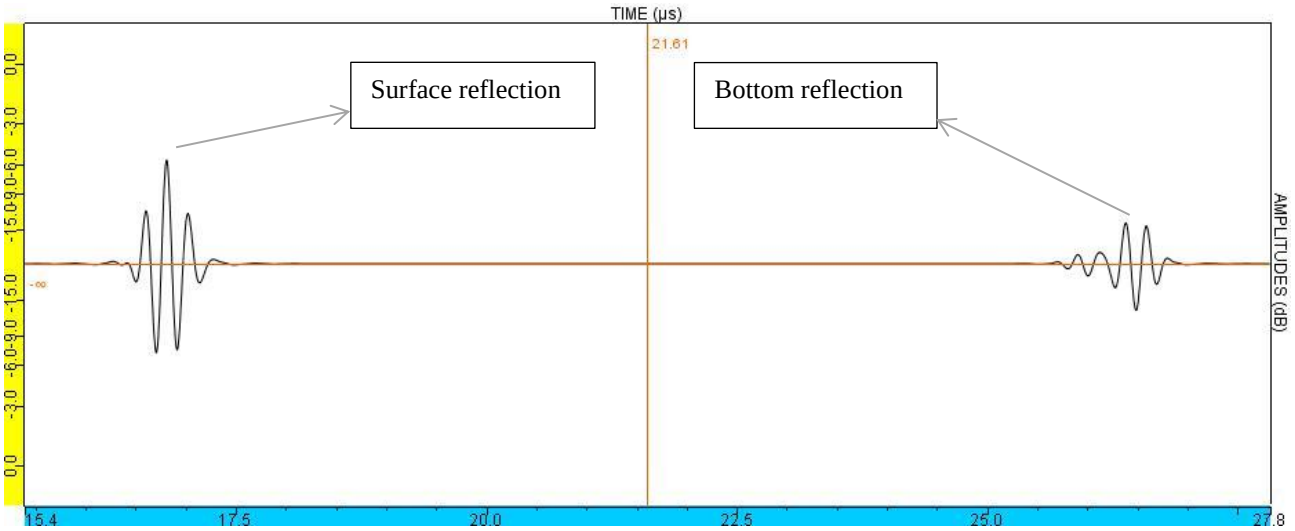

Fig. 6.3. A-scan image at no delamination position.

The difference between the amplitudes of the surface and bottom are is due to the attenuation and energy losses between the layers of A-320 elevator as shown in a figure 6.3

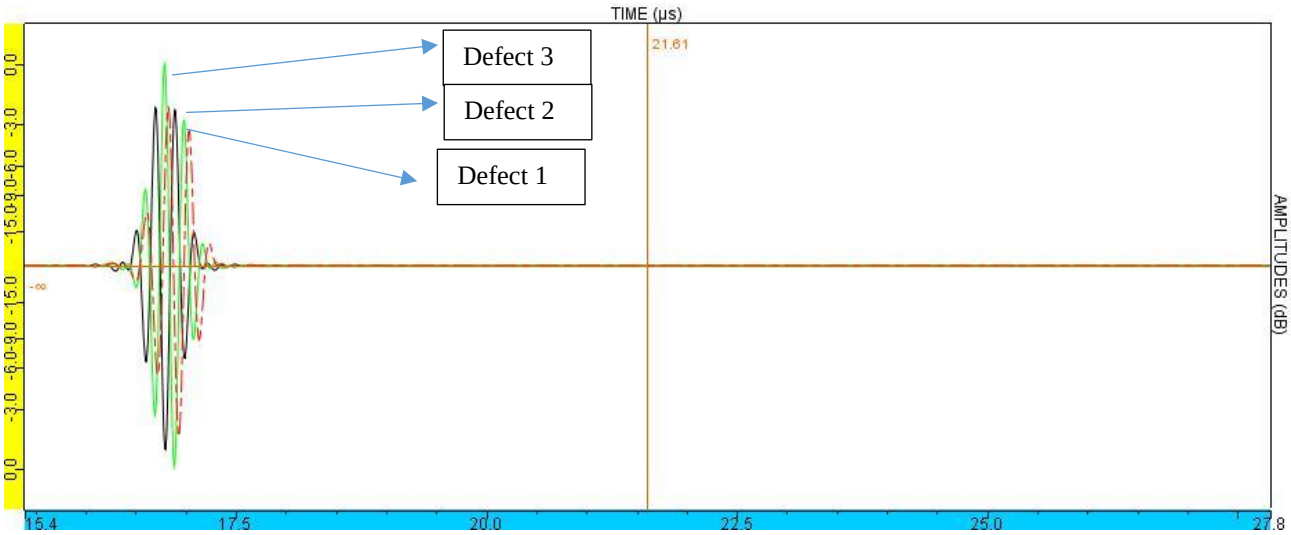

Fig. 6.4. A-scan image of the maximum amplitudes.

Figure 6.4 shows the maximum amplitude of the defects. The intensity of the defect3 has reached the highest amplitude -1dB at a 0.8mm depth. On the other hand, defect2 shows high 0dB at a 0.6mm depth. The maximum amplitude of defect1 is -0.6dB.

6.1.2. Results of Case Study2 by Using 10L128-64X7-NW1 PA (10MHz)

Similarly, the inspection of the same size defects is performed by using a 10MHz phased array transducer. However, the intensity has increased significantly by using a 10MHz PA transducer. The results are represented by B-scan and A-scan images as shown below.

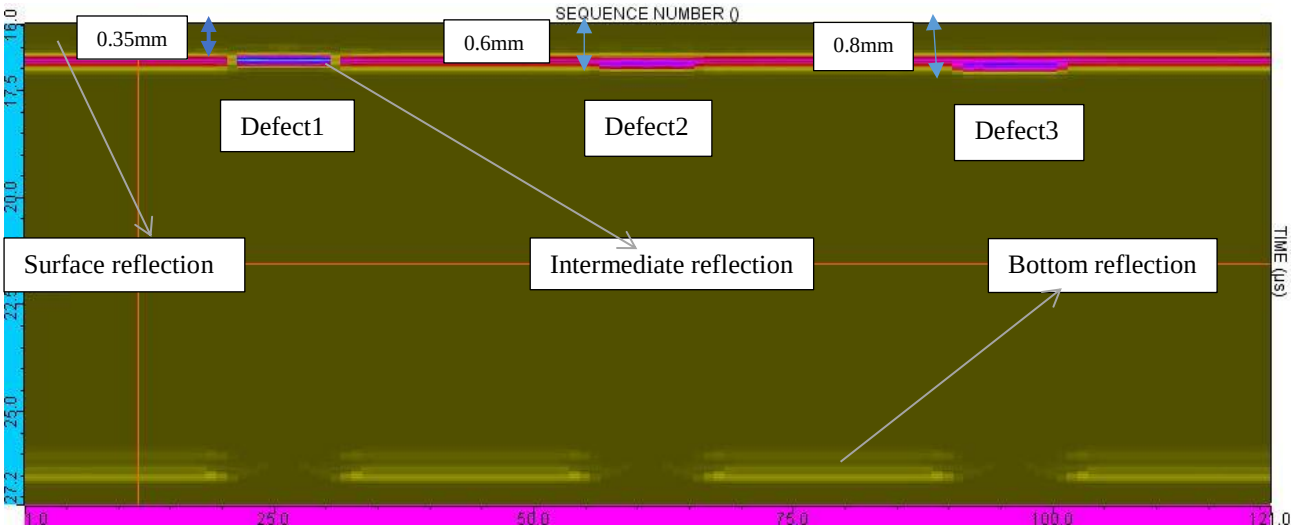

Fig. 6.5. B-scan image of A 10MHz PA transducer.

Figure 6.5 shows the B-scan image of case study2 at a 10MHz, where various deflections are shown such as surface, intermediate and bottom reflections. As the intensity increase, the resolution and accuracy of the defects increase as well. The maximum amplitudes of the defects are shown in a figure 6.6.

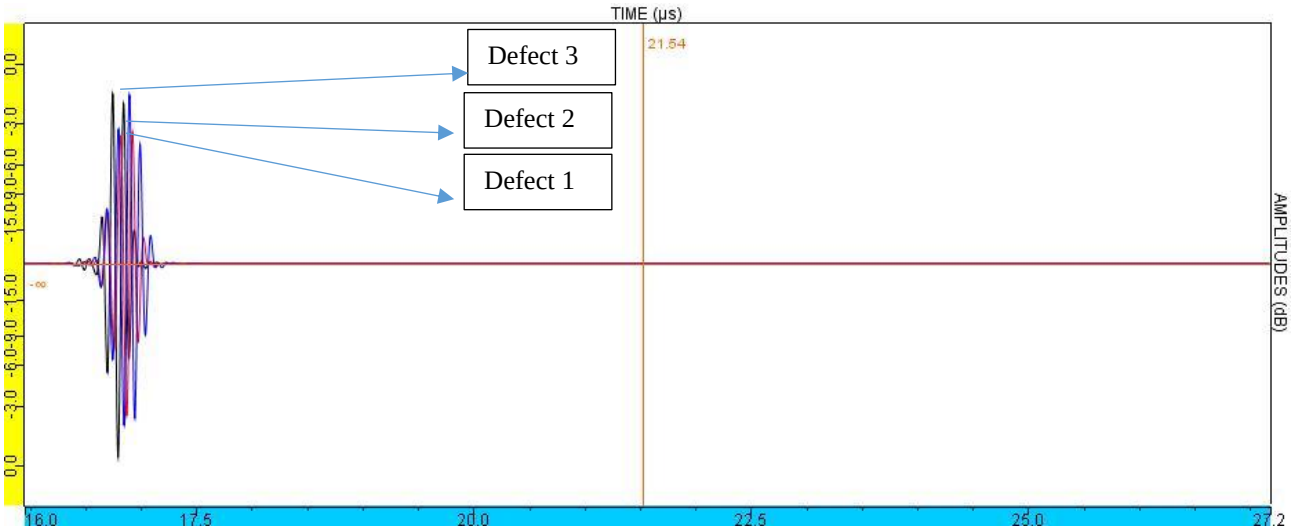

Fig. 6.6. A-scan image at a 10MHz frequency

Figure 6.6 represents the comparison of the same size defects at a 10MHz frequency, and at a different. However, the black signal shows the highest amplitude -10.2dB due to the reflection of delamination at 0.6mm from the upper surface. The highest measured amplitude is -8.2dB at a 0.35mm below the surface. The maximum amplitude at a 0.6mm depth is -9.6 and it is shown in blue color. The reference value is 16.654 points.

Table 6.1. Maximum amplitudes of the same size defects.

Frequency / Defect's Size	**0.35 mm depth**	**0.6 mm depth**	**0.8 mm depth**
	Measured Max Amp. (dB)	Measured Max Amp. (dB)	Measured Max Amp. (dB)
5 MHz frequency	-0.6	0	-1
10 MHz frequency	-8.1	-10.2	-9.6

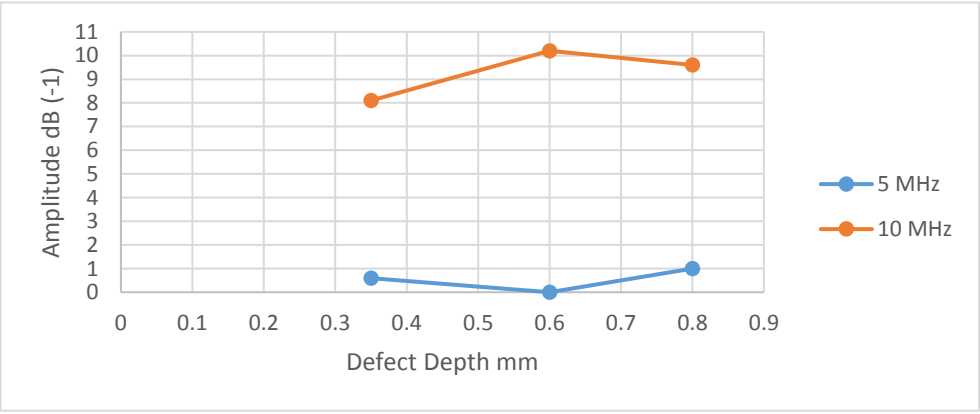

Fig. 6.7. Variation of the maximum amplitudes as a function of the defect's depth.

The maximum amplitudes has increased significantly at a 10MHz frequency as shown in a figure6.7. However, defect2 has reached the highest amplitude -10.2dB at a 10MHz frequency, and it sharply

increased to 0dB at a 5MHz frequency. The maximum measured amplitude of a defect3 is -1dB at a 5MHz frequency.

6.2. Results of Case Study3 by Using 5L128-128X7-NW3 PA (5MHz)

Case study3 is correspond to the different size defects. The inspection is performed by using 5L128-128X7-NW3 PA transducer. The aim of this task is to find the amplitudes of different size defects, then compare their intensities. The running simulation was at a 210 steps and 0.5mm step size, while the simulation setup is 2D. Similarly, this experiment consists of three sections, where each section corresponds to a specific depth. For example, Section1 is related to the different size defects at a 0.35mm depth, Section2 is related to the different size defects at a 0.6mm depth, and Section3 represents the defects at a 0.8mm depth.

6.2.1. Results of section1 - 5MHz

To find the influence of the ultrasound wave velocity of each material, different size defects are positioned at a different depths. However, in a section1, all the defects are located at a 0.35mm depth. The results are demonstrated by A-scan and B-scan images. This test is performed by using 5MHz PA transducer.

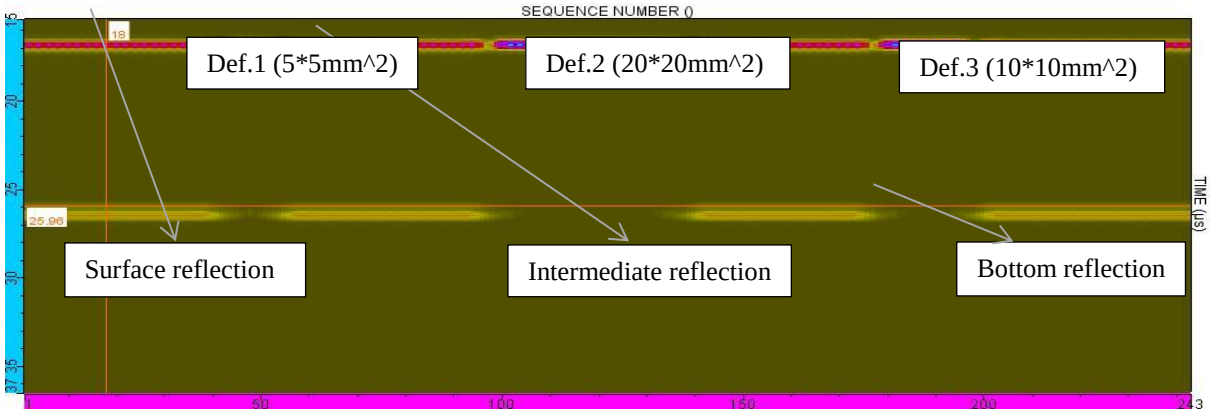

Fig. 6.8. B-Scan image of different size defects at 5MHz frequency.

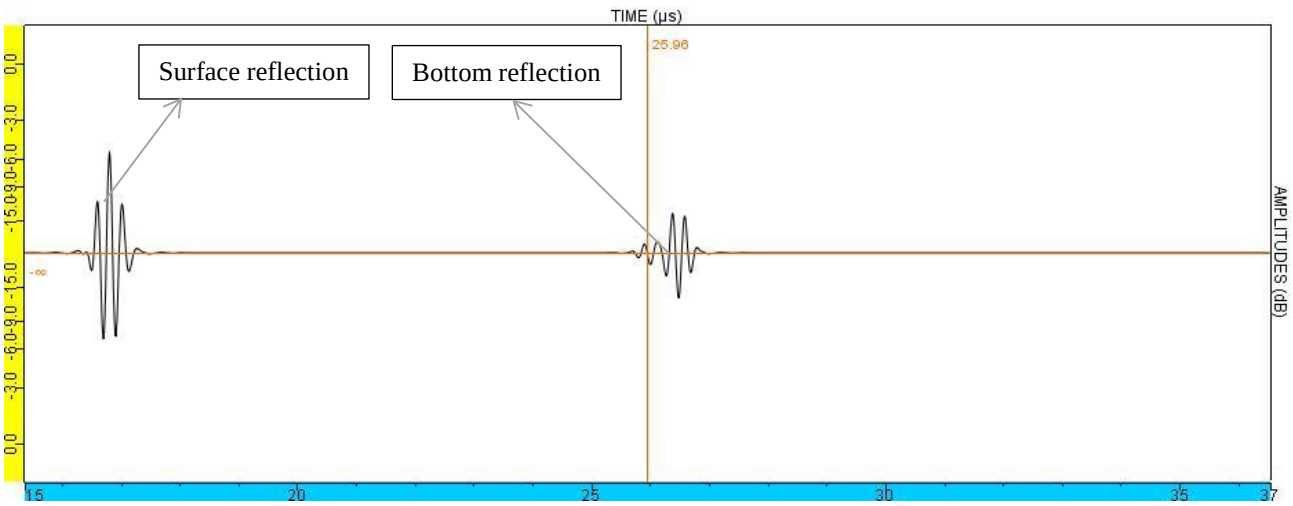

Fig. 6.9. A-Scan at no delamination of 5MHz frequency.

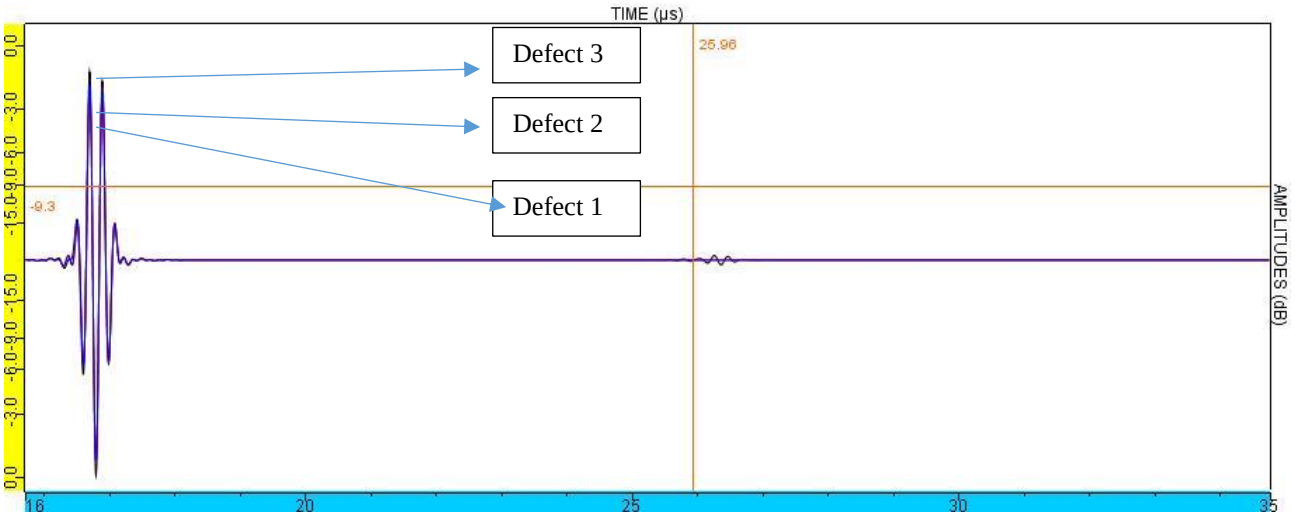

Fig. 6.10. Maximum amplitudes of the different size defects at 5MHz frequency.

Figure 6.28 represents the maximum amplitudes of the different size defects at a height 0.35mm from the surfside. The highest amplitude is a -0.4dB at the defect2 and defect3. The maximum amplitude is slightly increased to 0dB at a defect1, where the intensity is decreased.

6.2.2. Results of section2 – 5MHz

In the following section, all the defects are aligned at the same height, which it is a 0.6mm from the surface. However, the PA focusing type is a single point focusing and 5MHz PA transducer. The results are obtained by A-scan and B-scan images. A-scan image represents the intensity of the defects and B-scan represent the position of each defect as shown in the figures below.

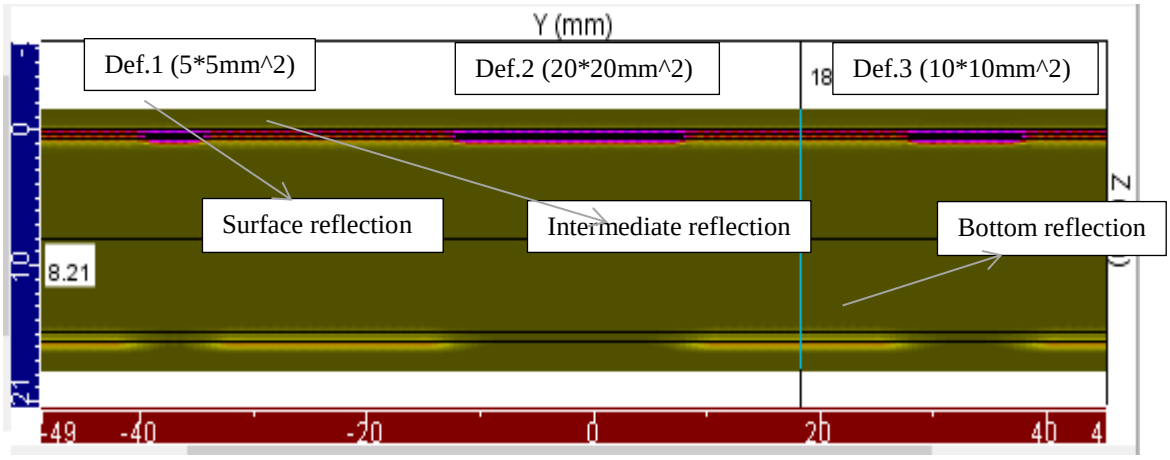

Fig. 6.11. B-scan image of different size defects at a 0.6mm depth.

Figure 6.11 shows a B-scan image with different reflections. The reflections are surface, bottom and intermediate. However, the amplitude are varied due to the ultrasound-wave velocity, attenuation and energy losses. Similarly, these results are obtained by using 5MHz PA transducer. Moreover, the depth of the all defects is a 0.6mm, which it is aligned at CFRP layer.

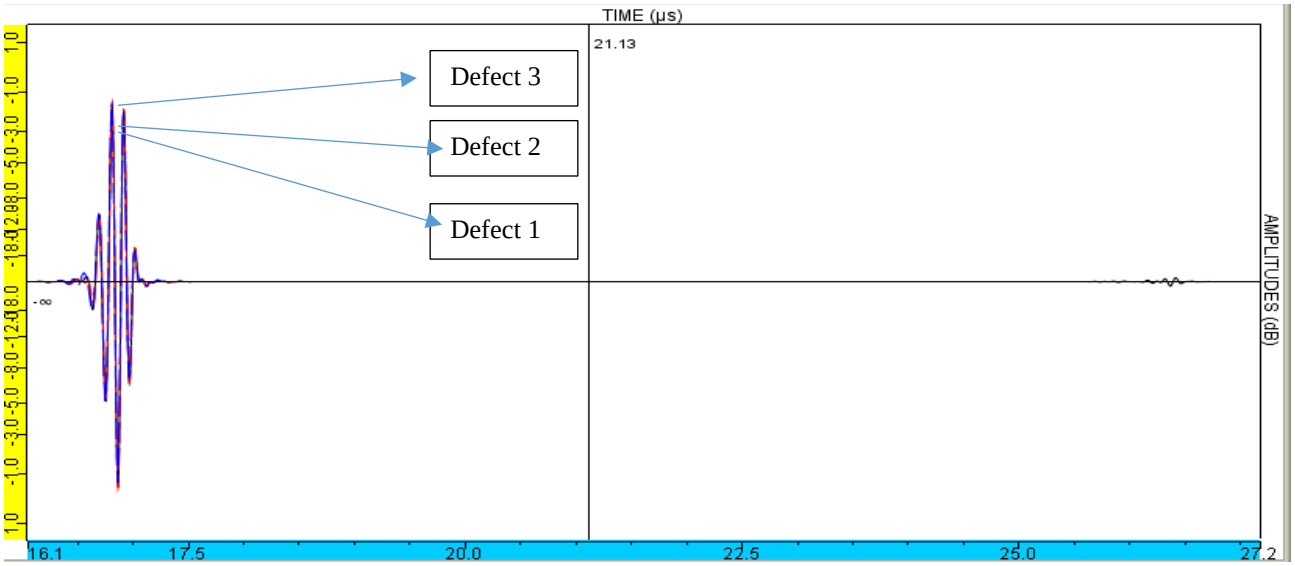

Fig. 6.12. A-scan image of the different size defects at a 0.6mm depth.

Figure 6.12 represents the maximum amplitudes of the different size defects at 0.6mm depth. However, the maximum intensity is a -1.6dB at a defect3 and -0.2dB at defect2. The maximum measured amplitude at the small size defect (5*5mm^2) is a -0.4Db. Moreover, the variation of the intensities is due to the wavelength for each layer because the A-320 elevator is a heterogeneous material.

6.2.3. Results of section3 – 5MHz

In a section3 all the defects are placed at a 0.8mm depth. However, the frequency is a 5MHz, and the focusing type is Single Point Focusing. The results are represented by B-scan and A-scan images as shown in the figures 6.13 and 6.14 respectively. Moreover, the run setup is consist of a 210 steps and 0.5mm step size.

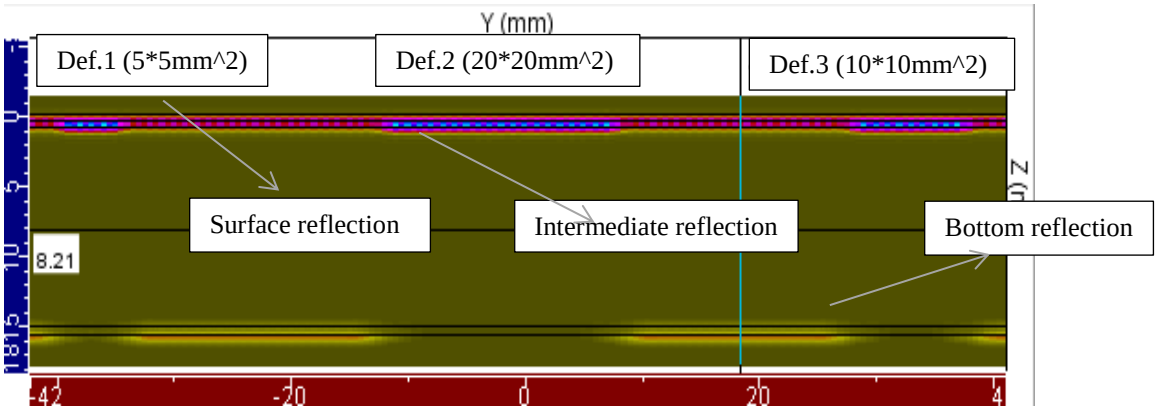

Fig. 6.13. B-scan image of the different size defects at a 0.8mm depth.

Figure 6.13 represents a B-scan image. The defects are aligned below the surface, and they are represented by blue color. However, all the defects are positioned at a 0.8mm depth. The spaces between the defects are equidistant of a 35mm. Moreover, the frequency of the given transducer is a 5MHz.

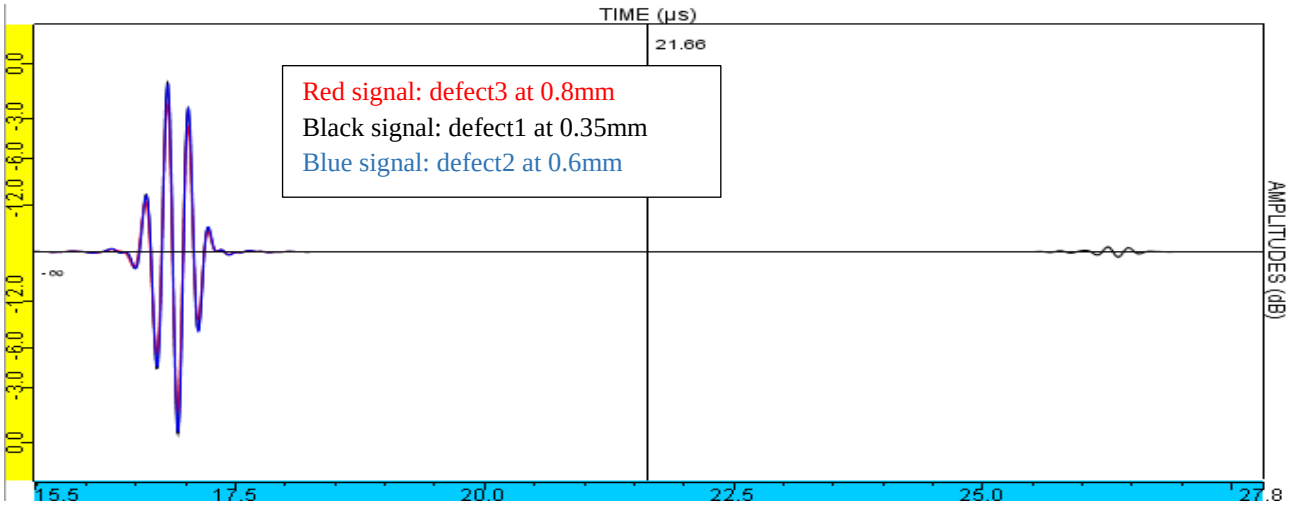

Fig. 6.14. A-scan image by using a 5MHz frequency PA at 0.8mm depth.

Figure 6.14 represents A-scan image of the different size defects at a 0.8mm depth. The defect2 has reached maximum amplitude -0.4dB, and it is increased to 0dB at a defect1. However, defect3 has reach peak amplitude of a -0.3dB. The variation of the amplitudes is due to the different size of the defects.

6.3. Results of Case Study3 by Using 10L128-64X7-NW1 PA (10MHz)

This test is performed by using a 10MHz PA transducer. Similarly, the inspection is consist of three sections, and each section represents a specific depth. However, the aim of this experiment is to determine the influence of the 10MHz frequency on each defect. There is an inverse proportional relation between the wavelength and the frequency. Moreover, the resolution and accuracy has increased at 10MHz frequency. The focusing type of the inspection is Single Point Focusing.

6.3.1. Results of Section1 – 10MHz

Section1 is related to the defects at a 0.35mm depth below the surface, and the inspection is performed by using a 10MHz PA transducer. There are 128 elements, and the width of each element is 1mm. However, the running setup consists of a 210 steps/0.5mm step size. The obtained results are represented by a B-scan and an A-scan image.

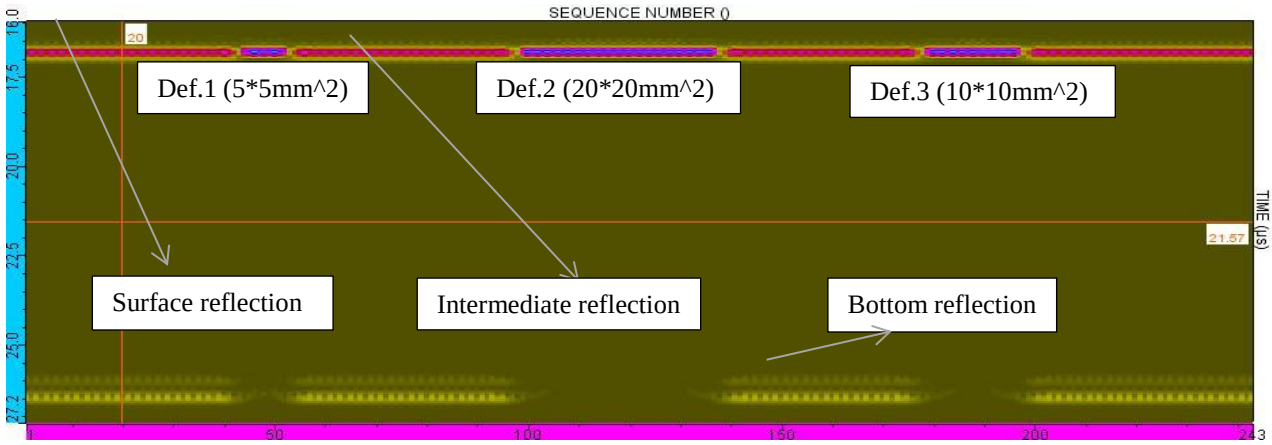

Fig. 6.15. B-scan image by using 10MHz PA transducer at a 0.35mm depth.

Figure 6.15 shows a B-scan image of 10MHz transducer. The resolution and accuracy of the defect1, defect2 and defect3 are significantly increased. Moreover, different reflections have received, such as surface, intermediate and bottom reflections. However, the defects are very clear and they are represented in blue color.

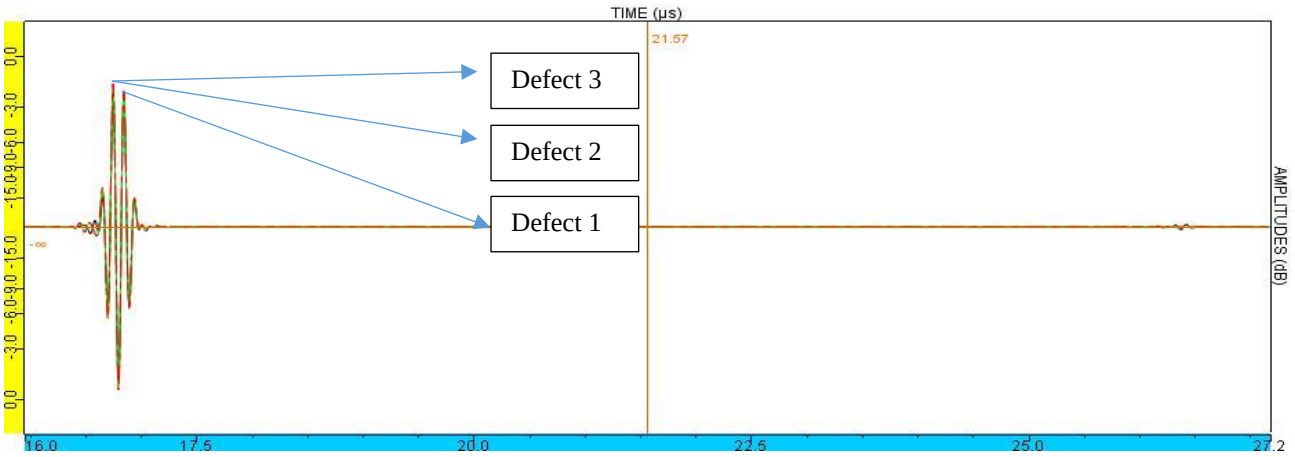

Fig. 6.16. A-scan image of different size defect at 5MHz PA.

Figure 6.16 represents the A-scan image of the three different size defects. However, defect2 and defect3 have reached the maximum amplitude of a -8dB, then the intensity is increased at defect1 to -7.7dB. The following results ensure the influence of the high frequency on detecting different size defects, where the amplitude is significantly increased as shown in a table 6.2.

Table 6.2. Maximum amplitudes of the three different size defects by using 5MHz PA.

Frequency / Defect's Size	**5*5 mm^2**	**10*10 mm^2**	**20*20 mm^2**
	Measured Max Amp. (dB)	**Measured Max Amp. (dB)**	**Measured Max Amp. (dB)**
5 MHz frequency	0	-0.4	-0.4
10 MHz frequency	-7.7	-8	-8

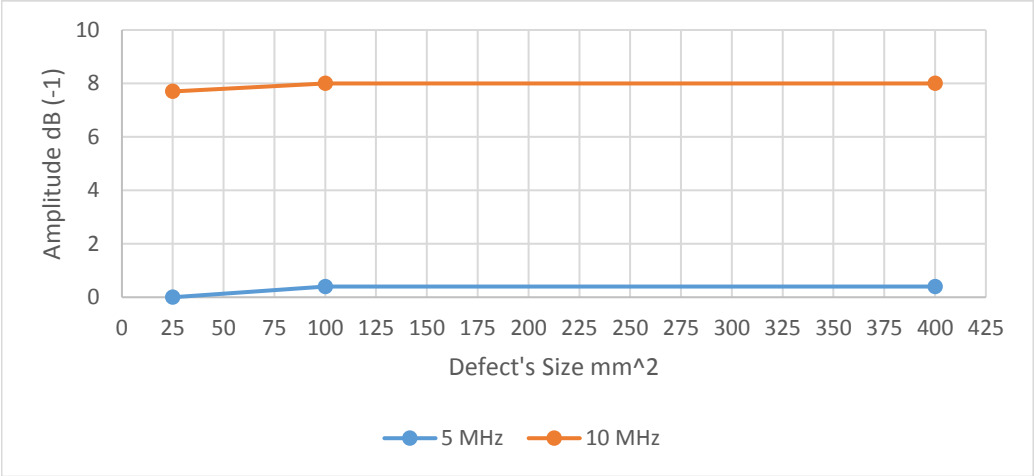

Fig. 6.17. Different size defects versus maximum amplitude at 5MHz and 10MHz.

6.3.2. Results of Section2 – 10MHz

In the following section, the defects are aligned consecutively at a same height 0.6mm below the surface. The defects size are 5*5mm^2, 20*20mm^2 and 10*10mm^2. However, the PA focusing type is a single point focusing, and the frequency of the PA transducer is a 5MHz. The results are obtained by A-scan and B-scan images. A-scan image represents the intensity and B-scan represent the position of each defect as shown in the figures below.

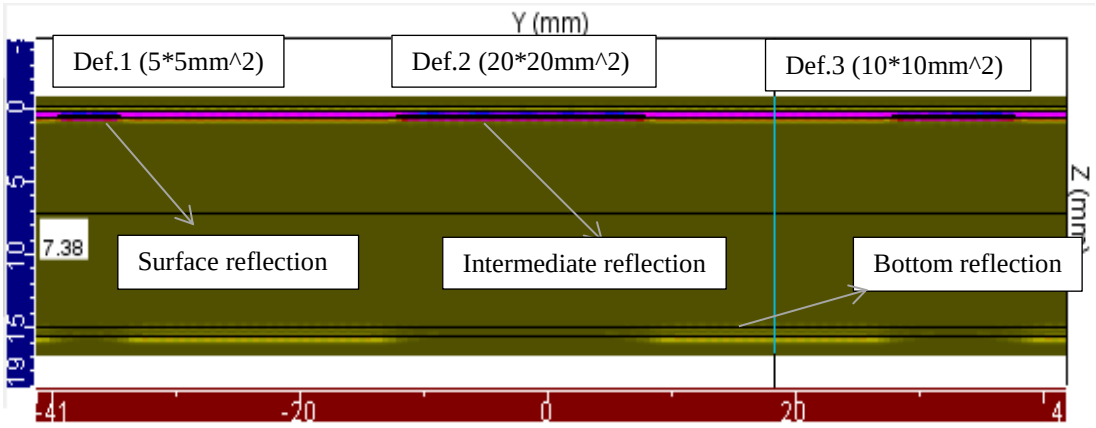

Fig. 6.18. B-scan image of a 5MHz PA transducer.

Figure 6.18 shows the different size defects at a 0.6mm depth. Similarly, the resolution and the accuracy have increased significantly at a 10 MHz PA transducer. Moreover, there are different reflections. The top line corresponds to the surface reflections, and the middle line is related to the intermediate reflections.

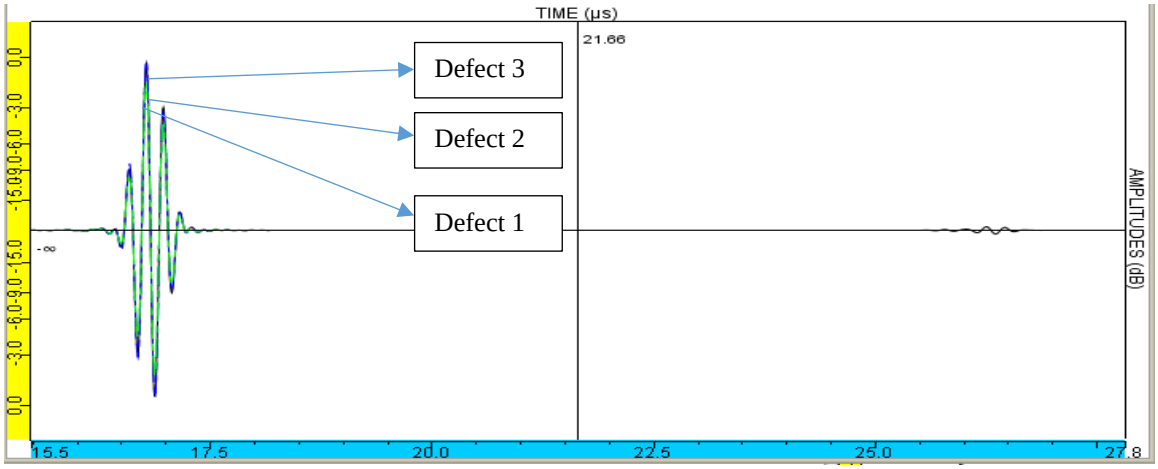

Fig. 6.19. A-scan image by using 10MHz PA at a 0.6mm depth.

Figure 6.19 represents A-scan image of the different size defects at a section2. The frequency is a 10MHz, and the focusing type is a single point focusing. However, the maximum amplitude has reached is -8dB at the defect2 and defect3. Then, the amplitude has increased to -7.7dB at a defect1. The intensity of the defects at the 10MHz frequency is higher than the intensity at a 5MHz as shown in a table 6.3.

Table 6.3. Maximum amplitudes at 5MHz and 10MHz frequencies.

Frequency / Defect's Size	**5*5 mm^2**	**10*10 mm^2**	**20*20 mm^2**
	Measured Max Amp. (dB)	**Measured Max Amp. (dB)**	**Measured Max Amp. (dB)**
5 MHz frequency	-0.4	-0.2	-1.6
10 MHz frequency	-7.7	-8	-8

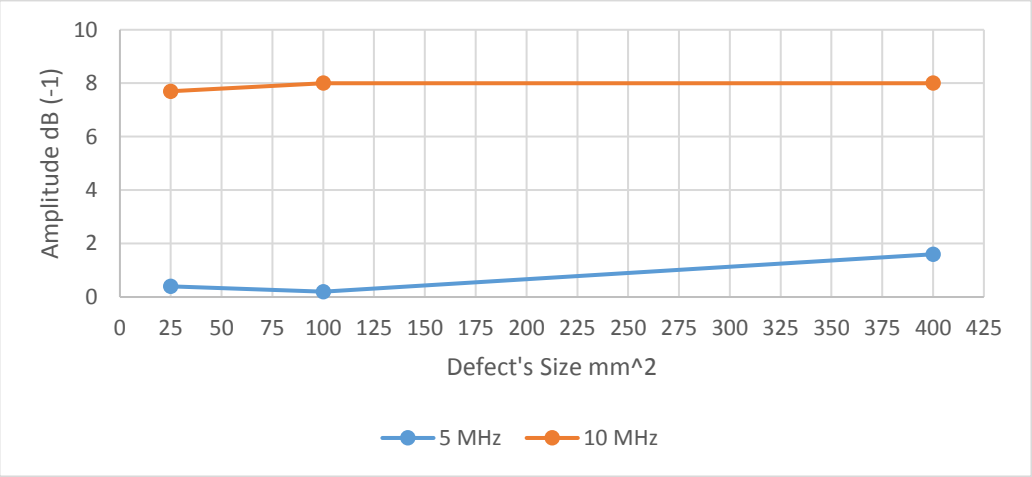

Fig. 6.20. Different size defects versus maximum amplitude at a section2.

6.3.3. Results of Section3 – 10MHz

Section3 represents the defects at a 0.8mm below the surface. The inspection is performed by using a 10MHz PA transducer that is consists of 128 elements. However, the focusing type is a Single Point Focusing. The results are represented by A-scan and B-scan images as shown below. The reference value is 8.123 points.

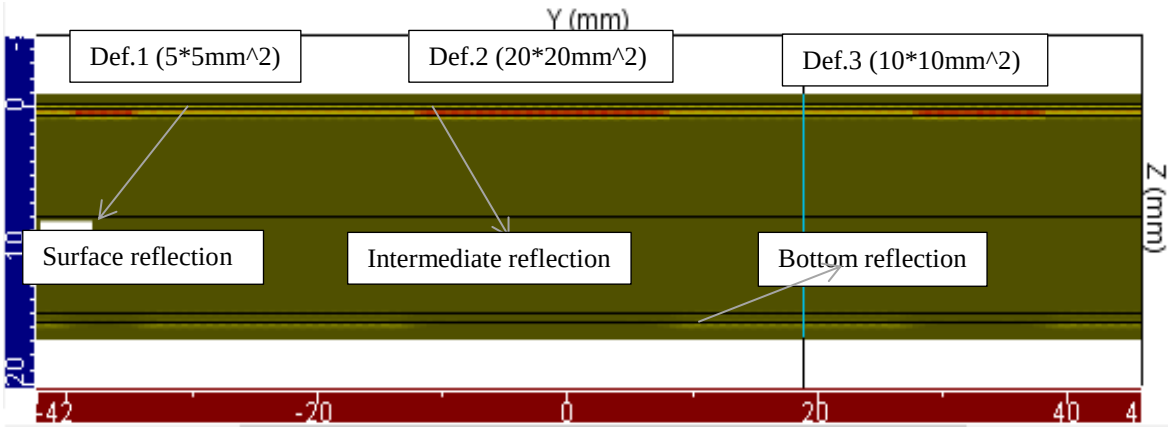

Fig. 6.21. B-scan image of section3 by using a 10MHz frequency.

Figure 6.21 represents the B-scan image of the different size defects. Similarly, same reflections have received at the top and bottom sides. The frequency is a 10MHz, and the PA transducer consists of

128 elements. The resolution and accuracy of the defects have been increased significantly by using a 10MHz frequency.

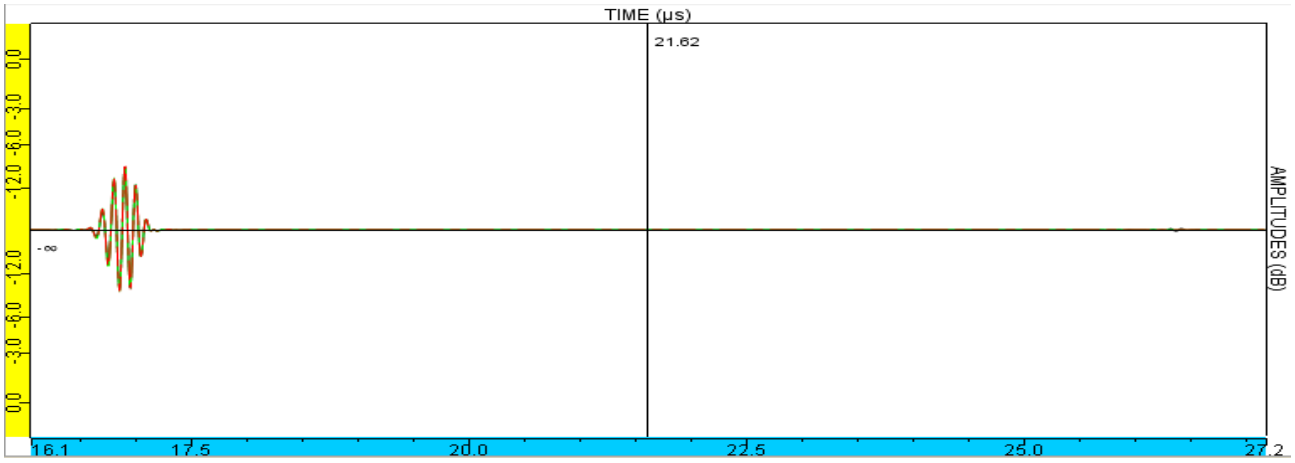

Fig. 6.22. A-scan image of the maximum amplitudes of a section3 at 10MHz frequency.

Figure 6.22 represents the maximum amplitude of the different size defects at 10MHz frequency. The intensity at 10MHz has increased significantly. The maximum amplitude of a defect2 is -9.5MHz. However, the intensity has slightly increased to reach -8.7dB at defect3. Moreover the intensity has significantly increased at 10MHz, and increased to 0dB at 5MHz frequency.

6.4. Results of POD Analysis

The POD analysis is correspond to the different size defects at 10MHz PA transducer. However, the defined characteristic is related to the length of 5mm, and the uncertain parameters are defined at the positions of x-axis and y-axis. The number of the characteristic values is 50 and 2 samples per character. The distribution type for all uncertain parameter is normal distribution as shown in a figure 6.23.

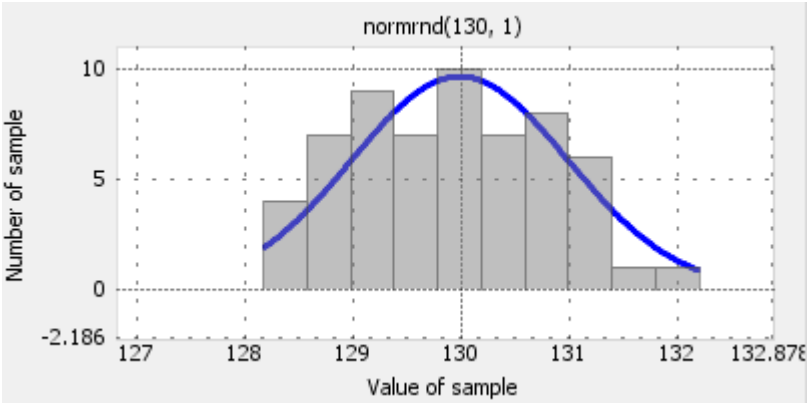

Fig. 6.23. Normal Distribution of the uncertain parameter (x-axis).

The computational method have used is called Monte-Carlo. However, Monte-Carlo method is a useful technique to express the probability of the uncertain parameters, and determine the interaction between the flaws.

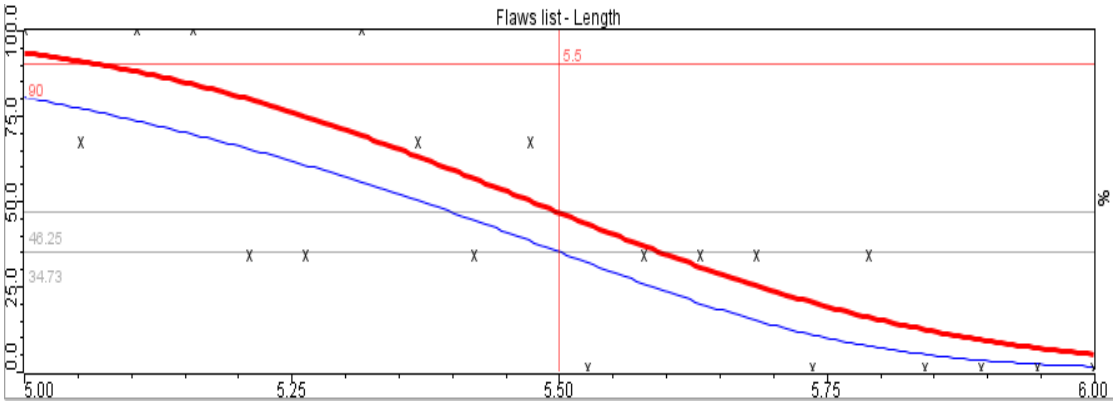

Fig. 6.24. POD curve.

Figure 6.24 shows the POD curve of the defect length. The probability of detection has decreased exponentially from 90.4% at 5mm to 6% at 5.9mm. However, the confidence level is 95%. Figure 6.25 shows the thresholds and residual plots.

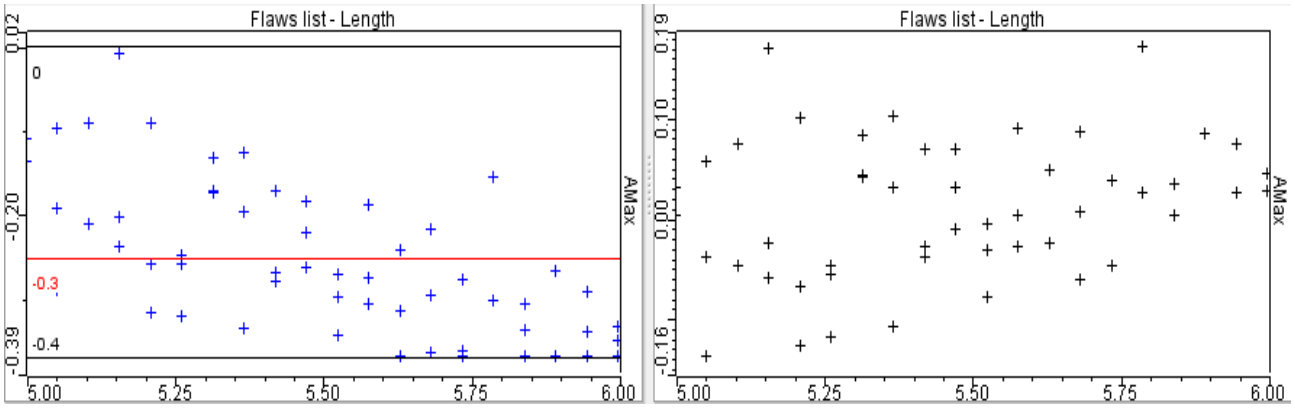

Fig. 6.25. Thresholds and residual plot.

Table 6.4. Thresholds

	Thresholds
Attenuation dB	-0.4
Detection dB	-0.3
Saturation dB	0

6.5. Conclusion

The 10 MHz PA transducer of a single point focusing is very effective to detect defects at CFRP of ultrasound velocity 3070 m/s as shown in study case 2. The maximum amplitude has reached is a -10.2 at a defect2, which represents a high intensity and strong reflecting signal. However, study case3 shows that 10MHz PA transducer of a single point focusing is more able to detect large defect such as defect2 and defect3, where the maximum amplitude has reached in most sections -8dB.

7 Modelling Results by Using PA Transducer – Null Delay Law

In the following chapter, the results of different study cases will be presented in a different sections. However, the frequencies of the PA transducer are 10MHz and 5MHz. Moreover, the focusing type is a Null Delay Law, where the beam is able to steer or focus. The running simulation is a 210 steps and 0.5mm step size, while the simulation setup is 2D. Furthermore, the case study3 consists of a three sections, where each section is related to a specific depth.

7.1. Results of Case Study2 by using PA transducer

The results of case study2 are related to the same size defects. The focusing type for this test is a Null Delay Law. The distance between the defects is 35mm, and the size of the all defects is 10*10mm^2 as shown in chapter6 figure 6.1. However, two types of transducers have been used such as 5L128-128X7-NW3 (5MHz) and 10L128-64X7-NW1 (10MHz).

7.1.1. Results of Case Study2 by Using 5L128-128X7-NW3 PA (5MHz)

The following results are correspond to a 5MHz frequency and PA transducer. However, the running setup is a 210 steps and 0.5mm step size. The simulation is performed by a 2D inspection. The PA transducer consists of 128 elements and 8 sequencing elements. Moreover, a different A-scan and B-scan images have been received as shown below.

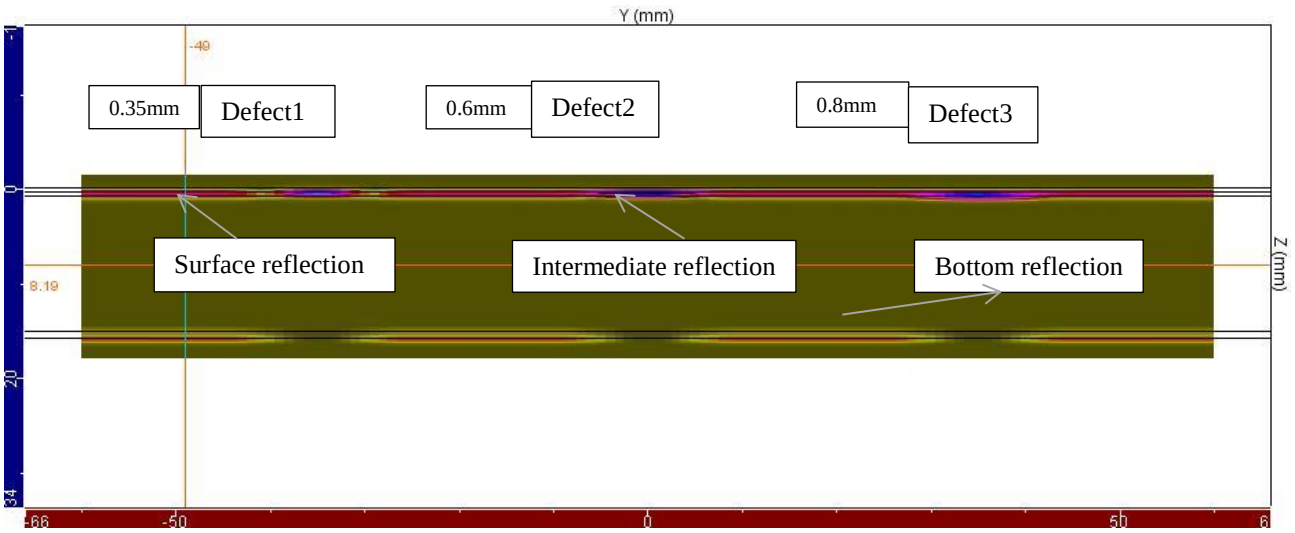

Fig. 7.1. B-scan image of the same size defects at a 5MHz frequency.

The reflections and position of the defects are possible to display by using B-scan image as shown in a figure 7.1. However, the defects are located at a three different depths, such as 0.35mm, 0.6mm and 0.8mm respectively. Figure 7.1 shows the same size for all defects.

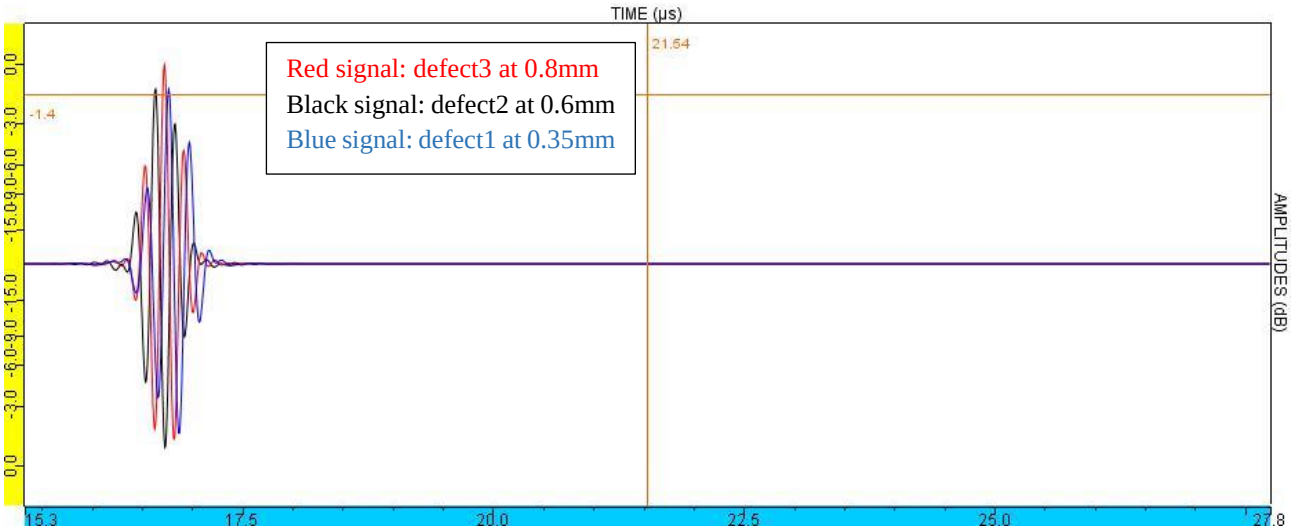

Fig. 7.2. A-scan of study case 2 by using 5MHz PA transducer.

Figure 7.2 shows the maximum amplitude of the same size defects. The intensity of the defect3 has reached the highest amplitude -1.2dB at a 0.8mm depth. On the other hand, defect2 shows high amplitude 0dB at a 0.6mm below the surface. The maximum amplitude of defect1 is -0.8dB. Therefore, the variation of the intensity is due to the defect's depth and the ultrasound velocity of each material.

7.1.2. Results of Case Study2 by Using 10L128-64X7-NW1 PA (10MHz)

The results of the case study2 are obtained by using 10MHz PA transducer. Similarly, the experiment has performed for the same size defects at different depths. However, the results are shown by B-scan and A-scan images. The focusing type is Null Delay Law.

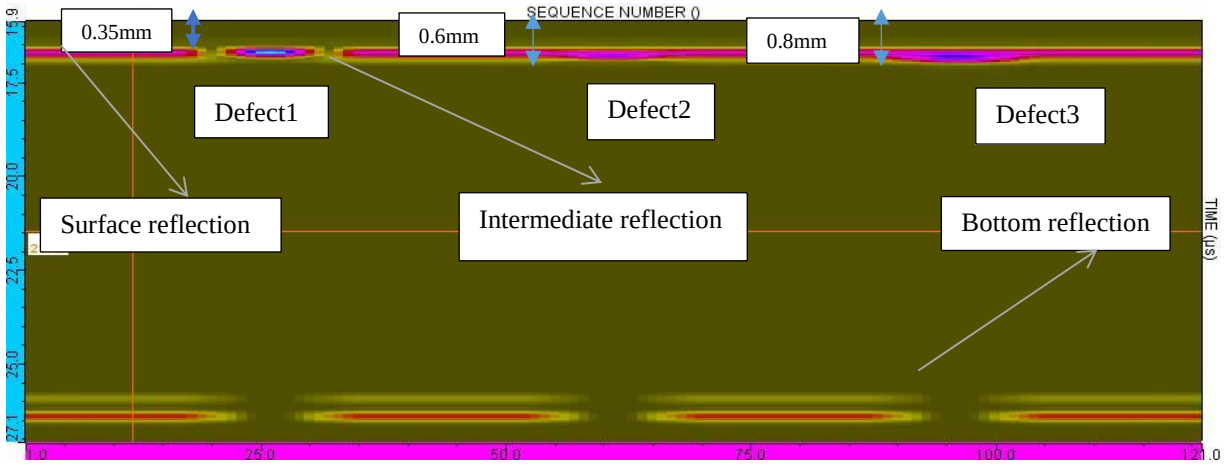

Fig. 7.3. B-scan image of a study case2 at 10MHz frequency.

Moreover, The resolution and accuracy have increased at a 10Mhz frequency as shown in a figure 7.3. However, different reflections are shown. The intensity/maximum amplitude at the defect increased significantly as well.

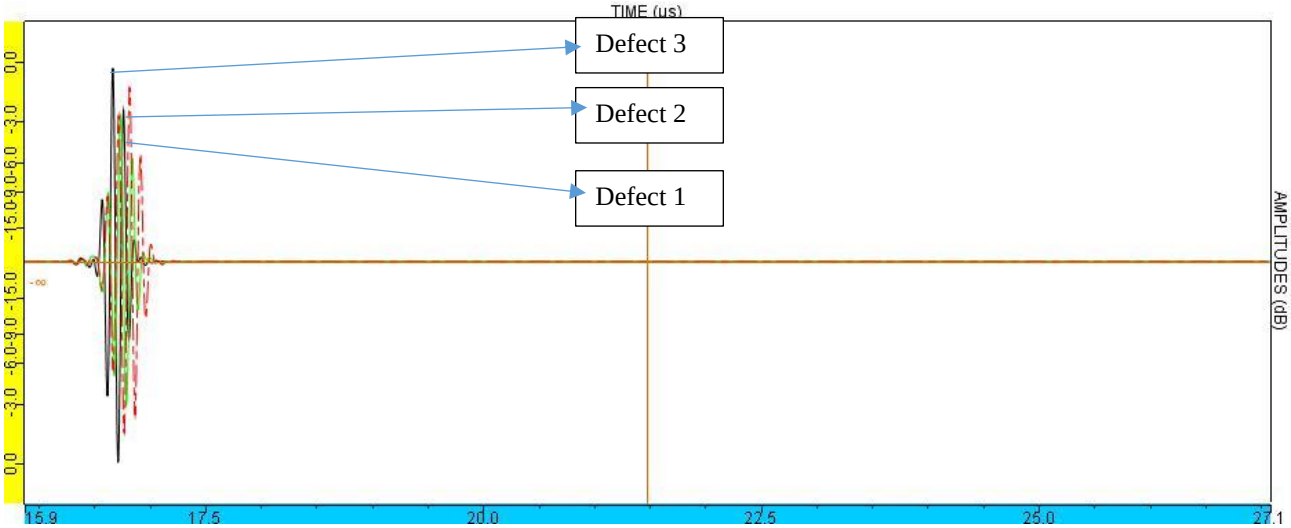

Fig. 7.4. A-scan image of the same size defects at a 10MHz frequency.

Figure 7.4 represents the maximum amplitudes of the same size defects at a 10MHz frequency. Defect2 has reached maximum amplitude -9.1dB, and then the intensity has increased to reach -6.4dB at defect1. However, at a 0.8mm depth, the maximum amplitude is a -7.6dB. Moreover, the intensity at a 10MHz is lower than the intensity of a 5MHz, which means that the reflections are stronger at 10MHz frequency as shown in the table 7.1. The variation of amplitudes is due to the different ultrasound velocity of the materials.

Table 7.1. Maximum amplitudes at 5MHz and 10MHz frequencies.

Frequency / Defect's Size	**0.35 mm depth**	**0.6 mm depth**	**0.8 mm depth**
	Measured Max Amp. (dB)	Measured Max Amp. (dB)	Measured Max Amp. (dB)
5 MHz frequency	-0.8	0	-1.2
10 MHz frequency	-6.4	-9.1	-7.6

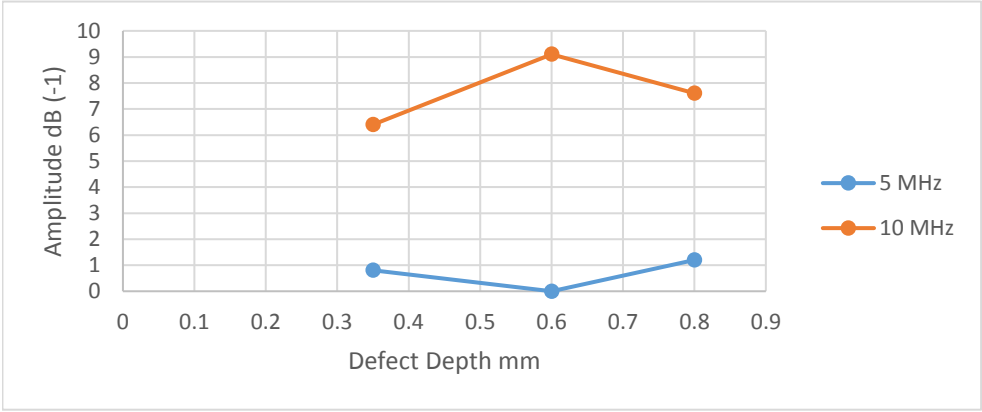

Fig. 7.5. Maximum amplitudes of section2 defects.

7.2. Results of Case Study3 by Using 5L128-128X7-NW3 PA (5MHz)

Case study3 is consist of three different sections. Each section corresponds to a specific depth. However, the inspection is performed by using 5MHz PA transducer of a 128 elements. The PA type is Null Delay Law. In non-linear delay law the reflected beam is flexible, and it could be steering/rotating or focusing. Moreover, the run setup consists of 210steps and 0.5mm step size.

7.2.1. Results of Section1 – 5 MHz

The results of section1 are shown by B-scan and A-scan images. All the defects are located at a 0.35mm below the surface. However, the frequency is 5MHz PA transducer.

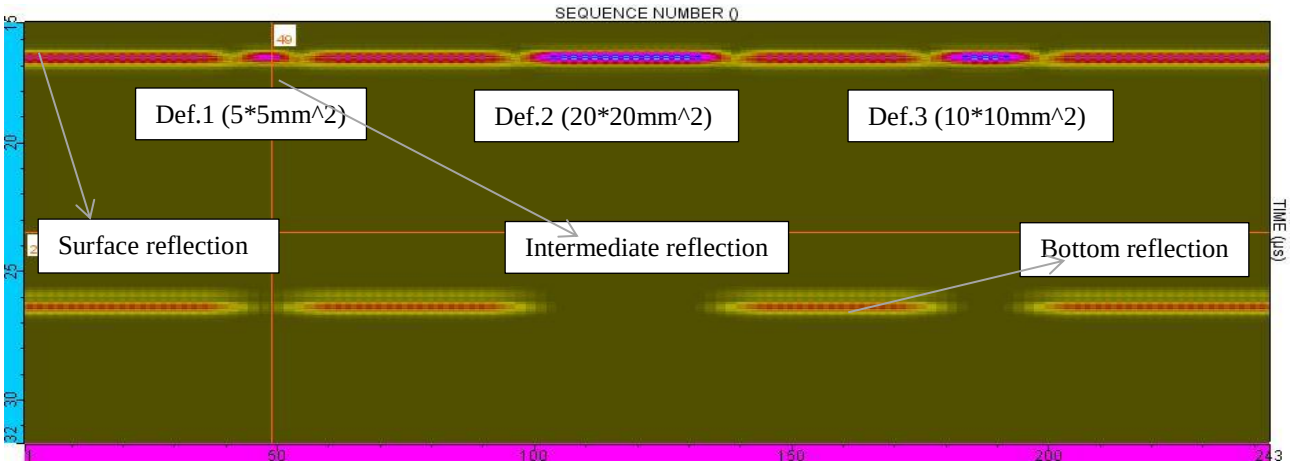

Fig. 7.6. B-scan image of the different Size defects at section1 and 5MHz frequency.

Figure 7.6 represents B-scan image of different size defects at a 0.35mm below the surface. However, the reflections are surface, intermediate and bottom reflections.

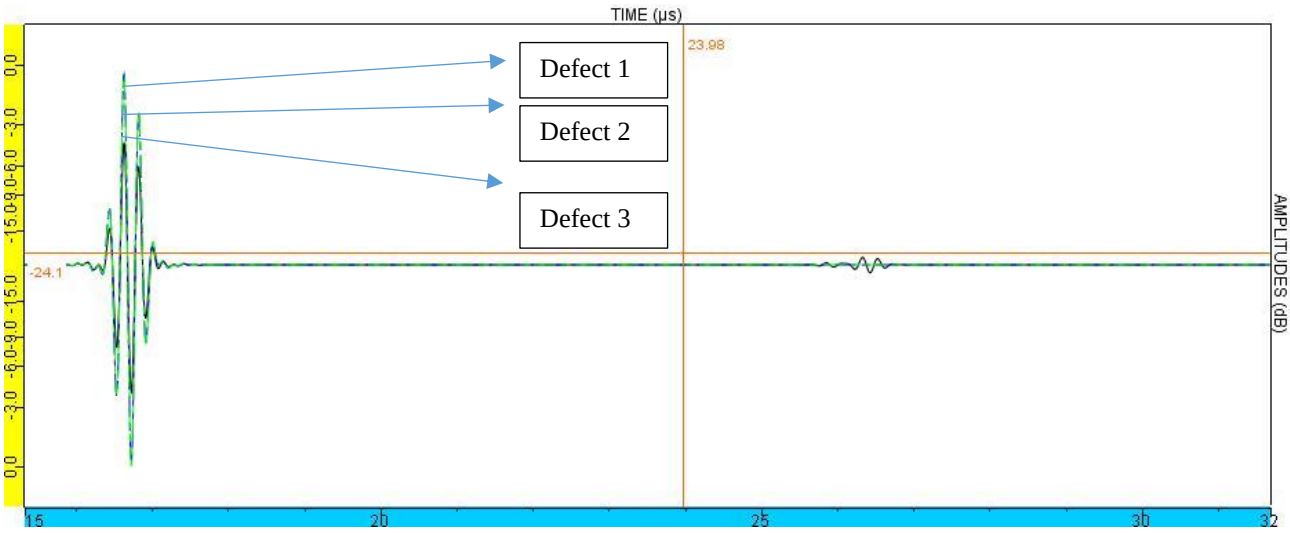

Fig. 7.7. A-scan image of the maximum amplitudes of a section1 defects at 5MHz frequency.

Figure 7.7 represents the maximum amplitude of the different size defects at a section1. Defect1 has reached -3.9dB maximum intensity, where the amplitudes of defect3and defect2 have increased progressively to reach 0dB. The frequency of the given transducer is 5MHz.

7.2.2. Results of sction2 – 5MHz

The defects in a section2 are aligned consecutively at a same height 0.6mm below the surface. The defects size are 5*5mm^2, 20*20mm^2 and 10*10mm^2 respectively. However, the PA type is a single point focusing. Similarly, the run setup is a 210 steps and 0.5mm step size. The simulation setup is a 2D.

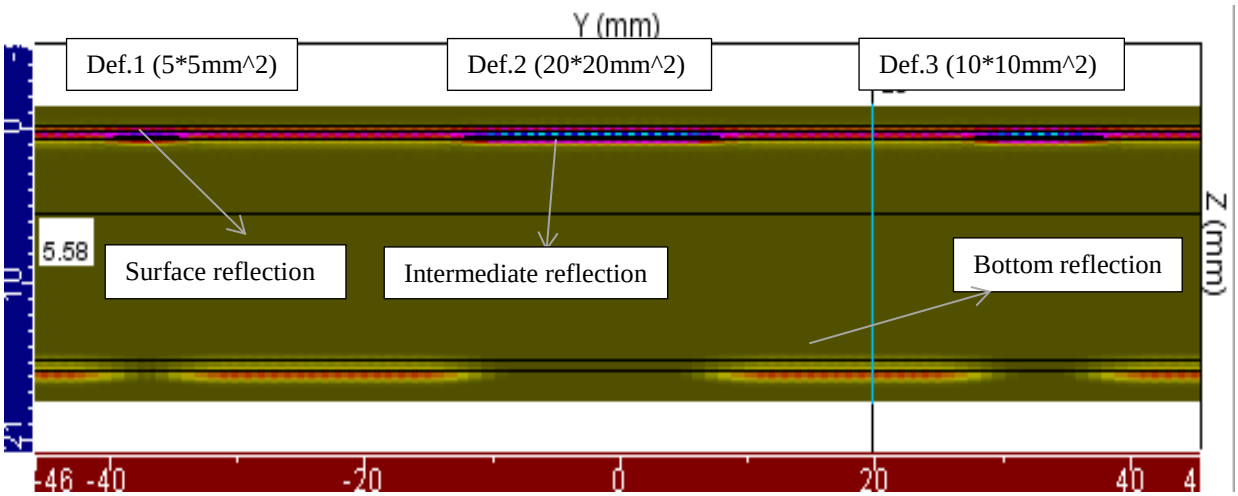

Fig. 7.8. B-scan image of a section2 at 5MHz frequency.

There are different reflection as shown in a figure 7.8, and each reflection is related to a specific location. The upper reflections are the surface reflection, and the lower part is a bottom reflection.

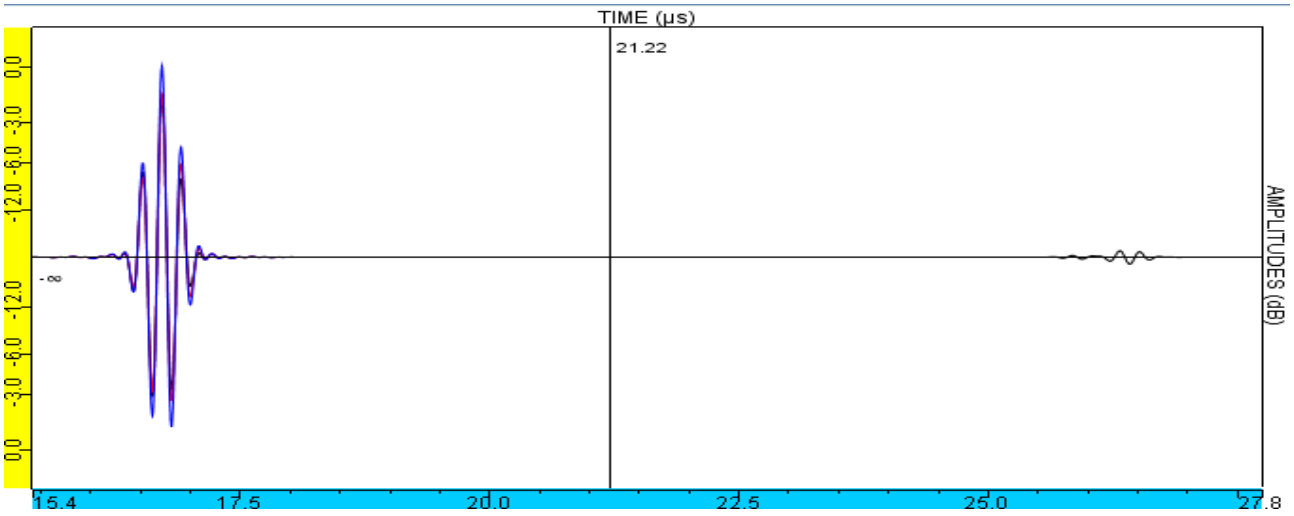

Fig. 7.9. A-scan image of the maximum amplitudes of the defects at a section2.

Figure 7.9 shows the comparison of the different defects. Defect1 has reached maximum amplitude -1.7dB. However, the amplitudes have slightly increased significantly to -1.4dB and 0dB at the defects 2 and 3 respectively.

7.2.3. Results of Section3 – 5MHz

The following results are related to the defects that are located at a 0.8mm below the surface. However, the test is performed by using a 5MHz PA transducer, 128 elements and 8 sequencing

elements. The pa type is a null delay law. Figure 7.10 represents B-scan image of the different size defects at a 0.8mm below the surface.

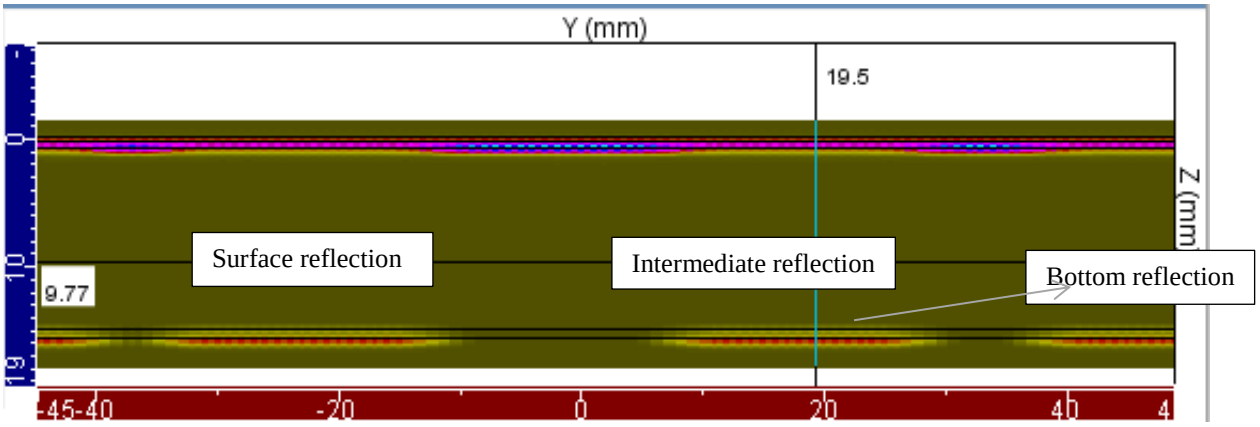

Fig. 7.10. B-scan image of different size defects at a section3 and 5MHz.

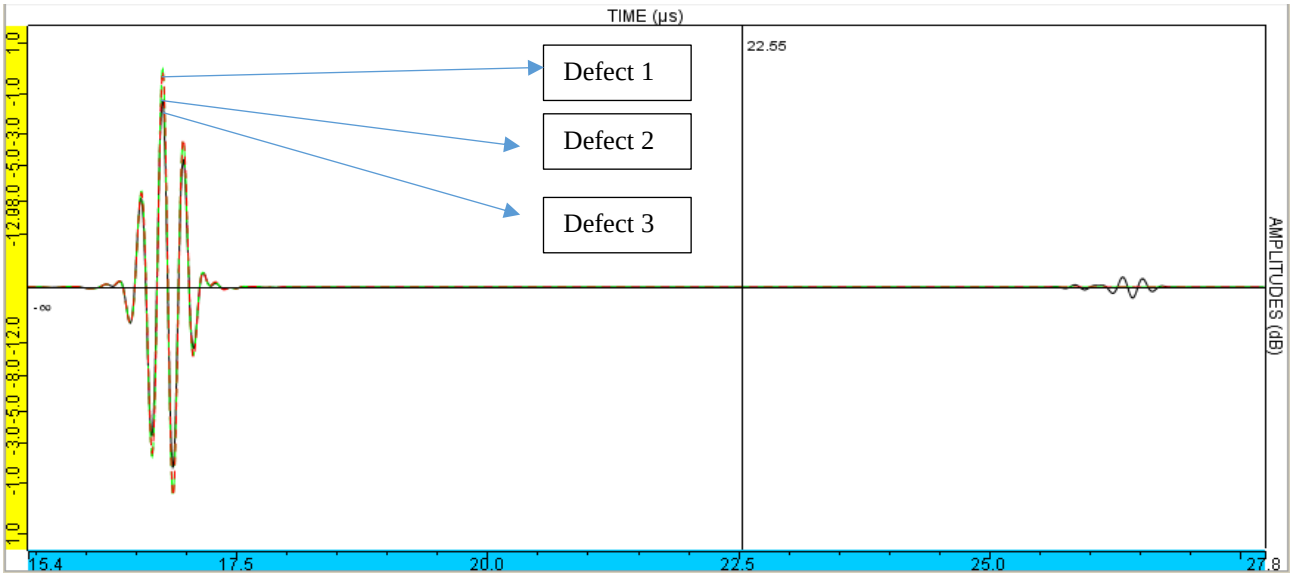

Fig. 7.11. A-scan image of the maximum amplitudes at a section3.

Defect1 has reached peak point at -1.3dB as shown in a figure 7.11. Then, the maximum amplitudes have increased to -0.1dB and 0dB at the defects2 and defect3 respectively.

7.3. Results of Case Study3 by Using 10L128-64X7-NW1 PA (10MHz)

This test is performed by using a 10MHz PA transducer. The aim of this experiment is to determine the influence of the 10MHz frequency on each defect. However, as the frequency increases the wavelength decreases. Moreover, the resolution and accuracy has increased at a 10MHz frequency. The focusing type of the inspection is Null Delay Law.

7.3.1. Results of Section1 – 10MHz

The defects in section1 are positioned at a same depth 0.35mm. The Ultrasound velocity at the given depth is 3040m/s. However, the intensity and maximum amplitudes have been increased by using a

10MHz PA transducer. Therefore, the resolution and accuracy have increased as well. The results are demonstrated by A-scan and B-scan images as shown below.

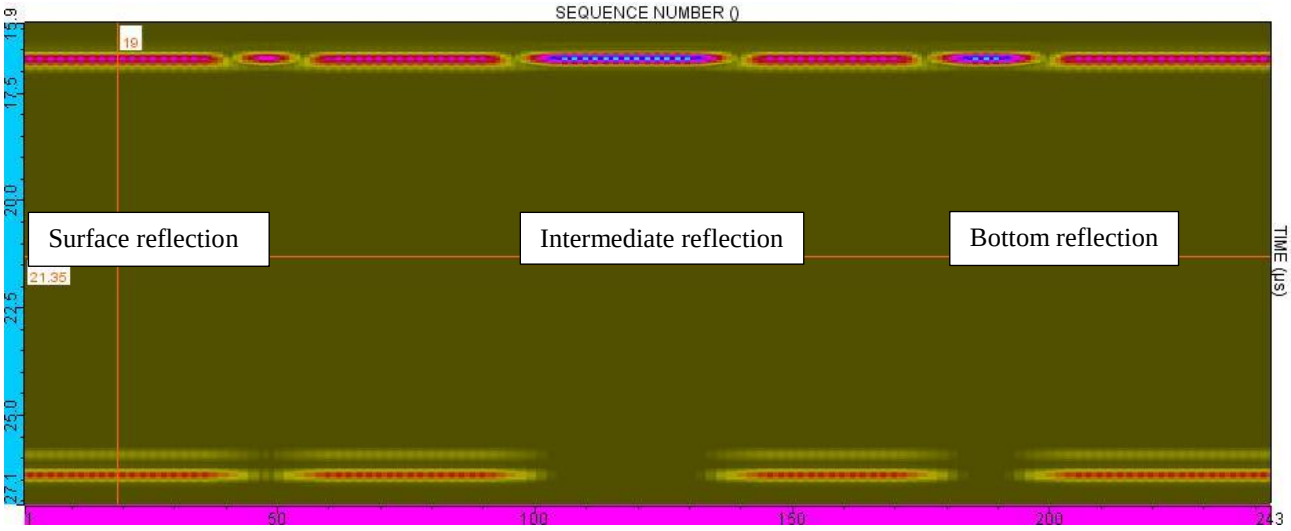

Fig. 7.12. B-scan image of a section1 at 10MHz.

Figure 7.12 shows a B-scan image of 10MHz transducer. Moreover, different reflections have received, such as surface, intermediate and bottom reflections. However, the defects are very clear and visible, where they are represented in blue color.

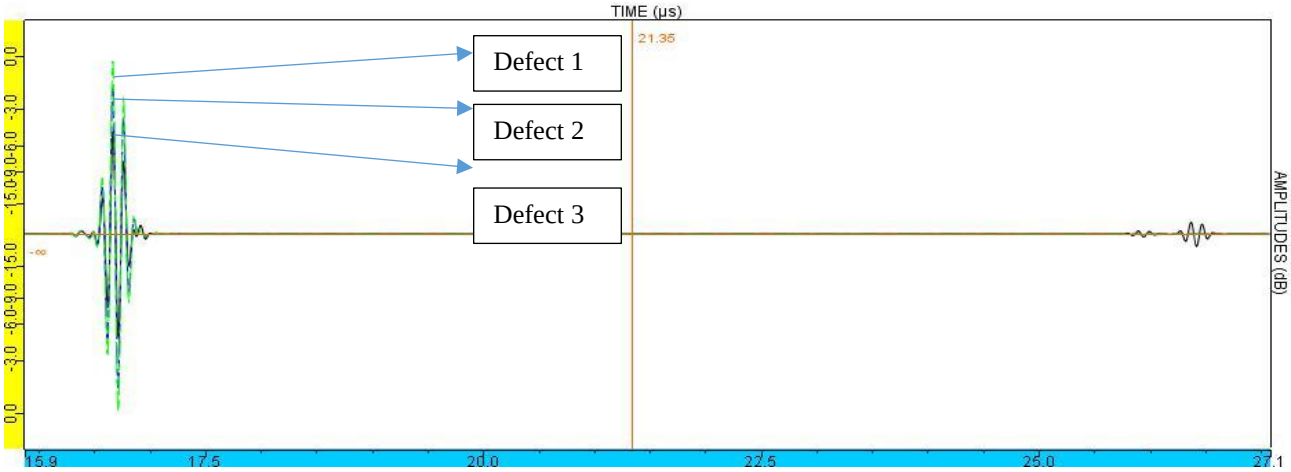

Fig. 7.13. A-scan image of the maximum amplitudes at a section1.

Figure 7.13 represents the comparison of the three different size defects by using 10MHz PA transducer. The maximum intensity is reached at a defect1 is -10.1dB, and it has increased to -5.8dB at defect2 and defect3 as shown in a table 7.2. The maximum amplitudes of a 10MHz frequency is higher than the amplitudes of 5MHz PA transducer.

Table 7.2 . Maximum amplitudes at section1.

Frequency / Defect's Size	**5*5 mm^2**	**10*10 mm^2**	**20*20 mm^2**
	Measured Amp. (dB)	Measured Amp. (dB)	Measured Amp. (dB)
5 MHz frequency	-3.9	0	0
10 MHz frequency	-10.1	-5.8	-5.8

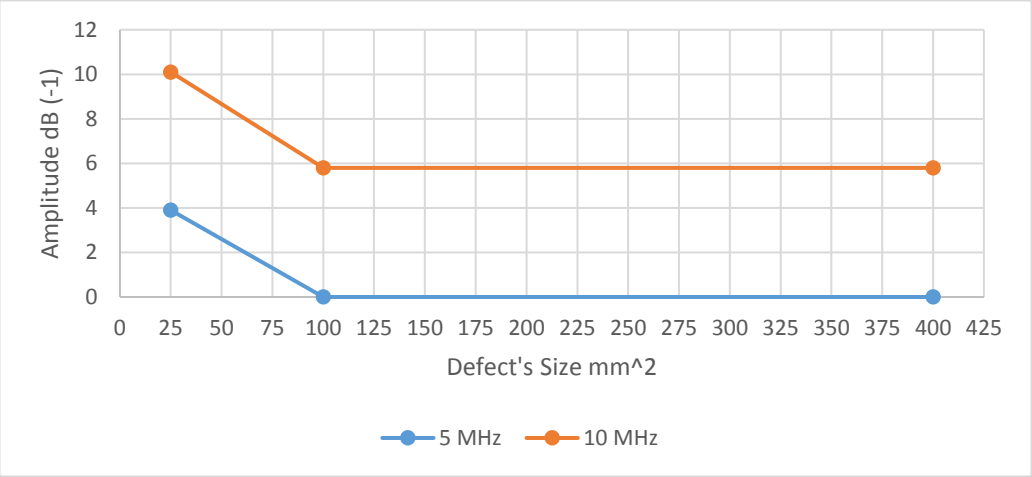

Fig. 7.14. Maximum amplitude versus defect's size at 5MHz and 10MHz frequencies.

7.3.2. Results of Section2 – 10MHz

In the following section, the defects are placed at a same height 0.6mm below the surface. However, the PA type is a Null Delay Law and 10MHz frequency. The results are obtained by A-scan and B-scan images. A-scan image represents the intensity and B-scan represent the position of each defect as shown in the figures below.

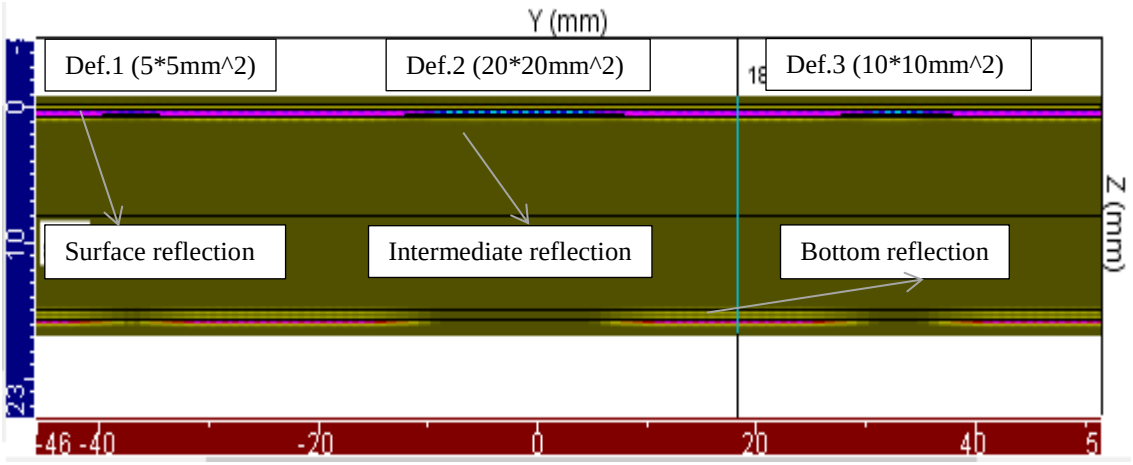

Fig. 7.15. B-scan image of different size defects at a section2.

Figure 7.15 represents B-scan image of the different size defects at a section2. The results are obtained by using a 10MHz PA transducer of 128 elementsHowever, the top and bottom reflection have been received. Moreover, the intensity of the defects has significantly increased at a 10MHz frequency.

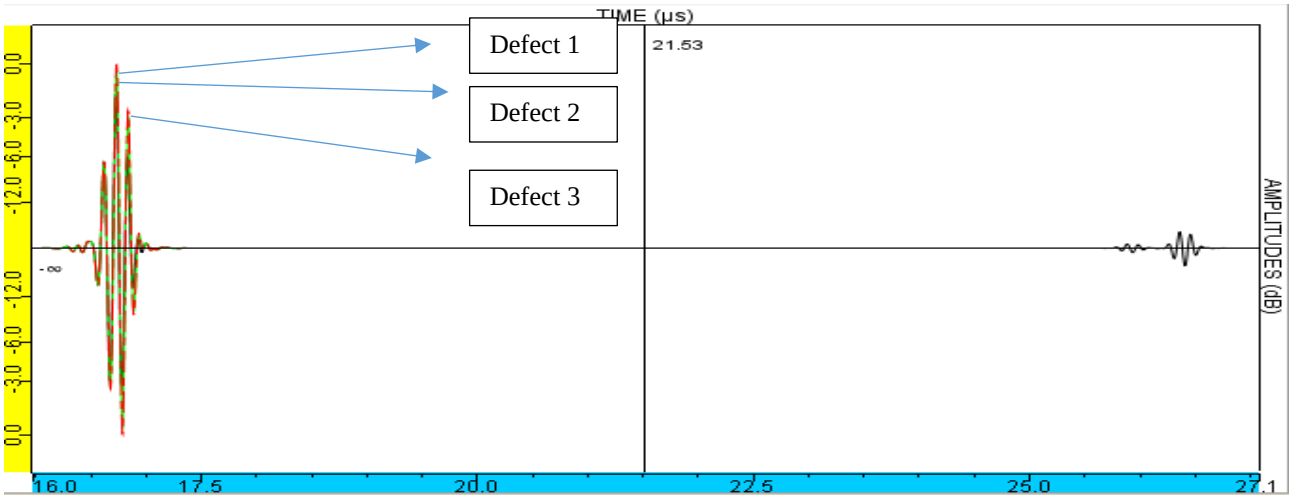

Fig. 7.16. Maximum amplitudes of different size defects at section2 and 10MHz frequency.

Figure 7.16 shows that the defect1 has reached maximum amplitude -10.7dB at 0.35mm depth. The measured amplitudes have increased to -9.2dB and -9.1dB at defect2 and defect3 respectively. However, the intensities of the defects at 10MHz is lower than the amplitudes of a 5MHz as shown in a table 7.3.

Table 7.3. Maximum amplitudes of different size defects at a 5MHz and 10MHz.

Frequency / Defect's Size	**5*5 mm^2**	**10*10 mm^2**	**20*20 mm^2**
	Measured Amp. (dB)	**Measured Amp. (dB)**	**Measured Amp. (dB)**
5 MHz frequency	**-1.7**	**-0.1**	**0**
10 MHz frequency	**-10.7**	**-9.2**	**-9.1**

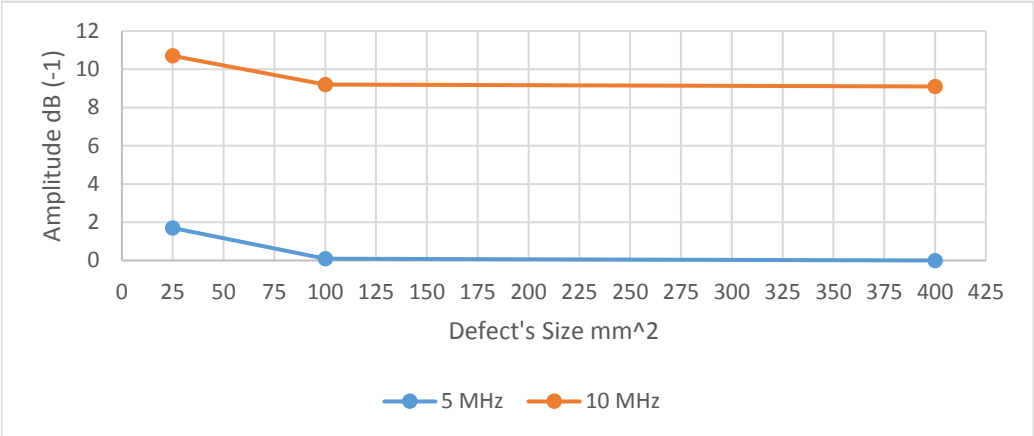

Fig. 7.17. Maximum amplitudes of different size defects at 5MHz and 10MHz frequencies.

7.3.3. Results of Section3 – 10MHz

The test is performed by using a 10MHz PA transducer, 128 elements and 8 sequencing elements. The focusing type is null delay law. Moreover, B-scan and A-scan images have been received as shown in the figures below.

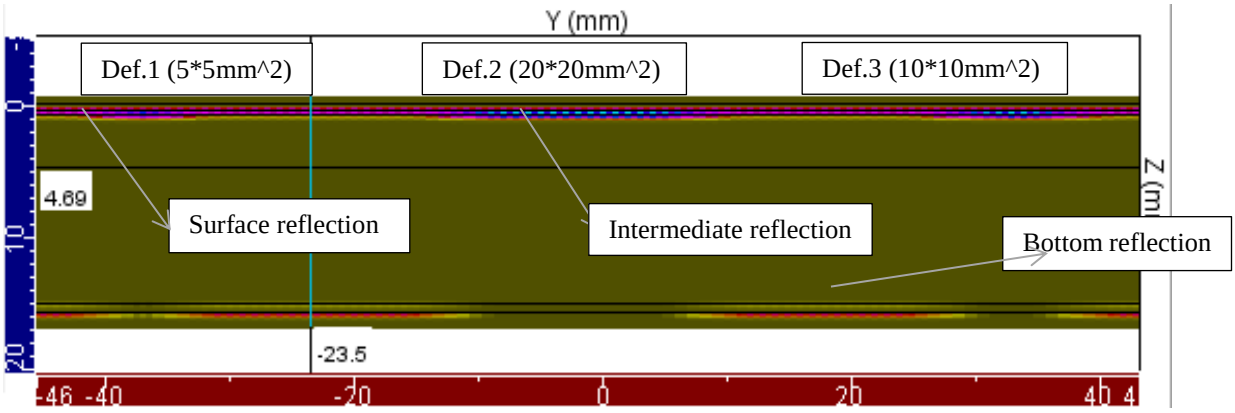

Fig. 7.18. B-scan image of the different size defects at a section3.

Figure 7.18 represents a B-scan image, where it shows different reflections. The upper reflections are related to the surface reflection, and the lower reflections correspond to the bottom reflections of the A-320 elevator. The inspection is performed by using 10MHz PA transducer and Null Delay Law focusing.

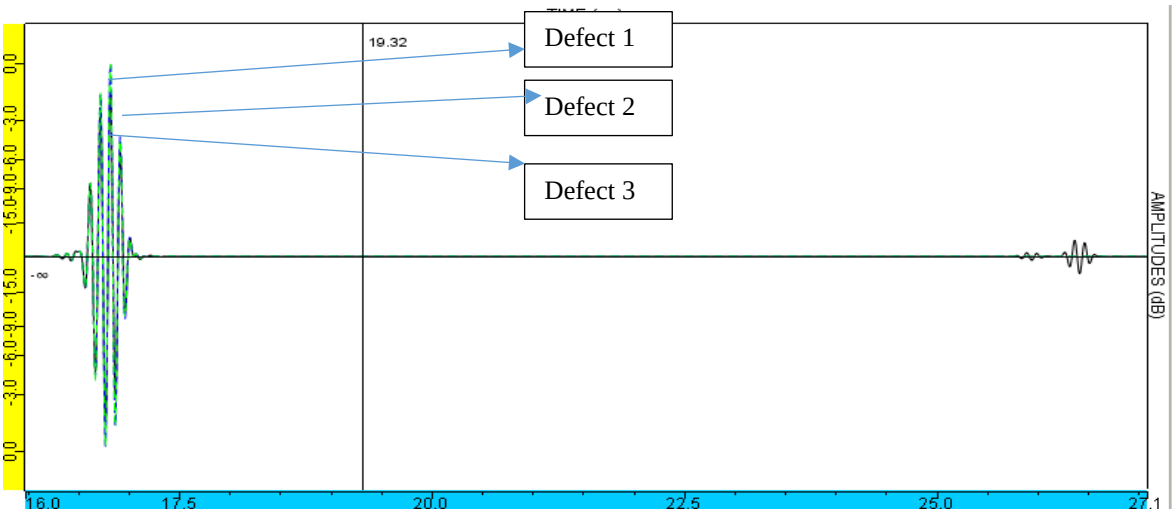

Fig. 7.19. Maximum amplitude of different size defects at a 5MHz frequency.

Figure 7.19 shows the comparison between the three different size defects. The maximum amplitude is -7.8dB at a defect1, and then it is increased to -6.5 at a defect2. However, the maximum amplitude of defect3 is -6.4dB. Moreover, the intensity at 10MHz frequency is -7.8Db, which is lower than the intensity at 0dB as shown in a table 7.4.

Table 7.4. Maximum amplitudes of the different size defects at 5MHz and 10MHz frequencies.

Frequency / Defect's Size	**5*5 mm^2**	**10*10 mm^2**	**20*20 mm^2**
	Measured Amp. (dB)	Measured Amp. (dB)	Measured Amp. (dB)
5 MHz frequency	-1.3	-0.1	0
10 MHz frequency	-7.8	-6.5	-6.4

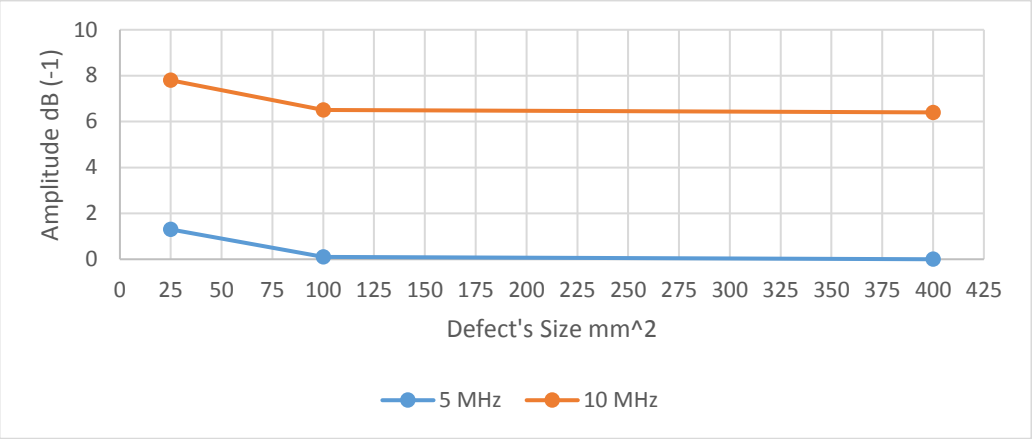

7.4. Results of POD Analysis

The following results correspond to the POD analysis of 10MHz PA transducer-Null Delay Law. The focusing type is a single point focusing. Similarly, same flaws/defects are set as define characteristics, and the position of the defects are defined as uncertain parameters such as the variables along x-axis and y-axis. The number of the characteristic values is 50, and there are 2 samples per character. The distribution type for the all uncertain parameter is a normal distribution as shown in a figure 7.20. The confidence level is 95.

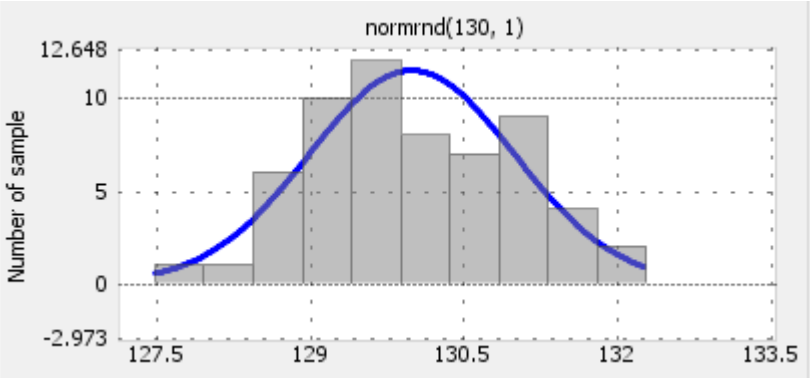

Fig. 7.20. Normal distribution of variable-x.

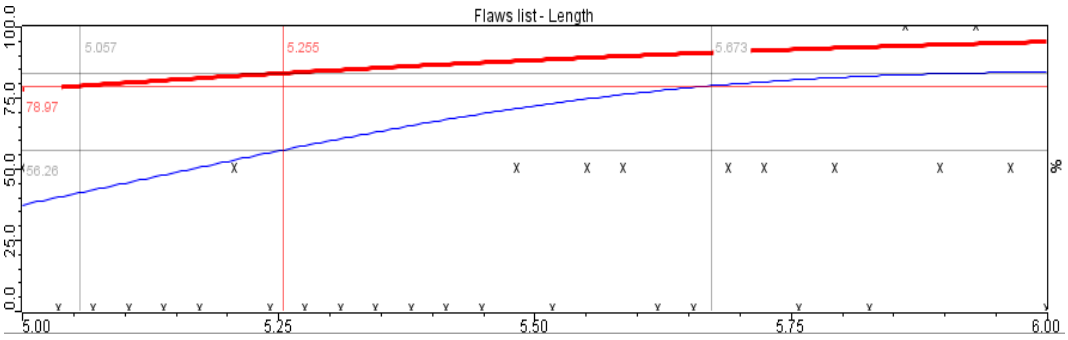

Fig. 7.21. POD Curve.

Figure 7.21 shows the POD curve. However, the POD is increasing progressively from 78.9% at 5mm to 95.5% at 5.9mm. Moreover, the attenuation and noises are presented by the thresholds plots as shown in a figure 7.22

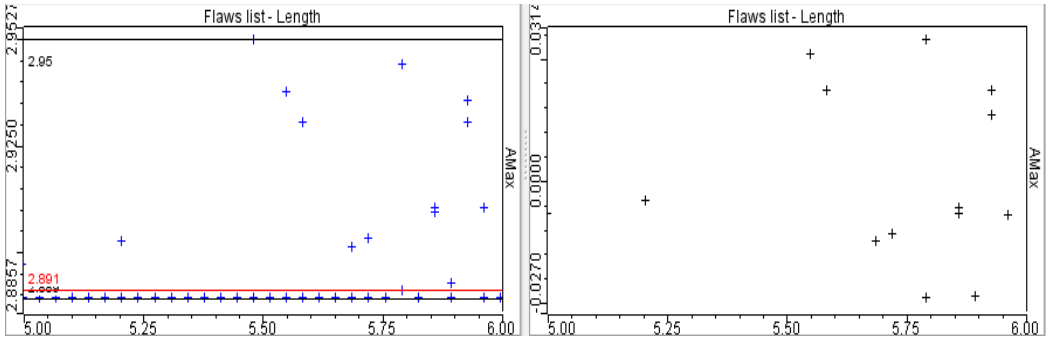

Fig. 7.22. Thresholds and residual plots.

Table 7.5. Thresholds values.

	Thresholds
Noise dB	-0.2
Detection dB	-0.2
Saturation dB	0

7.4.1. Conclusion

The results of the case study2 show that the 10MHz PA transducer of a null delay law type is highly effective to detect the defects at a 0.6mm depth since the CFRP material has high ultrasound velocity, which is relevant to 3070m/s. However, the maximum measured amplitude is -9.1dB. Thereforee, the small size defects are more likely possible to detect by using 10MHz PA of a null delay law rather than single point focusing. The maximum measured amplitude is a -10.7dB at a defect in section, which it shows very high reolution.

8 Experimental Results

The experimental results are correspond to A-320 elevator component, which it is a sandwich structure material. The test was done on the lower side surface of an A-320 elevator. The surface area of the A-320 elevator is 580*360mm^2. The A-320 elevator is made of three types of material that are stacked on each other. However, the investigation has done by using a 5L128-128X7-NW3 PA transducer of a 5MHz frequency. The results are displayed by using OMNISCAN$_{MX}$, where different images are obtained such as A-scan, B-scan, C-scan and S-scan.

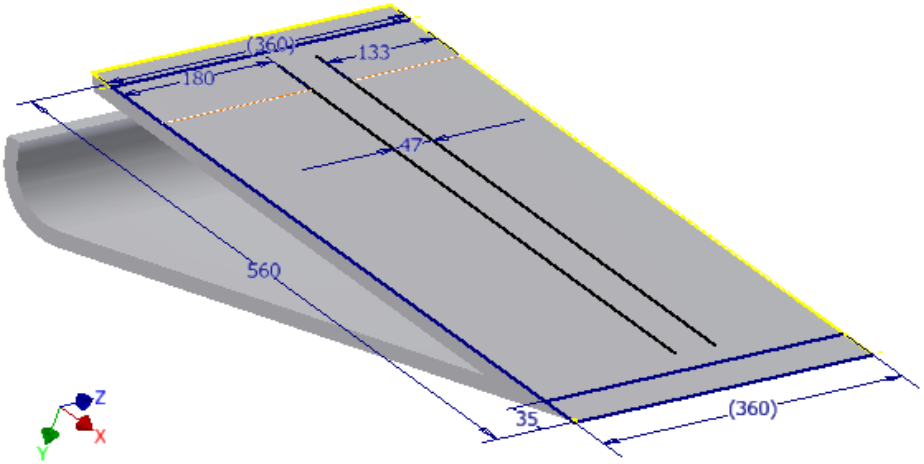

Figure 8.1. Isotropic view of A-320 elevator.

8.1. Experimental Procedures

The PA 5L128-128X7-NW3 transducer is connected to OMNISCAN$_{MX}$ tool. The OMNISCAN$_{MX}$ will automatically detect the type of the connected transducer. The Transducer is attached to a specific wedge SNW3-OL. The wedge is used to separate the signal's reflection between the surface and intermediate reflections of the defects because the inspecting defects are very near to the surface.

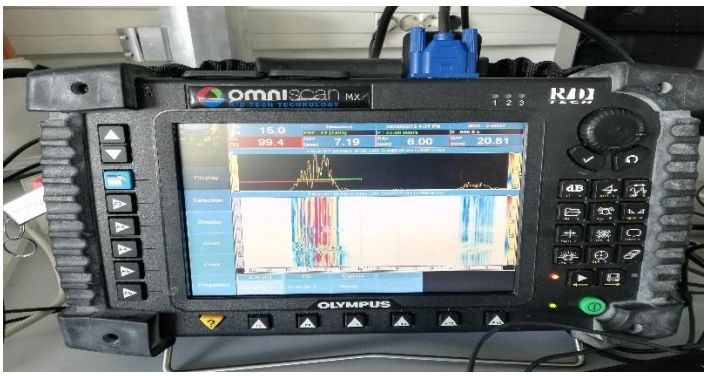

Fig. 8.1. OMNISCAN$_{MX}$ tool.

Table 8.1. Parameters of the experimental inspection.

Transducers	5L128-128X7-NW3
Material	Plexiglas
Material waves-sound velocity	2700 m/s

Geometry	Plate
Law configuration	Linear Sector
Wave type	Longitudinal
Thickness	14 mm
Focal depth	1 mm
Gain	20 dB

Second, a 5MHz transducer is placed on the bottom side surface of the A-320 elevator and coupling liquid/gel is used to detect the cracks. The inspection is divided into two zones. The first zone is a 218*120 mm^2. The second inspection area is 35*225 mm^2, and it is near the trailing edge. The inspection zones are shown by the green color, while the defects are represented in red color . Moreover, there are three defects as shown in a figure 8.2(a).

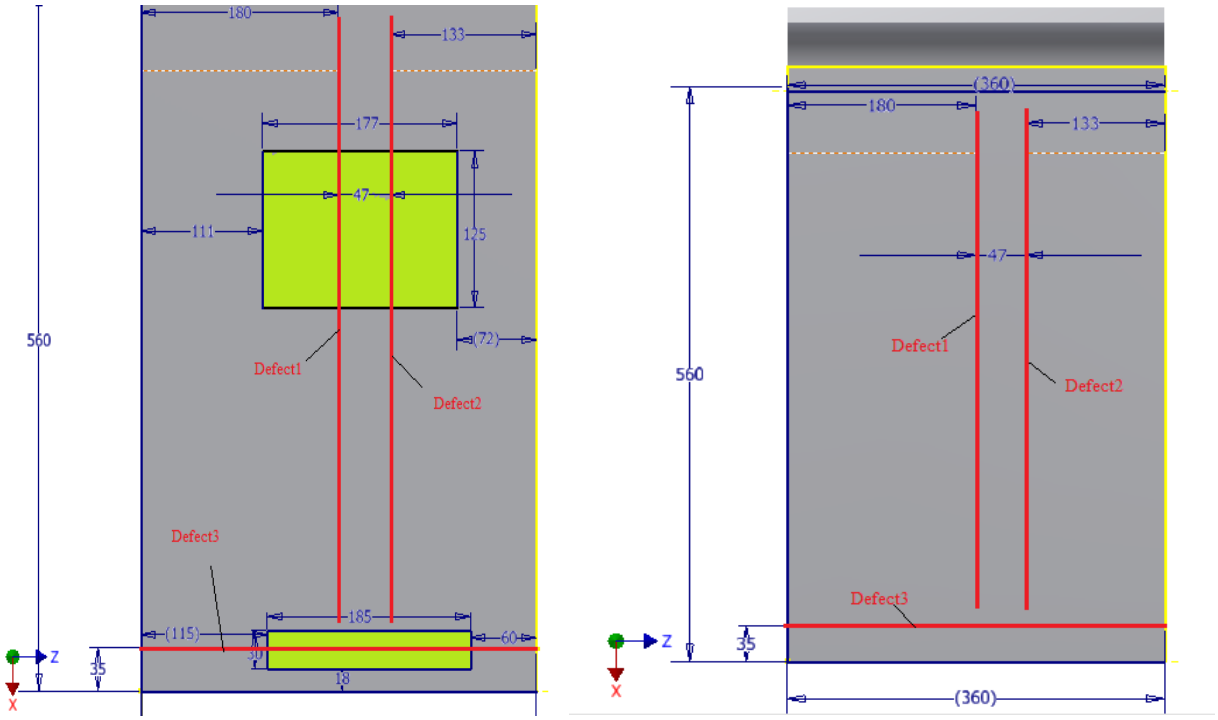

a) Inspection zones b) Vertical and horizontal cracks

Fig. 8.2. Top view of the inspection zones and defects

8.2. Results of the Experimental Inspection

The inspection has done for A-320 elevator by using 5L128-128X7-NW3 PA transducer. However, the cracks are visible, and they are consist of two parallel at a distant of 47mm. Moreover the other crack has been inspected near the trailing edge of the A-320 elevator as shown in a figure 8.2(b).

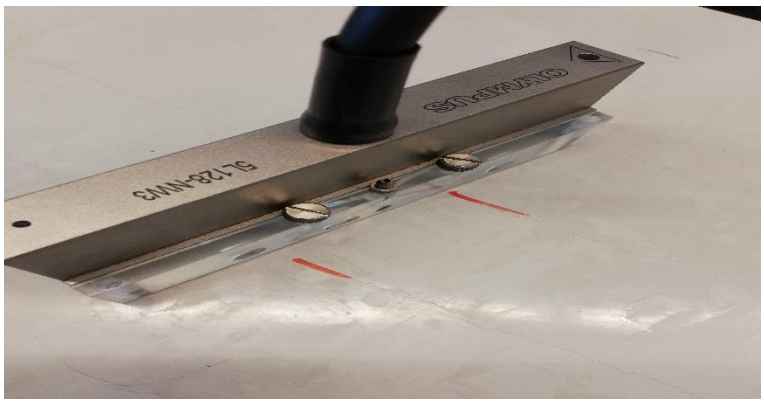

Fig. 8.3. Parallel cracks inspection.

Figure 8.3 represent the lab inspection using 5L128-128X7-NW3. However, the red marks represent the vertical cracks along the surface of the A-320 elevator. Figure 8.4 shows the A-scan and B-scan image of the parallel cracks.

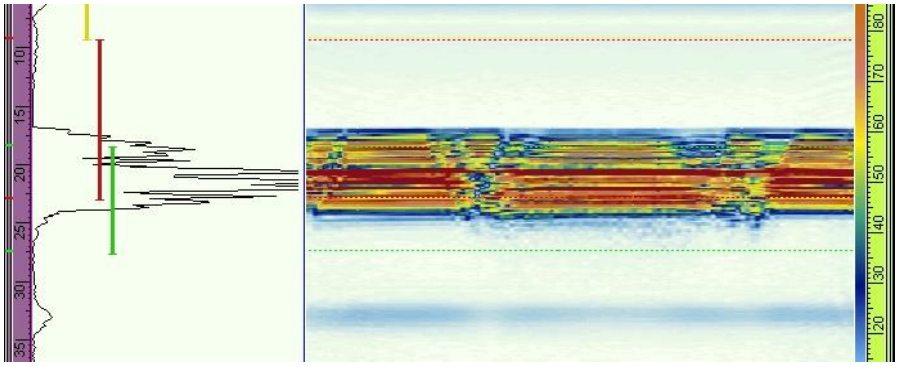

Fig. 8.4. A-scan and B-scan images of the parallel cracks.

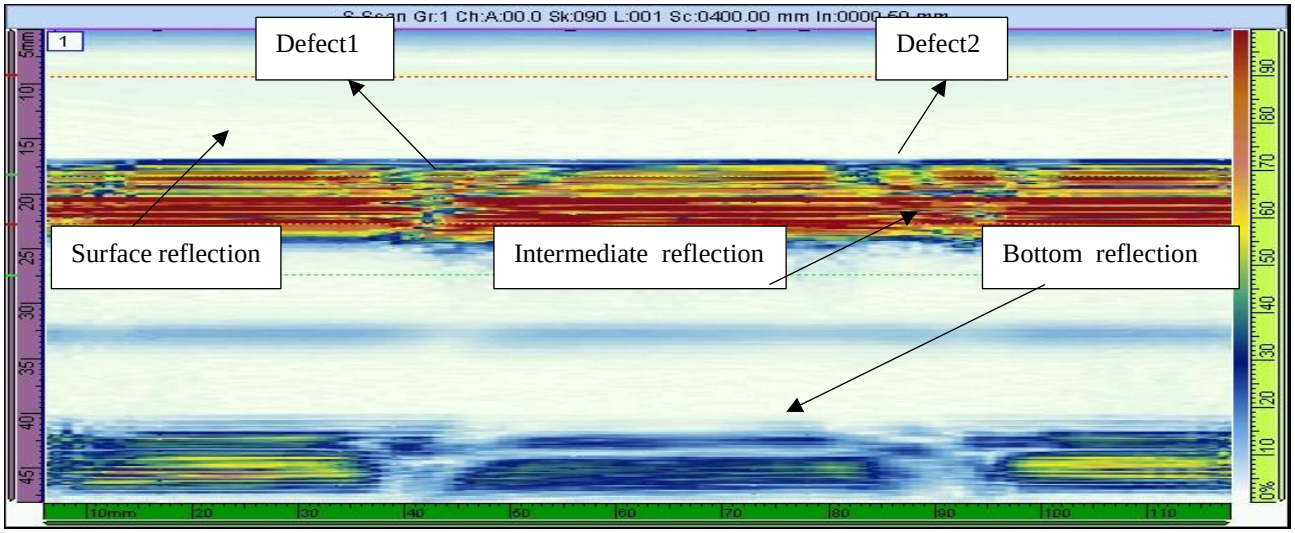

Fig. 8.5. Parallel cracks detection.

Figure 8.6 shows the A-scan and B-scan images of the horizontal crack near the trailing edge. Similarly, the inspection is performed by using 5MHz PA transducer of a 128 elements. Then, the

time intervals between signals have been recorded. However, the maximum depth of the cracks is calculated according to the following equation: $H= V_m.T_d /2$, where V_m=2700 m/s

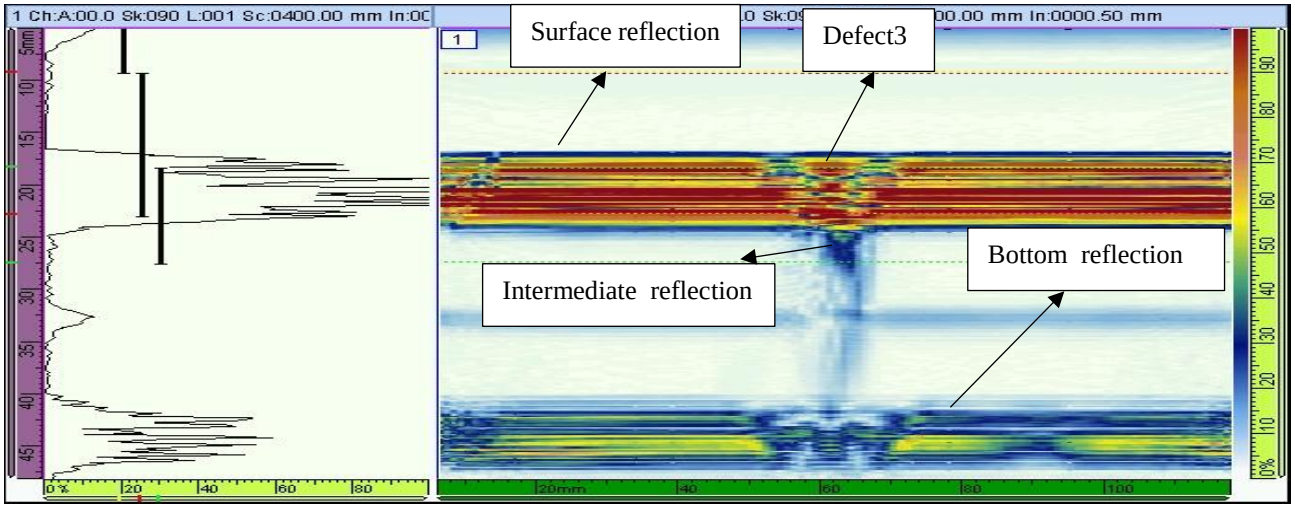

Fig 8.6. A-scan and B-scan image of a defect3.

Figure 8.6 shows the reflections at a crack3. However, crack3 is located near the trailing edge of an A-320 elevator. The time interval of the signals and the maximum depth of each crack are shown in a table 8.2.

Table 8.2. Time interval and defect depths.

	Defect1	**Defect2**	**Defect3**
Time Interval µs	[9.5,10.1]	[8.8,.2]	[8.5,9.35]
Depth mm	0.81	0.27	0.93

9 Comparison of the Results of Different Transducers

The Inspections are performed by using two different transducers. However, the frequency range is varied between 5MHz and 10MHz. The transducers are Single element probe and Phased Array transducer. Moreover, the PA transducer consists of 128 elements and two focusing types, such as Single Point Focusing and Null Delay Law.

9.1. Comparison of the Results between PA-Single Point Focusing and Single Element Probe

The results of the PA and Single element transducers have reached maximum amplitude at a defect2 in the case study2 inspections. The maximum measured amplitudes are -10.2dB and -9.7Db at 10MHz PA and 10MHz Single Element probe respectively. The results of a Single element probe in a study case3 show that the maximum amplitude is a -13.9dB at defect1 in a section2, which it represents a strong reflection. Then it is increased progressively to almost -6.4Db in section3. However, the PA results showed higher amplitudes on the larger size defects at both frequencies 5Mhz and 10MHz. The maximum amplitude of PA is a -8dB in study case3 and section2. Therefore, PA transducer is more preferable to detect medium and large size defects, and the Single Element Probe is able to detect small size defects such as 5*5mm^2.

9.2. Comparison of the Results between PA-Null Delay Law and Single Element Probe

In study case2 inspection, the results of both transducers PA and Single Element Probe have shown maximum amplitudes and high intensity at defect2. The maximum measured amplitude of defect2 is a -9.7dB by using 10MHz single element probe, and a -9.1dB by using a 10MHz PA transducer of a null delay law. Therefore, the inspection is very effective in CFRP material by using 10MHz Single Element Probe and less efficient for paint/adhesion inspection because week reflections have been received at defect1 which is equivalent to -6.4dB.

The results of case study3 show that the maximum measured amplitudes have reached peak values at defect1 of a section2, where the magnitudes are -13.9dB and -10.7dB by using a 10MHz single element probe and Phased Array transducer respectively. However, section2 represents the study case of the different size defects at 0.6mm depth (CFRP layer). Therefore, even in the inspection of different size defects, the strong reflections are at the CFRP material by using 10MHz Single Element Probe and 10MHz PA. The maximum amplitudes reached were at defect1, which means that the mentioned transducers are very efficient for the small size defect's inspection. Moreover, at 10MHz frequency the resolution and accuracy of the inspected defects are significantly increased in the results of both transducers.

9.3. Comparing the Results of PA (Single Point Focusing and Null Delay Law)

The results of the same size defects at a different depth (Case Study2) show that the reflections of signals using PA single point focusing transducer is stronger than the reflections of PA null delay law. The maximum amplitude measured at defect2 is -10.2dB, and slightly increased to -9.1dB by using 10MHz PA null delay law. Therefore, the resolution and intensity have been increased by using single point focusing PA. On the other hand, the 10MHz null delay law PA is more preferable to detect small size defects as it is shown in study case3 at a defect2 of a -10dB ma

10 Conclusion

1. A320- elevator is a sandwich structure component that it consists of different materials are stacked on each other. For this reason, limited NDT methods could be used. However, the selected technique for the investigation is UT. Ultrasonic testing is widely used in aerospace industries especially for composite materials inspection. UT methods are very efficient and reliable to detect surface and internal defects by using only one side surface. However, various ranges of frequencies is possible to use such as 5MHz and 10MHz. The results are shown by B-scan and A-scan images.
2. The results of the inspection by using PA transducer show high amplitudes in the most of the study cases. For example in study case3, the maximum amplitude has reached is -10.7dB at defect2 and -10.2dB in study case2, which indicates high intensity and resolution. In comparison with single point focusing PA, the 10MHz Single Element Probe is more able to detect small size defects such as 5*5mm^2, where maximum amplitude has reached is -13.7dB in study case3 at defect1.
3. In all the study cases, two values of frequency have been used which are 5MHz and 10MHz. The results shows that the maximum amplitudes of the 10MHz frequency is lower than the measured amplitudes of a 5MHz frequency. However, the resolution and accuracy are higher at 10MHz frequency.
4. A 10MHz PA transducer is selected as the best option for the non-destructive testing of the wing elevator.

.

List of references

1. Litera Steinchen W, Yang L, Kupfer G and Mackel P (2015) Non-destructive testing of aerospace composite materials using digital shearography Journal of Aerospace Engineering 212 1 21-30
2. Abdullah WSW, Yusof MY, Puad ANA and Hoque ME Analysis of corrosion in pressurized pipelines by advanced laser shearography (2016) Engineering e-55.
3. Santos F, Vaz M and Monteiro J (2014) A New Set-Up for Pulsed Digital Shearography Applied to Defect Detection in Composite Structures Optics and Lasers in Engineering 42 2 131-140 .
4. Hung YY, Chen YS, Ng SP, Liu L, Huang YH, Luk BL, Ip RWL, Wu CML and P.S. Chung. (2017) Review and Comparison of Shearography and active Thermography for Non-destructive Evaluation Material Science and Engineering 64 73-112.
5. Chetwynd, D., Mustapha, F., Worden, K. & Rongong, J.A. "Damage Detection in Plates using Transducers Mounted on Viscoelastic Damping Layers", Proceedings of the 3rd European Workshop on Structural HealthMonitoring, 2016.
6. Chetwynd, D., Mustapha, F., Worden, K., Rongong, J.A., Pierce, S.G. & Barton, J. "Damage Location in a Stiffened Composite Panel using Lamb Waves and Neural Networks", Proceedings of the 25th International ModalAnalysis Conference (IMAC XXV), 2017.
7. Chetwynd, D., Lew, T.L., Worden, K. & Rongong, J.A. "Damage Detection in an Aluminium Plate with an Active Constrained Layer Damping Treatment", Proceedings of the 7th International Conference on DamageAssessment of Structures, 2017.
8. Castellano, A.; Fraddosio, A.; Piccioni, M.D. Quantitative analysis of QSI and LVI damage in GFRP unidirectional composite laminates by a new ultrasonic approach. Compos. Part B Eng.2018, 151, 106–117.
9. Toyama, N.; Ye, J.; Kokuyama, W.; Yashiro, S. Non-Contact Ultrasonic Inspection of Impact Damage inComposite Laminates by Visualization of Lamb wave Propagation. Appl. Sci. 2018
10. J. Zemlicka, V. Kraus, M. Holik and J. Jakubek, Fast Spectroscopic Imaging with Pixel Semiconductor Detector Timepix and Parallel Data Reading, Journal of Instrumentation, submitted (2013)
11. U. Ewert, K.-U. Thiessenhusen, B. Redmer, Reduktion von Kreuzartefakten in der Laminographie, DGZfP Jahrestagung 2013, Dresden, Germany, May 6-8, 2013
12. A. Deresch , K.-U Thiessenhusen, U. Ewert, C. Bellon, Schnelle Shift-Average-Rekonstruktion für die koplanare Translationslaminographie, DGZfP Jahrestagung 2014, Potsdam, Germany, May 2014
13. U. Schnars, A. Kück, Application of POD Analysis at Airbus, 4th European-American Workshop on Reliability of NDE, June 2009, Berlin, Germany.
14. U. Ewert, B. Redmer, C. Rädel, U. Schnars,R. Henrich, K. Bavendiek, M. Jahn, "Mobile Computed Tomography for Inspection of Large Stationary Components in Nuclear and Aerospace Industries", Materials Transactions, Vol. 53, No. 2 (2012) pp. 308 to 310.
15. Dattoma, V. , Marcuccio, R. , Pappalettere, C. and Smith, G.M. (2012). Thermographic Investigation of Sandwich Structure made of Composite Material , NDT AND E International, 34(8): 515–520
16. Legendre, S. , Goyette, J. and Massicott, D. (2015). Ultrasonic NDE of Composite Material Structures using Wavelet Coefficients , NDT & E International, 34(1): 31–37

17. Favro, L.D. , Thomas, R.L. , Han, X. , Ouyang, Z. , Newaz, R.L. and Gentile, G.D. (2014). Sonic Infrared Imaging of Fatigue Cracks , International Journal of Fatigue, 23(Supplement 1): S471–S476 . Figure [34] reprinted with permission from Elsevier.
18. Osmont, D. , Devillers, D. and Taillade, F. (2010). Health Monitoring of Sandwich Plates based on the Analysis of the Interaction of Lamb Waves with Damages , In: Proceedings of SPIE – The International Society for Optical Engineering, 432(7): 290–301 .
19. Ma, X.Q. and Takemoto, M. (2012). Quantitative Acoustic Emission Analysis of Plasma Sprayed Thermal Barrier Coatings subjected to Thermal Shock Tests , Material Science and Engineering A, 308(1–2): 101–110
20. Kim, B. and Weiss, J. (2013). Using Acoustic Emission to Quantify Damage in Restrained Fiber-reinforced Cement Mortars , Cement and Concrete Research, 33(2): 207–214 .
21. Forest, L. , Gibiat, V. and Hooley, A. (2009). Impedance Matching and Acoustic Absorption in Granular Layers of Silica Aerogels , Journal of Non-Crystalline Solids, 285(1–3): 230–235
22. Vavilov, V.P., Burleigh, D.D.: Review of pulsed thermal NDT: physical principles, theory and data processing. NDT E Int. **73**, 28–52 (2015)
23. Cramer, K., Winfree, W., Hodges, K., Koshti, A., Ryan, D., Reinhard, WW.: Status of thermal NDT of space shuttle materials at NASA. In: Proceedings of SPIE "Thermosense-XXVIII", vol. 6205, p. 62051B1-9 (2016)
24. Burleigh D.A.: Portable, combined thermography/shearography NDT system for inspecting large composite structures. In: Proceeding of SPIE "Thermosense-XXIV" vol. 4710, pp. 578–587 (2002)
25. Balageas, D., Levesque, P., Brunet, P., Cluzel, C., Déom, A., Blanchard, L.: Thermography as a routine diagnostic for mechanical testing of composites. Quant. InfraRed Therm. J. **5**(1), 45–68 (2008)
26. Guo, X., Vavilov, V.P.: Crack detection in aluminum parts by using ultrasound-excited infrared thermography. Infrared Phys. Technol. **61**, 149–156 (2013).
27. Ibarra-Castanedo C., Genest M., Maldague X. (2013) Infrared vision: visual inspection beyond the visible spectrum. Integrated Imaging and Vision Techniques for Industrial Inspection: Advances and Applications, Zheng Liu Ed., Springer, New York (2013)
28. Schnars, U., & Henrich, R. (2016, September). Applications of NDT methods on composite structures in aerospace industry. In Conference on damage in composite materials, Stuttgart, Germany (pp. 1-8).
29. K. Deutsch, Phased array ultrasonic testing of heavy-wall seamless tubes by means of a testing portal, ECNDT, Moscow, June, 2010, pp.1–10.
30. F. Jenson, E. Iakovleva, N. Dominguez, "Simulation supported POD: methodology and HFET validation case", in Review of Progress in QNDE, 30, 2010.
31. N. Dominguez, V. Feuillard, P. Willaume, F. Jenson, "Simulation assisted POD of a Phased Array Ultrasonic Inspection in Manufacturing", in Review of Progress in QNDE, 31B, 2011.